SQT

OT/TRER 33 (Old Series)
OT REPORT 73-15

AN EXPERIMENTAL STUDY OF THE TEMPORAL STATISTICS OF RADIO SIGNALS SCATTERED BY RAIN

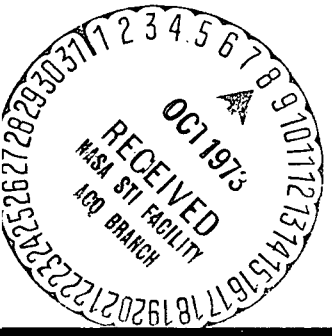

OT

U.S. DEPARTMENT OF COMMERCE/Office of Telecommunications

AN EXPERIMENTAL STUDY OF THE TEMPORAL STATISTICS OF RADIO SIGNALS SCATTERED BY RAIN

R. W. HUBBARD
J. A. HULL
P. L. RICE
P. I. WELLS

U.S. DEPARTMENT OF COMMERCE
Frederick B. Dent, Secretary

OFFICE OF TELECOMMUNICATIONS
John M. Richardson, Acting Director

JUNE 1973

For sale by the Superintendent of Documents, U.S. Government Printing Office, Washington, D.C. 20402

$ 1.55

UNITED STATES DEPARTMENT OF COMMERCE

OFFICE OF TELECOMMUNICATIONS

STATEMENT OF MISSION

The mission of the Office of Telecommunications in the Department of Commerce is to assist the Department in fostering, serving, and promoting the Nation's economic development and technological advancement by improving man's comprehension of telecommunication science and by assuring effective use and growth of the Nation's telecommunications resources. In carrying out this mission, the Office:

Performs analysis, engineering, and related administrative functions responsive to the needs of the Director of the Office of Telecommunications Policy in the performance of his responsibilities for the management of the radio spectrum;

Conducts research needed in the evaluation and development of telecommunications policy as required by the Office of Telecommunications Policy, Executive Office of the President, pursuant to Executive Order 11556;

Conducts research needed in the evaluation and development of other policy as required by the Department of Commerce;

Assists other government agencies in the use of telecommunications;

Conducts research, engineering, and anlaysis in the general field of telecommunication sciences to meet government concerns;

Acquires, analyzes, snythesizes, and disseminates information for the efficient use of telecommunications resources.

PREFACE

The experiment and measurements described in this report were performed under the Radio-Frequency Interference and Propagation Program (RIPP) administered by the National Aeronautics and Space Administration (NASA). The planning for this program was guided by a steering committee composed of members (and their technical advisors) representing the Federal Communications Commission (FCC), the Office of Telecommunication Management (OTM - now the Office of Telecommunication Policy), NASA, and the Institute for Telecommunication Sciences (ITS). The technical investigations were carried out by the ITS in two basic phases that spanned one year from September, 1970 to October 1971. This report covers only Phase I of the program, at which time precipitation scatter data were obtained on frequencies in both the S-band and X-band portions of the electromagnetic spectrum. The experimental period for Phase I was from late September, 1970, through January, 1971, and this report contains the computer analyses of data for this four-month period.

Phase II of the program included a reconfiguration of the experiment, that eliminated some of the original transmission paths and the X-band measurements. Computer analyses as noted in this report were not continued, and a manual analysis was performed by NASA for only the S-band data for the balance of the year. Results of this work are reported in a NASA document (1972) listed in the references.

Magnetic tape data for Phase II of the experiment are on file at the Institute for Telecommunication Sciences (ITS) laboratories in Boulder, Colorado, and are available for additional analyses.

Acknowledgements: This work has been supported by the National Aeronautics and Space Administration, initially through the Electronics Research Center and later through the Goddard Space Flight Center. The NASA Technical Officer is Dr. Jerome Eckerman. Portions of the modeling effort and much of the data reduction and analyses have been supported through Research and Development funds of the Department of Commerce.

TABLE OF CONTENTS

LIST OF FIGURES

LIST OF TABLES

AN EXPERIMENTAL STUDY OF THE TEMPORAL STATISTICS OF RADIO SIGNALS SCATTERED BY RAIN

R. W. Hubbard, J. A. Hull, P. L. Rice, and P. I. Wells *

ABSTRACT

A fixed-beam bistatic CW experiment designed to measure the temporal statistics of the volume reflectivity produced by hydrometeors at several selected altitudes, scattering angles, and at two frequencies (3.6 and 7.8 GHz) is described. Surface rain gauge data, local meteorological data, surveillance S-band radar, and great-circle path propagation measurements were also made to describe the general weather and propagation conditions and to distinguish precipitation scatter signals from those caused by ducting and other nonhydrometeor scatter mechanisms. The operating characteristics of the various system components used in the experiment are presented. The data analysis procedures were designed to provide an assessment of a one-year sample of data with a time resolution of one minute. The results to date cover the time interval of September 15, 1970 to January 31, 1971. The cumulative distributions of the bistatic signals for all of the rainy minutes during this period are presented for the several path geometries. These cumulative distributions of amplitude-time durations of hydrometeor scatter signals are compared with measured cumulative distributions of surface rain-rate measurements obtained for the same time periods. The surface rain-rate statistics are compared with long-term excessive precipitation data available for the southeastern United States.

Key Words: Propagation, Precipitation scatter, Rain-rate statistics, Coordination distances, Satellite/terrestrial communications, Frequency sharing.

*The authors are with the Institute for Telecommunication Sciences, Office of Telecommunications, U. S. Department of Commerce, Boulder, Colorado 80302.

1. INTRODUCTION

As an integral part of the Radio-frequency Interference Propation Program (RIPP) administered by the National Aeronautics and Space Administration (NASA), the Institute for Telecommunication Sciences (ITS) conducted an experiment at Langley, Virginia, to study the propagation/interference problem caused by scatter from precipitation.

The objective of this fixed-beam, bistatic CW experiment was to measure the temporal statistics of the volume reflectivity produced by hydrometeors at several selected altitudes and scattering angles, and to determine the relationship of these measured path-loss statistics to those of local surface rain-rate measurements. Extensive meteorological, surveillance radar, and great-circle path measurements were also made to describe general weather and propagation conditions.

When the earth terminals of a satellite communication system share frequency bands with terrestrial microwave systems, the addition of a new terminal to either system requires that it be established in such a manner that no harmful interference will result to either the new terminal or any of the terminals of the existing systems. It is necessary, therefore, in the planning, design, and construction of such systems to have estimates of expected interference to or from the proposed new system.

Current procedures for the estimation of interference between terrestrial radio systems and the earth stations of satellite communication systems are based upon reports of the CCIR, especially CCIR

Report 382 [1966a] as revised in New Delhi. The details of these procedures are given in reports by the Federal Communications Commission [1965], and the COMSAT Corporation (unpublished report 1969).

Many factors in the design and location of a telecommunication system can be optimized to provide a maximum ratio of wanted to unwanted signals. Propagation effects, however, are essentially beyond the control of the system designer. They enter into the system performance by introducing distortion of the desired signal. This may be independent of the ratio between the desired and undesired signal [CCIR, 1966b] (for example, phase interference due to multipath, pulse distortion, intermodulation, etc.) or may involve power fading and interference effects that degrade the quality of service by reducing the desired to undesired signal ratio. In the latter case, a "safety margin" can normally be applied to assure an adequate power level for the victim service. The goal of interference probability modeling is to develop a method for determining the required "safety margin" as a function of the probability of harmful interference that can be determined or predicted. The development of models for this purpose has been a contribution of the Institute for Telecommunication Sciences (ITS) and its predecessors over the past two decades [Rice et al., 1967]. The methodology and mathematical development of such models is based on the concept of service probability [CCIR, 1966c], and has been treated in a summer seminar series presented by ITS in 1970.

Since most telecommunications systems can tolerate interruption for relatively short, infrequent time periods and must operate on essentially a continuous basis in the absence of interference, the role of propagation is quite different in performance predictions from its role in interference probability predictions. For performance prediction models (in the absence of interference) only one dominant propagation

mechanism normally needs to be considered. The objective of such a model is to predict the probability that this mechanism will be present a high percentage of time and be sufficiently efficient to assure that an adequate signal will be propagated along the desired path. In contrast, the interference probability model that is of concern in this report involves several possible propagation mechanisms that can couple interfering signals between services sharing the same frequencies. Some of these mechanisms may be associated with more than one path. They may be highly efficient and may exist for long periods of time. In the performance prediction models, the statistical properties of the propagation mechanism are usually stated in terms of the distribution of hourly median values, while in the case of an interference probability model the statistical properties of rare events are needed.

In considering the aspects of sharing between space and terrestrial systems, CCIR Study Group 5 [CCIR, 1970] has identified seven propagation factors which should be considered in the development of methods to predict the interference between the services, namely: effects of terrain, effects of vegetation and buildings, the effects of random tropospheric inhomogeneities, the effect of tropospheric ducts or layers, scatter from hydrometeors, scatter from aircraft, terrain diffraction and tropospheric refraction. Among these factors, one that has been least understood in terms of the statistical parameters required to predict the interference potential, is scatter from hydrometeors. This particular factor is the subject of this study.

It is not feasible to measure the precipitation reflectivity directly in all system configurations that must be coordinated to prevent detrimental rain-scatter interference. Thus, there is a need for a model based upon an available data source, such as a meteorological parameter that is measured generally on a worldwide basis. The readily available data are primarily surface rain measurements.

The modeling required for this form of propagation interference consists of the selection of pertinent information regarding the temporal variations of geophysical parameters, and the electromagnetic wave interaction with these parameters, to provide an anticipated statistical performance of a given system. A primary concern in this work is a precipitation scatter model that will provide an appropriate statistical basis for the propagation factors associated with the scatter from hydrometeors. The physics of scattering by hydrometeors and turbulent layers has been treated and experimentally validated as described in a recent report by Crane [1970a]. His work has developed models that compare radar backscatter and bistatic scatter phenomena for both turbulent layer scattering and scatter by precipitation. These models are based upon the reflectivity η associated with the scatter region, which was measured directly in the validating experiment with a high-power precision radar system.

The statistics of surface rainfall rates discussed in section 5.3 and in Rice and Holmberg [1972] are based on close examination of ten years of surface data for 49 measuring stations in the U.S. Recorded rainfall rates are ratios of the depth of water collected in standard rain gauge instruments and the period of time of the record, ranging from 5 to 180 minutes, and are expressed in mm/hr. In order to estimate the rainfall rates within a shorter period of time (i.e., one minute), extrapolation techniques were applied, and a model for the cumulative time statistics of one-minute rainfall rates was developed. Two basic "modes" are defined, with different average rainfall rates, $\overline{R}_1$ and $\overline{R}_2$. The data base for the model is large enough to describe an "average year" (from 1951 - 1960) for each of several climatic zones in the U.S.

The fixed-beam experiment at Langley, Va. was designed to obtain measured rainfall rates with short resolution times, in order to directly develop the type of cumulative statistics used in the Rice and Holmberg model over the span of a one-year measurement interval. In addition, bistatic CW measurements were made of the volume reflectivity caused by hydrometeor scattering at several scattering angles. The surface rain-rate measurements obtained are reordered into a cumulative distribution and compared with the statistical prediction for an average year, using the Rice and Holmberg model. A long data sample will permit an empirical relation between the surface rain-rate statistics and the altitude-dependent volume reflectivity statistics to be made. Using these relationships, we may then apply the model to other locations (climatic regions) to predict the interference probability based on surface rain measurements for that location.

This report discusses the physics of the experiment, some statistical limits of rain scatter, and the expected tropospheric path loss for the geometric configuration of the experiment. The geometric configuration is described, and the system operating characteristics required for the evaluation of the observed signals and events are presented. The data processing and reduction procedures for both the rain gauge and radio path loss measurements are described, and the cumulative data for a four-month period of the experiment are presented. Finally, some comparative analyses of surface rain-rate and radio data are presented to demonstrate the performance of the system, and to indicate the level of confidence that can be placed in the resultant data.

2. DESCRIPTION OF THE EXPERIMENT

2.1 Physics of the Experiment

Precipitation scattering of radio energy in the frequency bands shared by terrestrial microwave and satellite communications systems has been clearly established [Carey and Kalagian, 1969; Gusler and Hogg, 1970] as a dominant source of potential mutual interference in these systems, for time periods exceeding the present allowable limits established by the Federal Communications Commission (FCC).

The Virginia fixed-beam experiment was designed to provide measurements of the path loss variations caused by hydrometeor scattering at four discrete altitudes and at two frequencies representative of the low and high ends of the present bands allocated for satellite-terrestrial communication systems. Surface rain-rate measurements were made at the sub-points of the common volumes defined by the intersection of several transmitter antenna beams and the receiver main beam (see figure 1, page 28). From these measurements, the long-term statistics of the path loss (or volume reflectivity) are accumulated, as are the corresponding surface rain-rate statistics. Unwanted signals can occur in a given communication system configuration by means other than hydrometeor scatter; for example, atmospheric ducting. Thus, it was necessary to obtain sufficient ancillary meteorological data during this experiment to permit separation of the non-rain scatter mechanisms that are possible, assuring that the statistics of the path loss measurements are properly interpretable. The design of this fixed-beam propagation experiment has emphasized measurements that permit proper identification of scatter signals due to rain and hail in the common volumes.

Most of the physics involved in the experiment, whether meteorological or electromagnetic in nature, are visible in the bistatic radar equation

$$\bar{p}_r(\theta,\varphi) = \frac{p_t(\theta',\varphi')\lambda^2}{64\pi^3} \int_{(V)} \frac{g_t g_r \eta}{S_t^2 S_r^2}\, dv \left[e^{-\int_0^{S_i} \beta_{ab}(r)dr} \quad e^{-\int_{S_i}^{S_t} \beta_{ex}(r)dr} \right.$$

$$\left. e^{-\int_{S_o}^{S_r} \beta_{ex}(r)dr} \quad e^{-\int_0^{S_o} \beta_{ab}(r)dr} \right] \qquad (1)$$

where

$\bar{p}_r(\theta,\varphi)$	is power received in the direction (θ,φ) in watts,
$p_t(\theta',\varphi')$	is power transmitted in the direction (θ',φ') in watts
θ and φ	are respectively the azimuth and elevation angles in a polar coordinate system with their origin at the receiver,
g_r and g_t	are the appropriate gain factors for the receiving and transmitting antennas relative to isotropic,
S_t and S_r	are the ray ranges from the transmitter and receiver, respectively, to the element of common volume dv in meters,
S_i	is the ray distance from the transmitter to the near "edge" of the scattering substance in meters,
S_o	is the ray distance from the receiver to the near "edge" of the scattering substance in meters,
β_{ab}	is clear atmosphere absorption (or attenuation) coefficient of a beam,
β_{ex}	is the attenuation caused by precipitation and/or turbulence,
V	is the volume of the scattering region in cubic meters,

η is the local reflectivity of material in the common volume, V, in inverse meters,

λ is the wavelength of incident and scattered power in meters, and

$\oint_V$ denotes the volume of integration.

The important physical aspect of the experiment is the reflectivity of energy by hydrometeors in the intersection of the transmitter and receiver antenna beams, which determine the common volume, V.

Thus, the reflectivity factor, η, is the key unknown in equation (1). The experiment will distinguish between clear air turbulence and rainfall, although there remains a problem of discrimination in a convective precipitation situation where both turbulence and heavy rainfall can coexist with near-forward scattering. The precise reflectivity encountered in any given common volume intersection is generally not known. In the case of precipitation, the reflectivity is dependent upon the size and distribution of the hydrometeors within the common volume. To determine η precisely requires that measurements be made directly in the common volume, for example, the backscatter measurements made with a precision monostatic radar in the work noted previously by Crane [1970a].

The attenuation and absorption terms in equation (1) may generally be neglected at the lower (S-band) frequencies used in this experiment without appreciable error. At the X-band frequencies, attenuation due to rain can be significant if the rain fills a major part of the beam of both the receiving and transmitting antennas. However, if the rain is concentrated in and near the common volume (of primary interest here), the attenuation may also be neglected at these higher frequencies.

The effect of the terrain and obstacles such as buildings or trees in the immediate foreground of the antenna can be a significant factor. Terrain or other obstacles should be considered when determining the effective power radiated from, or received by, an antenna at any specific direction (θ, φ). Also, the gain factors g_t and g_r include the effects of directivity and polarization of the transmitting and receiving antennas in the interference problem. Considerable effort (private communication from R. R. Bergman and L. G. Hause, 1970, of the ITS staff) was expended toward the determination of the antenna patterns and hence the description of the antenna gains in a particular direction for use in (1). Receiving antenna pattern measurements were made using a small target transmitter located on a tower at Poquoson, Virginia. Representative transmitter antenna patterns were measured on the antenna range maintained by NASA at Langley, Virginia. Assuming that there is no attenuation or angular dependence of the scattered power in the reflectivity factor η, a simplified version of the bistatic radar equation (1) may be used, where the antenna gain factors are as determined above. The simplified equation is

$$p_r = \frac{p_t \lambda^2 g_r g_t \bar{\eta} V}{64\pi^3 S_t^2 S_r^2} \qquad (2)$$

where p_r and p_t are now, respectively, the mean power received and transmitted along the main axes of the antenna beams, and S_t and S_r are now the range values measured to the intersection of the axes within the common volume intersections. The average reflectivity factor $\bar{\eta}$ may be related to the radar reflectivity value Z by

$$\bar{\eta} = \frac{\pi^5}{\lambda^4} |k|^2 Z \qquad (3)$$

where $|k|^2$ is a parameter dependent upon the dielectric properties of the scatter material. In the case of rain and for frequencies between 1 and 35 GHz, $|k|^2 \approx 1$ [Crane, 1970a], and is taken as 0.93 (an approximate value for water). For purposes of this experiment, $\bar{\eta}$ may thus be approximated by

$$\bar{\eta} = 0.93 \pi^5 \lambda^{-4} Z \times 10^{-18} \qquad (4)$$

where Z is in the units of mm^6/m^3 as derived from rain distribution theory, and $\bar{\eta}$ is in m^{-1}.

For most of the common volumes in the Viginia experiment, the volume of intersection between antennas may be approximated by a thin cylinder, the intersection of a pencil beam (receiver) with the broader beam of the transmitting antennas. In these cases, the volume is given approximately by

$$V = \pi/4 (\alpha_r S_r)^2 \alpha_t S_t \csc \theta \qquad (5)$$

where

α_r is the half-power beamwidth of the receiving antenna in radians,

α_t is the half-power beamwidth of the transmitting antenna in radians, and

θ is the scattering angle in degrees (the supplement of the angle between antenna axes at the scatter intersection.)

Substituting (4) and (5) into (2) yields

$$p_r = \frac{(p_t \lambda^2 g_r g_t)(0.93 \pi^5 \lambda^{-4} Z \times 10^{-18})(\pi/4)(\alpha_r^2 \alpha_t \csc \theta)}{64 \pi^3 S_t} \quad . \tag{6}$$

Rearranging terms of (6) and adding a factor to account for all line losses we may express the total power at the receiver input terminal in dB as

$$\begin{aligned} P_r = {} & P_t + G_r + G_t - L_t - 20 \log \lambda + 10 \log Z - 10 \log S_t \\ & + 10 \log A + 10 \log (0.93) + 10 \log (\pi^5 \times 10^{-18}) \\ & - 10 \log (64 \pi^3) \end{aligned} \tag{7}$$

where

P_r = $10 \log p_r$ dBm,
P_t = $10 \log p_t$ dBm,
G_r = $10 \log g_r$ dB,
G_t = $10 \log g_t$ dB,
L_t = total line losses in dB, and
A = $(\pi/4) \alpha_r^2 \alpha_t \csc \theta$.

Evaluating terms in (7), and inserting the transmitter power used in the experiment, 10 watts (40 dBm), results in

$$\begin{aligned} P_r = {} & -148.4 + G_r + G_t - L_t - 20 \log \lambda + 10 \log Z \\ & - 10 \log S_t + 10 \log A. \end{aligned} \tag{8}$$

Two nominal transmission frequencies were used in the Virginia experiment as noted earlier. Each of these was subdivided into a number of transmitting frequencies as outlined in section 2.3. For the purpose of equation (8), the wavelengths may be determined for the nominal frequencies without significant error in later calculations. Thus the nominal frequencies and freespace wavelengths are

$f_s = 3.672$ GHz,

$\lambda_s = 300/3672 = 0.0817$ meters,

$f_x = 7.834$ GHz, and

$\lambda_x = 300/7834 = 0.0383$ meters.

The receiving antenna at the Langley, Virginia, earth station (ES) was a 30-ft parabolic dish, common to both the S- and X-band frequencies. The measured gains of this common-feed antenna were, respectively,

$(G_r)_s = 47.5$ dB at 3.672 GHz, and

$(G_r)_x = 50.8$ dB at 7.834 GHz.

The transmitting antennas used were 10-ft parabolic dishes at S-band and 6-ft parabolic dishes at X-band. The gains of the transmitting antennas were, respectively,

$(G_t)_s = 38.8$ dB at 3.672 GHz, and

$(G_t)_x = 41.0$ dB at 7.834 GHz.

Substituting the above values into (8) yields

$$(P_r)_s = -40.74 - L_t + 10 \log Z - 10 \log S_t + 10 \log A \text{ and} \quad (9)$$

$$(P_r)_x = -28.41 - L_t + 10 \log Z - 10 \log S_t + 10 \log A \quad (10)$$

for the S- and X-band frequency cases, respectively. The remaining nonnumerical terms in (9) and (10) are functions of particular systems and path geometry, with the exception of Z. The accepted relationship* between the radar reflectivity Z and the rain rate R_v in the scatter volume is given by

$$Z = 200 R_v^{1.6} \quad (11)$$

where R_v is in mm/hr, and Z is in mm^6/m^3.

Equation (11) can be converted to logarithmic form as

$$10 \log Z = 23 + 16 \log R_v. \quad (12)$$

When (12) is substituted into (9) and (10), these equations become

$$(P_r)_s = -17.74 - L_t - 10 \log S_t + 10 \log A + 16 \log R_v \text{ and} \quad (13)$$

$$(P_r)_x = -5.41 - L_t - 10 \log S_t + 10 \log A + 16 \log R_v. \quad (14)$$

---

*Note: The relation $Z = 200\ R^{1.6}$ appears to be the best empirical fit for lower rain-rates. For rain-rates exceeding 75 mm/hr, the expression $Z = 400\ R^{1.4}$ becomes a better fit. [Austin, 1969]

These equations may be further simplified to the form

$$(P_r)_s = K_s + 16 \log R_v \text{ dBm and} \quad (15)$$

$$(P_r)_x = K_x + 16 \log R_v \text{ dBm} \quad (16)$$

where K_s and K_x are constants in dB determined from the individual path parameters.

The values of these constants have been computed and are given in table 1 for all of the bistatic path configurations in the Langley experiment. Their values may be viewed as the level of detectable rain scatter signal that will be received over each path, if R_v is assumed to be 1 mm/hr. The individual path and site parameters involved in the computations may be found in table 6 of section 3.

The above development is based on an approximation of the common volumes, assuming the intersection of two cylinders as in (5). A more accurate computation of the common volumes has been carried out by M. J. Miles of the ITS staff (private communication, 1970) using conical beam patterns defined by the half-power points of the transmitter and receiver antenna beams. The computer-derived values from this procedure are also given in table 6, section 3. The difference between the two estimates of the volumes is largest for the path configurations associated with the Quantico site (D_{11} and D_{16}, see table 1.). A quantitative comparison of these values results in less than 1 dB difference in the calculated value of the K factors for the Quantico paths. Thus it is concluded that the approximation of the volumes as computed from the cylindrical geometry of (5) is adequate.

For the purposes of this experiment, equations (15) and (16) may be used in either of two ways to evaluate the measurements.

Table 1. Path Constants for Equations (15) and (16)

Site & Path	f	K_s dB	K_x dB
Quantico (TS-1)			
D_{11}	f_1	-124.8	
E_{11}	f_1	-124.7	
D_{16}	f_6		-118.6
E_{16}	f_6		-118.4
Norfolk (TS-2)			
C_{22}	f_2	-112.5	
Ft. Lee (TS-3)			
C_{33}	f_3	-124.1	
D_{33}	f_3	-124.2	
C_{37}	f_7		-119.5
D_{37}	f_7		-119.6
Eastville (TS-4)			
B_{45}	f_5	-123.0	
C_{45}	f_5	-123.0	
D_{44}	f_4	-125.8	
E_{45}	f_5	-123.1	
B_{48}	f_8		-118.4
C_{48}	f_8		-118.4
E_{48}	f_8		-118.4

Path Designators:

a. The letter designates the propagation path or elevation of the common volume intersection as

A = great circle path,
B = 5,000 ft common volume,
C = 10,000 ft common volume,
D = 20,000 ft common volume,
E = 30,000 ft common volume, and
F = Off path.

b. The subscripts are as C_{mn}, where

m = transmitter site (TS) number as
1 = Quantico,
2 = Norfolk,
3 = Ft. Lee,
4 = Eastville, and
n = frequency number as
1, 2, 3, 4, 5 - S-band
6, 7, 8 - X-band

First, the measured interference power at the receiver for any bistatic path can be used directly to compute an effective rain-rate (R_e) at the common volume associated with that path. Second, the measured rain-rate at the surface of the earth (R_s) may be used to compute the expected scatter power if the surface rate corresponds to the actual rate in the common volume. Both of these techniques are used in the analysis of data (section 5), but not in real or chronological time. For example, it is not anticipated that the calculated values of R_e will correlate closely in real time with the measured values of R_s, as the time correlation between these parameters with respect to any particular surface rain gauge instrument will generally be destroyed by the non-homogeneous nature of storms, and by wind shears which occur during a storm. It is expected, however, that if the values of R_s and received power P_r reordered from chronological time to a rank ordering of magnitude values over a reasonably long period, agreement will be found between the statistics of the two measured values.

In addition, there must be a height dependence associated with an interchangeability between surface rain-rate measurements and effective rain-rates or reflectivity measured from common volumes aloft. For example, if the antenna beams intersect 30,000 ft above the surface, very little rain in the scatter volume is expected [CCIR 1971]. The fixed-beam experiment described here is not designed to determine this height dependence in any precise sense. To do so would require a tremendous amount of additional data to be recorded directly from the common volume, as in the case of the precision radar used by Crane [1970a]. The results of the fixed-beam experiment will indicate however, some empirical height dependence for the particular region of the experiment, for common volumes up to 30,000 ft. It is expected that height dependence models will be developed from future experimental and analytical work that is being carried out by Crane [1970a], Austin [1971], and Altman [1970]; one promising model has been proposed recently by Dutton and Dougherty [1973].

2.2 Sensitivity of the Experiment

The maximum sensitivity of the experiment for the parameters of interest can be estimated from equations (15) and (16), using the values of K_s and K_x in table 1 and known characteristics of the receiver. For example, the minimum detectable signals at the receiver were approximately

$$P_r(\min)_s = -130 \text{ dBm}$$

$$P_r(\min)_x = -125 \text{ dBm}$$

for all of the S- and X-band channels, respectively. These values can be used as the minimum received power level in equations (15) and/or (16), and thus provide an estimate of the minimum detectable rain rate. Solving either (15) or (16) for R_v, we find, for the minimum effective rain-rate $R_e(\min)$,

$$R_e(\min) = \log^{-1} \frac{P_{r(\min)} - K}{16} . \tag{17}$$

In addition, equations (4) and (11) may be used to compute the minimum detectable values of $\bar{\eta}$ and Z, respectively. The values of these parameters for the range of antenna/path configurations of table 1 are presented in table 2. Note that the values are based upon the assumption that each common volume intersection is completely filled by precipitation.

Table 2. Sensitivity Values of the Experiment

System & Path	R_e (min) mm/hr	Z (min) mm^6/m^3	$\bar{\eta}$ (min) m^{-1}
S-band			
D_{11}	0.47	58.8	3.76×10^{-10}
E_{11}	0.47	58.8	3.76×10^{-10}
C_{22}	0.08	3.6	2.32×10^{-11}
C_{33}	0.43	51.3	3.27×10^{-10}
D_{33}	0.43	52.5	3.35×10^{-10}
B_{45}	0.37	39.8	2.54×10^{-10}
C_{45}	0.37	39.8	2.54×10^{-10}
D_{44}	0.55	75.8	4.84×10^{-10}
E_{45}	0.37	40.7	2.60×10^{-10}
X-band			
D_{16}	0.40	45.7	6.03×10^{-9}
E_{16}	0.39	43.6	5.75×10^{-9}
C_{37}	0.45	56.2	7.42×10^{-9}
D_{37}	0.46	57.5	7.59×10^{-9}
B_{48}	0.39	43.6	5.75×10^{-9}
C_{48}	0.39	43.6	5.75×10^{-9}
E_{48}	0.09	4.1	5.42×10^{-10}

2.3 Statistical Nature of the Experiment

As stated previously, it is not feasible to measure the precipitation reflectivity directly in all system configurations that must be coordinated to prevent detrimental rain-scatter interference. Thus, it is necessary to develop a model based upon a more common data source, such as a meteorological parameter that is measured generally on a world-wide basis. The readily available data are primarily surface rain measurements.

The Virginia experiment was designed to collect data for a sufficient period of time to obtain a reliable statistical base, and to "catch" some relatively rare rainfall events in the experimental network. A minimum base of either rainfall or radio transmission loss statistics is estimated to require operation of the experiment for a period of at least one full year. Observation of the rare rainfall events, which consist of high rainfall rates that occur on the order of 1 to 5 minutes out of a year, appears to offer a serious challenge. However, the task is perhaps not as difficult as it seems because of the physical nature of very high rainfall rates.

A year, which would be a totally inadequate sampling period for catching an extreme value of 24-hour rainfall, may be a minimum reasonable period for catching near-extreme one-minute rainfall rates, as the highest one-minute rate might be expected to fall within a year. The reason lies in the saturation effect at very high rainfall rates; i.e., there is a physical limit to the rainfall rate that may exist for very short periods of time. For example, the highest value of Z that has been reliably measured with calibrated weather radars is about 10^7 mm^6/mm^3 [Donaldson, 1961]; this presumably represents a near-instantaneous value. Assuming that this measurement is due to rain (more likely it was due to hail [Rinehart et al., 1968]), the implied

rainfall rate is on the order of 1000 mm/hr. The world record one-minute rainfall rate was for some time thought to be 1.23 inches (or 1800 mm/hr) recorded at Unionville, Maryland, in 1956 [Critchfield, 1960], but this record was apparently caused by sticking of the rain gauge in use there [Private comm. R. K. Crane, 1970]. Credible one-minute records are on the order of 0.65 to 0.69 in., and correspond to rainfall rates of roughly 1000 mm/hr. These records represent the peak rainfall rates culled from hundreds of operational rain gauges throughout the world over a period of time of 50 years or more (one such record dates back to 1911).

The rainfall rage statistical model of Rice and Holmberg [1972] indicates that for the Virginia area, or for Norfolk in particular, the number of hours of rainy minutes, T(R), at rates exceeding any sufficiently high rate, R, is

$$T(R) = T_1 \exp(-0.03R) \text{ hours}, \qquad (18)$$

where $60\,T(0) = 437$ is the number of rainy minutes per year of Mode 1 (heavy, convective) rain. From (18), the rain-rate for the rainiest minute per average year is 204 mm/hr; for a 30-year period the rainiest minute should be 318 mm/hr, whereas the return period for a rate of 1000 mm/hr is on the order of 2×10^9 years at a median location.

On the other hand, during the period from 24 September through 31 January, the 10,000-ft subpoint rain gauge in the Virginia experiment registered 1.5 minutes of data with a rain-rate on the order of 100 mm/hr, and 7 seconds of rain at the rate of about 120 mm/hr. Based on experience to this date, it seemed entirely reasonable to assume that, during the balance of the first full year of operation, one-minute rain-rates on the order of 200 mm/hr would be measured. A one-minute rate of approximately 150 mm/hr was measured at the

Poquoson tower site during August 1970, before the experiment was operational. The effect of an increase in rain-rate on the received power via rain scatter can be estimated by using an equation of the form of (11) as

$$Z = aR^b. \tag{19}$$

The coefficient a is relatively unimportant in estimating the effect of increases in R, but the value of the exponent b is crucial. For example, assuming a typical value of b to be 1.5, the effect of changing R from 200 to 1000 mm/hr will be to increase Z, and thus the received power, by about 11 dB.

The accuracy with which we can estimate the effects of the extreme values of R on radio systems depends on how accurately we can extrapolate from $R \approx 200$ mm/hr to $R \approx 1000$ mm/hr (or less). Again, assuming a in (19) to be relatively stable as a function of R and assigning the error in the extrapolation process to errors in the assumed value of b at very high R, an absolute error of 0.25 (17%) in b, (i.e., b = 1.75 or 1.25 when 1.5 was actually used) results in an error of only 1.75 dB in the calculated value of Z or transmission loss at $R \approx 1000$ mm/hr. More realistically, extrapolating from R = 150 mm/hr (assuming 200 mm/hr is not recorded) to R = 330 mm/hr (a 4.8-dB increase in received power) to construct a 30-year distribution would involve an error under these assumptions of only 0.8 dB. The longer the Virginia experiment is operative the more likely is the probability of capturing the rare events (high rain-rates) and hence reducing the extrapolation errors.

2.4 Path Loss Calculations

It is instructive to consider the fixed-beam experiment as an actual example of a satellite-terrestrial communication systems problem, in which the two services share a common frequency band.

When frequency assignments are made on a coequal basis to these services, site locations must be coordinated in such a way that no intolerable mutual interference will result. The site separations are then determined on the basis of a "coordination distance" which will meet the established criteria.

Procedures for calculating coordination distances are established internationally by Recommendation 1A, Final Acts of the Extraordinary Conference to Allocate Frequency Bands for Space Communication Purposes (EARC) [EARC, 1963]. Report 382 of the CCIR [CCIR, 1966a] and various documents of the XIIth CCIR Plenary, New Delhi, [CCIR, 1970] recommend modifications to these procedures, and FCC Regulation 25 [FCC, 1966] establishes somewhat modified procedures for the U.S. The EARC Recommendation 1A establishes -145 dBW as the maximum permissible unwanted signal level at the input to an earth station receiver from any single terrestrial station (TS) transmitter with an output equal to P_{TS} dBW and an antenna gain (minus feeder loss) equal to G_{TS} dB relative to an isotropic antenna. Coordination distances are calculated in terms of these quantities, the maximum earth station (ES) antenna gain (minus feeder loss) G_{ES} at each azimuth and an earth station site shielding factor F_s, where applicable. This recommendation also establishes the minimum permissible sum of basic transmission loss and site shielding factor, $L_b + F_s$, as

$$L_b + F_s = P_{TS} + G_{TS} + G_{ES} + 145 \text{ dB}, \qquad (20)$$

for 4 GHz.

Allowable site shielding factors, F_s, are listed in Report 382 [CCIR, 1966a] as a function of the minimum angle of elevation of a horizon obstacle as seen from the earth station for each applicable azimuth. In current radio regulations, the maximum value of F_s is now 15 dB.

In CCIR Report 382 [CCIR, 1966a], it is proposed that the maximum value of F_s should be 25 dB*. A maximum allowable value, $P_{TS}+G_{TS} = 42$ dBW in the overlapping portions of cochannel bandwidth assignments between a terrestrial station and an earth station, is proposed by the CCIR.

Coordination distances at 4 GHz to the simulated earth station at Langley in the directions of Quantico, Norfolk, Fort Lee, and Eastville, respectively, are based on the relative gain of the earth station in the direction of these terrestrial sites, and assume an effective isotropic radiated power (EIRP) of 42 dBW at a hypothetical terrestrial station. Using the methods outlined in Recommendation 1A of the EARC, the coordination distances to the Langley earth station are shown in table 3.

It is necessary to add a correction factor to L_b when coordination distances at 8 GHz are considered. These correction factors appear in the Recommendation 1A of the EARC [1963] and were used to calculate the coordination distances at 8 GHz, which are also given in table 3.

All values used in calculating the coordination distances were derived from the propagation curves for Zone A as given in the Final Acts of EARC mentioned above. The curves apply to both 4 and 8 GHz using the correction factors given for the higher frequency. The receiving antenna gain was derived from a curve especially fitted to the actual antenna pattern measurement [Rice et al., 1970].

It will be noted that all transmitter-receiver combinations in the Virginia experiment are within the calculated coordination distance; therefore, it would be necessary to consider the probability of interference

---

*Note: Recommendations from the International Working Group Meeting at Geneva, February 1971, indicate values up to 50 dB may be achieved.

before frequency assignments for such stations could be considered. A comparison between the calculated coordination distances and the actual great circle (GC) path distances is shown in table 3.

Table 3. Comparison of Coordination and Actual Distances

Transmitter Site (TS)	Great Circle Distance from ES (km)	Calculated Coordination Distance (km)	
		4 GHz	8 GHz
Quantico (TS-1)	178.86	200	160
Norfolk (TS-2)	16.73	117	100
Ft. Lee (TS-3)	85.20	120	100
Eastville (TS-4)	50.67	125	100

For each of the transmitter-receiver combinations, it is also desirable to know the expected path loss characteristics which would produce a side-lobe-coupled unwanted signal. Each antenna at the transmitter sites will have a different gain in the direction of the receiver site and the receiving antenna will have different gains in each of the four directions to the transmitter sites. The specific antenna gains were obtained by the curve-fitting procedure outlined by Rice et al. [1970]. The relative antenna gains were obtained by considering the three-dimensional antenna pointing and great-circle path configurations. The difference between the vertical and horizontal polarization gains of the antennas was also considered. A computer program was used to calculate the relative gain factors along each great circle path, employing the derived antenna curves mentioned above.

The expected path loss for the different sites under the climatological conditions of Virginia was calculated using the ITS tropospheric prediction methods [Longley and Rice, 1968]. A prediction for each of the great circle paths was derived, based on these methods.

Using the above basic transmission loss models, antenna gain patterns, a power input to the antenna of 10 watts, and an estimated feeder line loss of 3 dB, the expected signal strength at the receiver for each of the antennas at the four transmitter sites was calculated using the relation

$$P_{ES} = P_{TS} + G_{TS} + G_{ES} - L_b, \tag{21}$$

where L_b is the path loss exceeded 99.9% of the time. The results are tabulated in table 4 for conditions of no site shielding.

The tabulated signal levels are expected to be exceeded not more than 0.1 percent of the time, with a probability of 0.5. Since the receiver noise threshold was -130 dBm for the S-band and -125 dBm for the X-band channels, it can be seen that the expected signal for 0.1 percent of the time thus exceeds the threshold level on all of the great-circle paths where the full gain of the transmitter antenna is realized. Also the off-path and 10,000 ft paths at both frequencies at Norfolk are seen to provide side-lobe interference via tropospheric propagation. The Quantico antenna pointed at the 20,000 ft intersection may also provide an interference signal about 0.1 percent of the time.

Similarly one can calculate the transmission loss for which the expected signal will be equal to the receiver sensitivity from the relation

$$L_b(\text{Min. Sig.}) = P_{TS} - \text{Receiver Threshold} + G_{TR} + G_{ES}. \tag{22}$$

Table 4. Calculated Values of Path Loss
Side-lobe to Main-lobe Coupling--Tropo. Scatter

Transmitter Site	Freq.	Path	Common Volume (ft)	Received Power (0.1%) (dBm)	% Time Rec. Sig. Exceeds Threshold
Quantico (TS-1)	f_1	A_{11}	GC	-111.7	6.0
		D_{11}	20 k	-124.7	0.11
		E_{11}	30 k	-135.3	< 0.01
		F_{11}	Off Path	-136.5	< 0.01
	f_6	A_{16}	GC	-120.8	0.5
		D_{16}	20 k	-144.5	< 0.01
		E_{16}	30 k	-145.2	< 0.01
Norfolk (TS-2)	f_2	C_{22}	10 k	-114.3	32.0
		F_{22}	Off Path	-107.3	97.0
Ft. Lee (TS-3)	f_3	A_{33}	GC	-115.9	1.4
		C_{33}	10 k	-148.1	< 0.01
		D_{33}	20 k	-157.3	< 0.01
	f_7	A_{37}	GC	-124.3	0.15
		C_{37}	10 k	-155.3	< 0.01
		D_{37}	20 k	-164.5	< 0.01
Eastville (TS-4)	f_4	A_{44}	GC	-106.9	10.0
		D_{44}	20 k	-154.3	< 0.01
	f_5	B_{45}	5 k	-138.8	< 0.01
		C_{45}	10 k	-146.9	< 0.01
		E_{45}	30 k	-157.8	< 0.01
	f_8	A_{48}	GC	-121.4	0.3
		B_{48}	5 k	-152.1	< 0.01
		C_{48}	10 k	-160.2	< 0.01
		E_{48}	30 k	-171.1	< 0.01

The percentage of time that the signal should exceed the receiver threshold for the calculated path loss can be read from the transmission probability curve for the respective paths. This percentage of time is given in the final column of table 4. These estimates show that the Eastville and Quantico great-circle paths at the lower frequency and the Norfolk paths should experience signals above threshold for significant periods during a typical year. These calculations utilize

the antenna patterns as smoothed by the curve-fitting technique; consequently, the actual results may show some significant deviations from these calculated results, based on the actual sidelobe patterns that existed. Also, the effect of terrain shielding has not been accounted for in these calculations. Data obtained from the great-circle measurements noted previously can be compared with the predictions in table 4.

3. EXPERIMENT CONFIGURATION

The geographic locations of the simulated* earth station (ES) and terrestrial stations (TS) are shown on the pictorial map of figure 1. A 30-ft receiving antenna was used at the simulated ES and was aligned along a great circle path toward Quantico (TS-1) at a fixed elevation angle of 13° 30'. Transmitting antennas at the four simulated terrestrial microwave radio relay stations were aligned to provide four common volume intersection points, at elevations along the receiver main beam of 5,000, 10,000, 20,000, and 30,000 ft. At Norfolk and Quantico an antenna was pointed "off-path" to provide the effect of a transmitter antenna main beam not intersecting but passing near the receiver antenna main beam. At the three forward stations, Quantico, Ft. Lee, and Eastville, a transmitter antenna was aligned along a great circle path toward the ES to provide a reference tropospheric propagation path loss measurement.

The experiment was designed around eight continuously recording receiver channels each with a nominal 2 kHz bandwidth. There were five

*The term "simulated" here is intended to imply antenna gain, sensitivity, etc., and not geometrical alignment or configuration of a typical satellite-terrestrial sharing system.

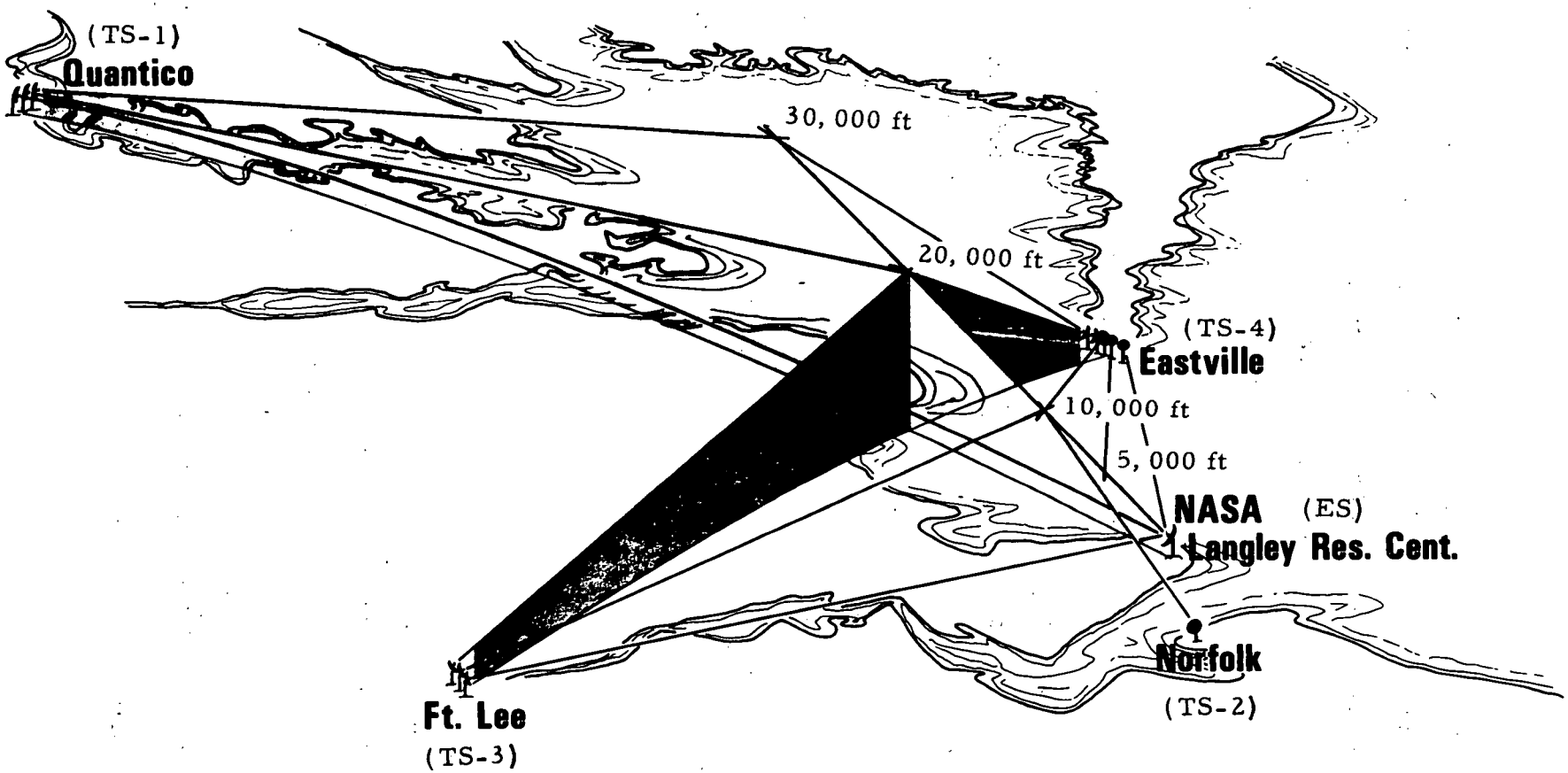

Figure 1. Configuration of the RIPP fixed-beam experiment.

lower frequency channels separated by 72 kHz, nominally at 3.672 GHz. The three high frequency channels were nominally 7.834 GHz, separated by 153.6 kHz.

Sixteen transmitting antenna beams (nine at S-band frequencies and seven at the X-band) located at the four simulated TS were aligned to intersect the ES main beam at the common volume altitudes listed above. The receiver antenna was equipped with a wideband feed system designed to receive both the S- and X-band signals, and was aligned with its main beam centered in the great circle plane passing through Langley and Quantico. Table 5 is a complete listing of all fixed-beam facilities showing location, site designation, transmitter frequencies, antenna code, antenna purpose, and antenna pointing angle. Table 6 lists the common volumes as computed by the conical method noted previously and presents all of the range parameters to the common volume locations, the scattering angle involved at the beam intersections, the antenna gains relative to isotropic, and the nominal line losses associated with each transmitter antenna. Line losses at the receiver are not tabulated as they were calibrated out of the system using the calibration technique described later. The listed parameters include all of those necessary to compute the K factors in table 1. The path designations used throughout this report are those of table 1.

Table 5. Fixed Beam Antenna Orientations

Location	Site	Frequency, Hz	Antenna	Purpose	Azimuth	Elevation
Quantico	TS-1	f_1, 3,671,928,000	A_{11}	G.C. to ES	152° 13.4'	0° 18'
			E_{11}	30 k ft.	152° 13.4'	3° 15.8'
			F_{11}	Off path	148° 13.4'	0° 18'
			D_{11}	20 k ft.	152° 13.4'	1° 46.9'
		f_6, 7,833,600,000	A_{16}	G.C. to ES	152° 13.4'	0° 18'
			E_{16}	30 k	152° 13.4'	3° 15.8'
			D_{16}	20 k	152° 13.4'	1° 46.9'
Norfolk	TS-2	f_2, 3,672,000,000	C_{22}	10 k	337° 17.8'	5° 47.5'
			F_{22}	Off path	344° 43.4'	0° 48'
Ft., Lee	TS-3	f_3, 3,672, 072,000	A_{33}	G.C. to ES	101° 6.6'	0° 48'
			C_{33}	10 k	93° 43.2'	1° 58.9'
			D_{33}	20 k	84° 58.5'	4° 35.9'
		f_7, 7,833, 753,600	A_{37}	G.C. to ES	101° 8.3'	0° 48'
			C_{37}	10 k	93° 43.2'	1° 58.9'
			D_{37}	20 k	84° 58.5'	4° 35.9'
Eastville	TS-4	f_4, 3,671,856,000	A_{44}	G.C. to ES	237° 58.5'	0° 48'
			D_{44}	20 k	265° 50.2'	6° 10.8'
		f_5, 3,672,144,000	E_{45}	30 k	276° 59.0'	8° 21.5'
			C_{45}	10 k	252° 28.1'	3° 14.8'
			B_{45}	5 k	245° 14.3'	1° 34.1'
		f_8, 7,833,446,400	A_{48}	G.C. to ES	237° 58.5'	0° 48'
			E_{48}	30 k	276° 59.0'	8° 21.5'
			C_{48}	10 k	252° 28.1'	3° 14.8'
			B_{48}	5 k	245° 14.3'	1° 34.1'
Langley	ES		Fixed Beam		332° 47.9'	13° 14.8'

Table 6. Experiment Configuration Parameters

SITE	PATH	f	h_v^* (ft)	L_t (dB)	θ (Degrees)	α_r (Rads.)	R_r (km)	α_t (Rads.)	R_t (km)	G_r (dB)	G_t (dB)	V $(km)^3$
Quantico (TS-1)	D_{11}	f_1	20 k	6.1	15.4	.0112	26.4	.0332	153.4	47.5	38.8	1.096
	E_{11}	f_1	30 k	6.1	16.3	.0112	39.5	.0332	140.9			2.062
	D_{16}	f_6	20 k	4.2	15.4	.0051	26.4	.0258	153.4	50.8	41.0	.2158
	E_{16}	f_6	30 k	4.2	16.3	.0051	39.5	.0258	140.9			.4075
Norfolk (TS-2)	C_{22}	f_2	10 k	3.4	8.8	.0112	13.2	.0332	29.7	47.5	38.8	.1118
Ft. Lee (TS-3)	C_{33}	f_3	10 k	3.4	57.0	.0112	13.2	.0332	77.8	47.5	38.8	.0465
	D_{33}	f_3	20 k	3.4	68.0	.0112	26.4	.0332	72.2			.1544
	C_{37}	f_7	10 k	3.1	57.0	.0051	13.2	.0258	77.8	50.8	41.0	.0092
	D_{37}	f_7	20 k	3.1	68.0	.0051	26.4	.0258	72.2			.0307
Eastville (TS-4)	B_{45}	f_5	5 k	3.4	88.0	.0112	6.6	.0332	50.5			.0064
	C_{45}	f_5	10 k	3.4	81.0	.0112	13.2	.0332	51.2	47.5	38.8	.0267
	D_{44}	f_4	20 k	6.1	67.0	.0112	26.4	.0332	55.1			.1224
	E_{45}	f_5	30 k	3.4	56.0	.0112	39.5	.0332	61.5			.3394
	B_{48}	f_8	5 k	3.1	88.0	.0051	6.6	.0258	50.5			.0013
	C_{48}	f_8	10 k	3.1	81.0	.0051	13.2	.0258	51.2	50.8	41.0	.0053
	E_{48}	f_8	30 k	3.1	56.0	.0051	39.5	.0258	61.5			.0677

*h_v = elevation of common volume. Other symbols are defined in section 2.1.

The transmissions from each transmitter site were received at the ES through separate receiver channels, and thus, clear identification of the source of each signal can be achieved. The low and high frequency antennas at each transmitter site were fixed in position, as indicated earlier, to point to specific locations. The transmission frequencies were switched at one-minute intervals in an established and fixed sequence, and were monitored and synchronized from the receiver site by means of a dedicated telephone line telemetry system. The transmitted power at all frequencies was held constant at a level of 40 dBm (± 0.2 dB) by means of an electronic control system at each transmitter. The receiver channels were calibrated automatically at two-hour intervals by introducing a known signal level through a precision attenuator and a directional coupler mounted directly behind the antenna feed horn. This calibration covered a 60-dB dynamic range in steps of 10 dB. This wide dynamic range was achieved through the use of logarithmic compression circuits in the IF stages of the receiver.

The output of the eight receiver channels was recorded on both analog magnetic tape and a strip chart recorder. In addition to the received signal levels, the recorders were encoded with a time signal which permitted the referencing of all data to local time as well as the decoding of the one-minute transmitter sequence intervals. The strip chart was used for visual monitoring of the experiment in real time, for annotating the data in real time, and for back-up to the magnetic tape as an archival data record.

The one-minute antenna switching sequence was performed in a four-minute timing cycle, which permitted the monitoring of a total of 32 path combinations with the eight frequencies involved. Four of these combinations represent a minute during which a transmitter was switched to a dummy load and only the receiver noise level was recorded. This provided a means of monitoring the long term receiver performance during the experiment. Two off-path signals, one each from Quantico (F_{11}) and Norfolk (F_{22}), and six great circle paths (A_{11}, A_{16}, A_{33}, A_{37}, A_{44}, and A_{48}) were monitored. The remainder of the available time-frequency combinations were used to monitor and record the sixteen paths derived from TS common volume intersections with the ES main beam. Some of these 32 combinations (C_{22}, F_{22}, A_{44} and D_{44}) were sampled for two minutes in every four-minute cycle. The complete matrix of the time-frequency switching system is shown in table 7.

An overall block-diagram of the fixed-beam experiment is shown in figure 2, in which only one of the four terrestrial transmitting sites is indicated. These sites were all configured in a similar fashion, the basic difference being the number of transmitters located at any one site. The latter may be seen from table 5.

Signals that were directed over the great-circle paths in the configuration noted above were received in the side-lobes of the ES receiving antenna whenever propagation conditions permitted this form of interference. In order to provide a reference for this interference mechanism, a second great-circle path receiver system was installed. Three horn type antennas were located at the ES receiving site, directed toward the three forward TS sites at Fort Lee, Quantico, and Eastville.

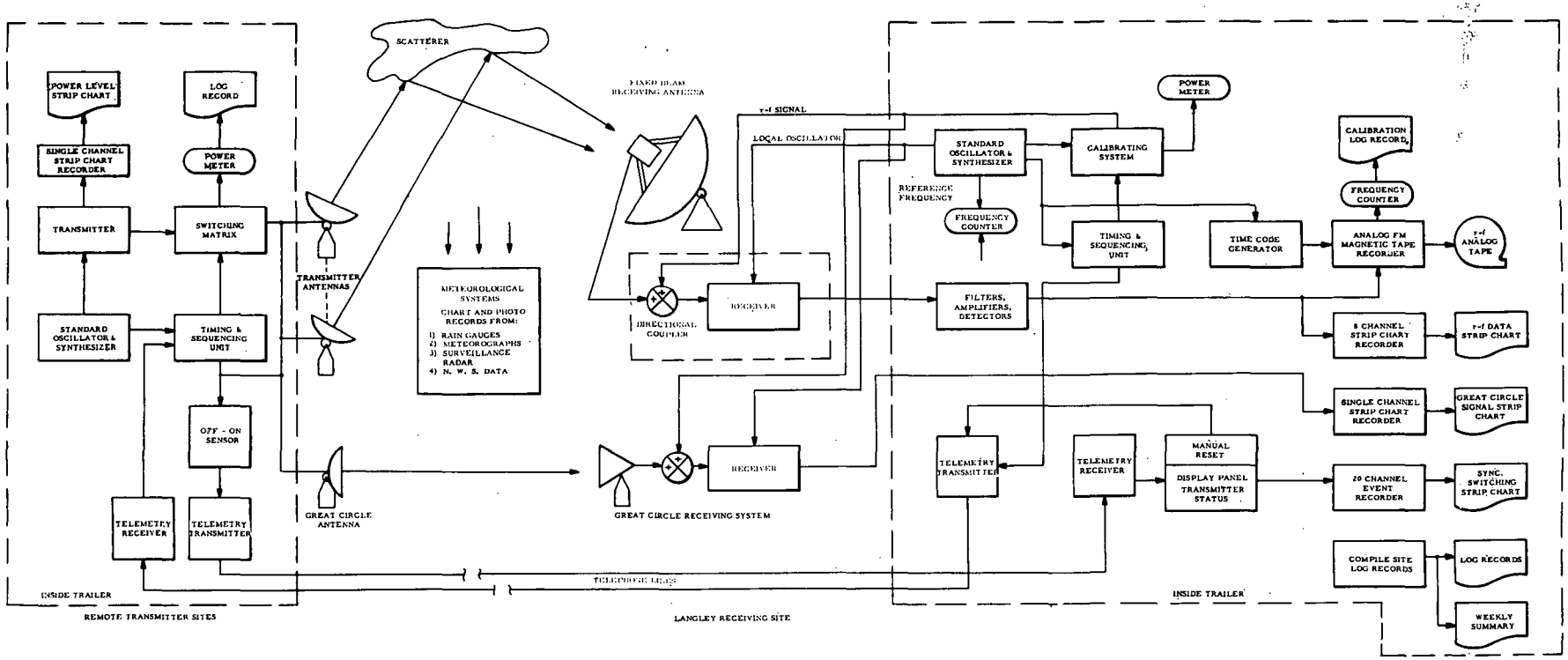

Figure 2. Block diagram of the RIPP fixed-beam experiment.

Table 7. Antenna/Path Switching Sequence

Transmitter Location & Site No.	Frequency / Time	Antenna/Path Sequence			
		Time Block			
		1	2	3	4
Quantico TS-1	f_1	A_{11}	E_{11}	F_{11}	D_{11}
	f_6	A_{16}	E_{16}	off	D_{16}
Norfolk TS-2	f_2	C_{22}	F_{22}	C_{22}	F_{22}
Fort Lee TS-3	f_3	A_{33}	off	C_{33}	D_{33}
	f_7	A_{37}	off	C_{37}	D_{37}
Eastville TS-4	f_4	A_{44}	A_{44}	D_{44}	D_{44}
	f_5	off	E_{45}	C_{45}	B_{45}
	f_8	A_{48}	E_{48}	C_{48}	B_{48}

Data were recorded over the same four-minute cycle (one minute for each path and one minute off) on an independent strip chart recorder. This system is also noted in the diagram of figure 2.

A summary of the facilities and parameters associated with the transmit and ES receiver sites are presented, respectively, in tables 8 and 9. Characteristics of the great-circle receiving system are shown in table 9. Specific data concerning the transmitting and receiving systems are presented in tables 10 and 11.

The experiment also included a rather comprehensive system of meteorological instrumentation indicated in a separate block of figure 2. Instruments to measure pressure, temperature, and relative

Table 8. Transmitting Site Summary

TRANSMITTER SYSTEM	X-BAND	S-BAND
Antenna Gains	41.0 dB	38.8 dB
Antenna Pointing Accuracy	± 15'	± 15'
Transmitter Output Power	10 Watts	10 Watts
Output Power Stability	±0.2 dB/wk	±0.2 dB/wk
Frequency (nominal)	7.834 GHz	3.672 GHz
Frequency Stability	5×10^{-10}/day	5×10^{-10}/day
TRANSMIT SITE	NUMBER OF ANTENNAS	
	6-FOOT DIA.	10-FOOT DIA.
A) Eastville (TS-4)	4	5
B) Ft. Lee (TS-3)	3	3
C) Quantico (TS-1)	3	4
D) Norfolk (TS-2)	0	2

Table 9. ES Receiving Site Summary

CW SYSTEM	X-BAND	S-BAND
Antenna Gain	50.8 dB	47.5 dB
Beamwidth	0.4^{o}	0.6^{o}
Receiver Noise Figure	7.5dB	8 dB
Receiver Gain Stability	± 1 dB	± 1 dB
Frequency Stability	5×10^{-10} / day	5×10^{-10} / day
GREAT CIRCLE SYSTEM		
Antenna Gain	19.2 dB	
Receiver Noise Figure	7.5 dB	
Receiver Gain Stability	± 1 dB	
Frequency Stability	5×10^{-10} per day	
RADAR SYSTEM (VERLORT)		
Antenna Gain	Nominal 35 dB	
Frequency	2850 MHz	
Peak Output Power	200 kW	
Range	125 nm	
TELEMETRY		
4 leased land lines, voice grade		

Table 10. CW Transmitting System Summary

	Frequency			
Antenna	3.672 GHz		7.834 GHz	
Diameter	10 ft		6 ft	
Gain (above isotropic)	38.8 dBi		41.0 dBi	
Beamwidth	1.8°		1.5°	
Sidelobes	-22 dB		-21 dB	
Transmission Line	50 ft	3.4 dB	50 ft	3.1 dB
Loss	100 ft	6.1 dB	100 ft	4.2 dB
TWT Amplifier				
Power Output	10 watts		10 watts	
Gain (minimum)	35 dB		35 dB	
Microwave Source				
Maximum Power Output	+ 16 dBm		+ 10 dBm	
Frequency Stability	5×10^{-10} per day		5×10^{-10} per day	
RF Switches				
VSWR	< 1.2		< 1.2	
Power Rating	10 watts		10 watts	
Life	$> 10^6$ switches		$> 10^6$ switches	
Power Meter				
Accuracy	± 0.05 dB		± 0.05 dBm	
Stability (on 5 dBm scale used)	± 0.2 dB		± 0.2 dB	

Table 11. CW Receiving System Summary

	Frequency	
Antenna - 30 ft. Parab.	3.672 GHz	7.834 GHz
Gain	47.5 dB	50.8 dB
Beamwidth	0.6°	0.4°
Sidelobes	-21 dB	-18 dB
Directional Coupler Loss	0.2 dB (max)	0.2 dB (max)
Diplexer Loss	0.5 dB	0.4 dB
Image Noise	3.0 dB	3.0 dB
Tunnel Diode Amplifier		
Noise Figure	4.9 dB	4.4 dB
Gain	20 dB	20 dB
Bandwidth	≈400 MHz	≈400 MHz
Local Oscillator		
Frequency stability	5×10^{-10} per day	5×10^{-10} per day
Injection Power	+ 7 dBm	+ 7 dBm
Mixer-Amplifier		
Noise Figure	7.5 dB	8.0 dB
Gain (RF-IF)	32 dB	32 dB
Bandwidth	3 MHz	3 MHz
IF Center Frequency	10 MHz	10 MHz
IF Amplifier		
Frequency Response	0.25 to 150 MHz	
Gain	20 dB	
Output (Full Gain)	1 V p-p (50 ohms) at 1 dB gain compression	
Filter, Crystal		
Pass band ripple	± 1.5 dB	
Isolation	70 dB	
Bandwidth (3 dB)	2 kHz	
Logarithmic IF Amplifiers		
Center Frequency	10 MHz	
Bandwidth	3 MHz	
Dynamic Range	80 dB	
Log Accuracy	± 1 dB over 60 dB	
	± 2 dB over 80 dB	
Outputs	Video, d-c coupled	
	IF, limited	

humidity were placed at the three forward transmitting sites and at a meteorological site (Poquoson tower) near the ES. These meteorograph instruments recorded continuously, and were checked, calibrated, and had their recording charts replaced at weekly intervals. Tipping bucket rain gauge instruments were located under each of the common volume intersection points and at the ES meteorological site. These instruments also recorded continuously and were calibrated to indicate the accumulation of each 0.01-inch of rain at rain-rates up to 7 inches per hour (177.8 mm/hr). The rain gauges were capable of operating up to 45 days on a single chart record.

This meteorological data collection system was augmented by radiosonde data taken twice daily at four locations surrounding the test site; namely, Wallops Island, Dulles Airport (near Washington, D.C.), Cape Hatteras, and Greensboro, North Carolina. Monthly weather summaries were also collected from Weather Bureau stations in the area.

A primary augmentation of the above surface meteorology data and the radiosonde measurements was provided by an S-band surveillance radar located at the ES receiving site. This Very Long Range Tracker (VERLORT) radar was dedicated full time to the experiment and was equipped with both PPI and RHI displays which were photographed to provide sequential records of the progress of a storm. A complete summary of all the subsystems in the meteorological configuration is presented in table 12. These data were collected for synoptic weather descriptions and for detailed application in properly identifying propagation conditions and particular interference mechanisms.

Table 12. Meteorological Subsystems

Subsystem	No.	Location	Data	Accuracy	Calibration	Maintenance
Rain Gauges	5	Poquoson and common volume sub-points	Rain Rate	± 1/2% to 20%	Bi-Monthly	Weekly
Meteorograph	4	Poquoson, Ft. Lee, Eastville & Quantico	Temp.	± 1°F	Weekly	Weekly
			Rel. Hum.	± 1% to 3%		
			Pressure	± 0.01"		
Surveillance Radar (Verlort)	1	Langley	Qual. Refl. (Rain) on PPI & RHI	Qualitative	As Req'd	As Req'd
Nat'l WX Service Data	Fax Wx Maps, Radar Maps, Radar Photos Fax & Film, Rawinsonde Data by TTY & Fax Recorder Charts, Local WX Data Incl. Rain Gauge Data.					

4. DATA PROCESSING AND REDUCTION PROCEDURES

An overall data flow diagram for the Virginia fixed-beam experiment is shown in figure 3, which serves to illustrate the interface between meteorological and radio data as well as the detailed interference analysis procedure outlined in this section. All of the data records were collected at the Langley experiment sites and returned to the Institute for Telecommunication Sciences in Boulder, Colorado, for processing. Data were recorded in several different ways as indicated in figure 3. The basic radio interference data were recorded on analog magnetic tape, and the rain-rate (R) record was a paper chart that was driven by a mechanical clock on each rain gauge instrument.

A great deal of preliminary editing was applied to these data before further processing took place. For example, a strip chart recording of all the radio signals was made at the Langley ES in parallel with the

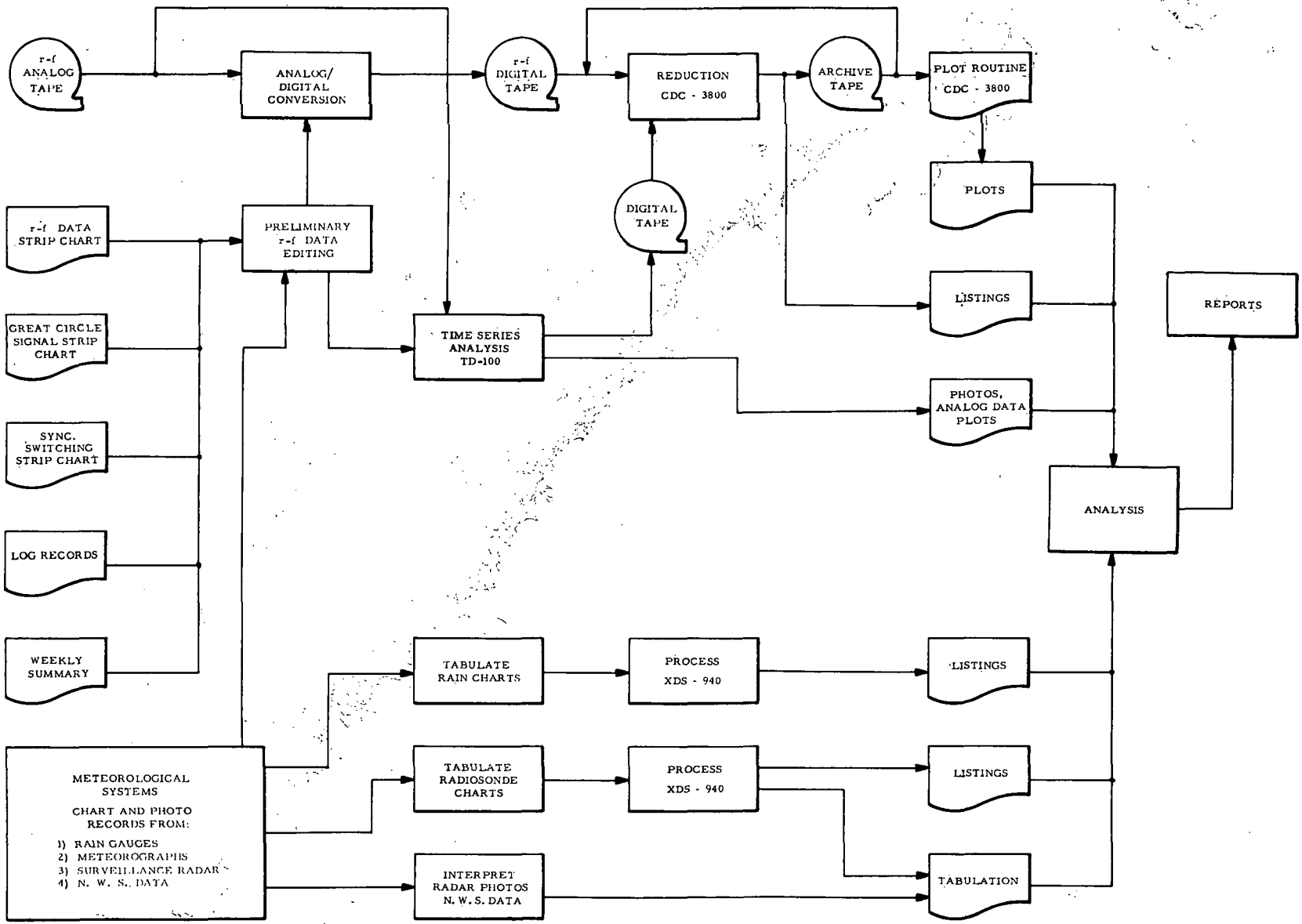

Figure 3. Data processing and analysis flow diagram.

magnetic tape recording. These charts as well as the rain gauge records were first visually scanned to determine periods of significant events. The latter may be periods in which radio signals were received either in the presence or absence of precipitation, measured precipitation within the configuration of the experiment, or any other significant weather or meteorological observation that could have an effect on the propagation mechanisms of interest. The times of occurrence and duration of these events were logged, and a listing of the data collected in both the radio and the meteorological systems was made. Each event period was compared with daily station-log reports and weekly system summary reports to determine the validity and accuracy of the data. For example, it was necessary to determine if all of the radio channels were in operation during the event, and if not, the outage time noted for each frequency. Also, each event period was given an initial classification such as "heavy convective rain," or as a period of "non-precipitation." In the latter case, the meteorological data were scanned for evidence of the presence of atmospheric layers or other phenomena that could explain any radio signals arriving via ducting and/or other non-precipitation scatter mechanisms.

Time correlations were sought in the data editing process process between the radio, meteorological, and radar data. These observations served to separate convective storm periods from other periods (such as cyclonic rains) or to simply isolate periods of reception when no precipitation was observed.

4.1 Radio Data

The bistatic radio data and great-circle path data were recorded on a 1-inch, 14-channel, analog, magnetic tape recorder and an eight-channel strip chart recorder mentioned previously. The data recording system is outlined in figure 4, and a typical sample of a recording for frequency f_3 is shown in figure 5. The switching sequence for the four-minute cycle is noted in this figure, and several significant precipitation interference signals are seen from the 5000 and 10, 000 ft common volumes during the third and fourth minutes of the timing cycle. A very low level signal may also be seen on the great-circle path, A_{33}.

The significant periods of rain scatter and/or other data were identified and selected for digital processing, using the editing procedures noted above. The analog tape recorded signals for the selected periods were played back through an analog-to-digital (A/D) conversion system. All eight data tracks from the analog magnetic tapes were digitized simultaneously in the A/D system for the selected event periods, using channel multiplex and sample/hold techniques. The length of each digitized event period is established by the length of the longest single-channel data record. Thus, some channels from the analog tapes were digitized for periods of time when there were no significant data; a fact which should be kept in mind in reading the sample data tabulation presented later in this section.

The pertinent factors involved in the analog playback-A/D process are shown in table 13.

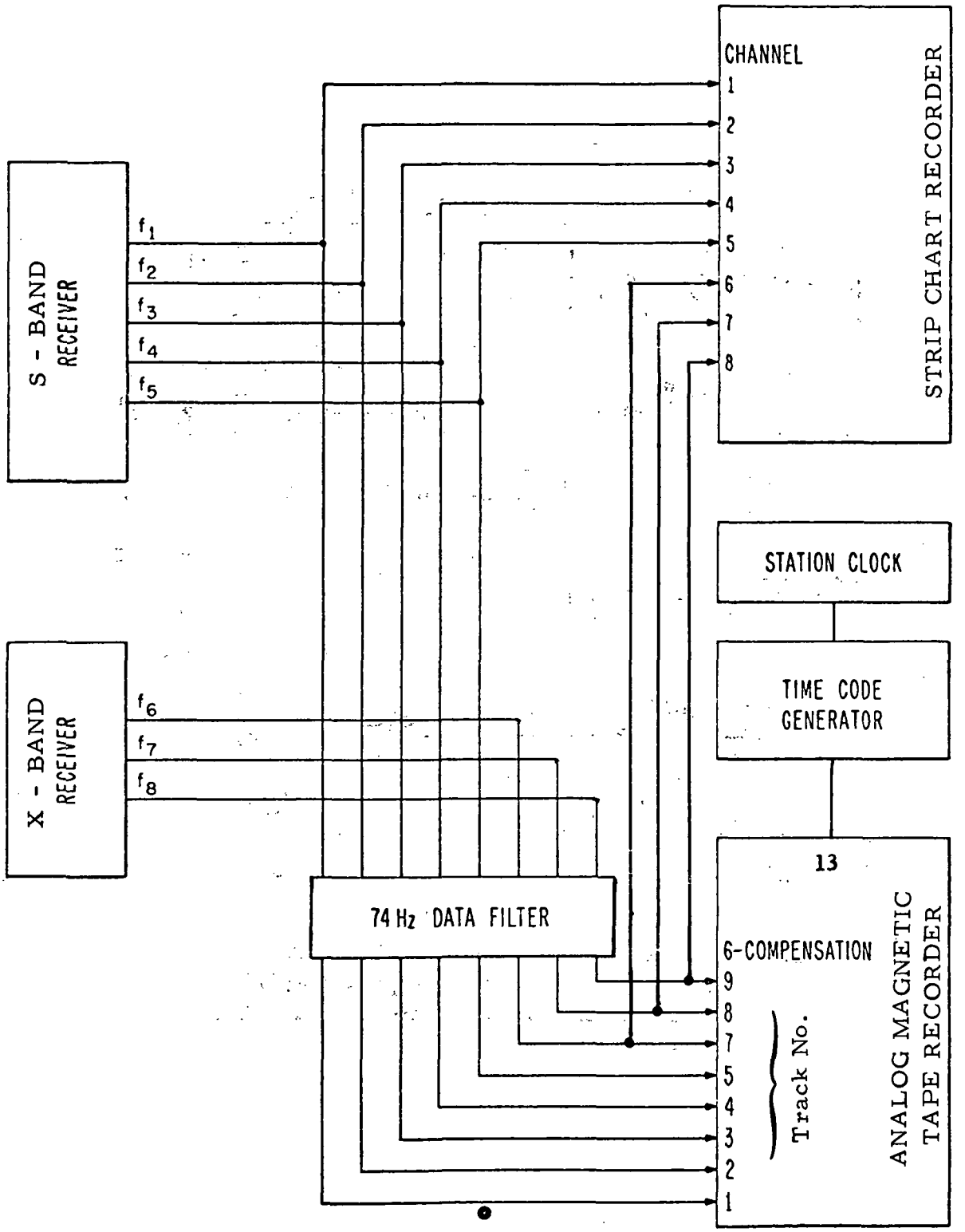

Figure 4. Data recording diagram for the RIPP fixed-beam experiment.

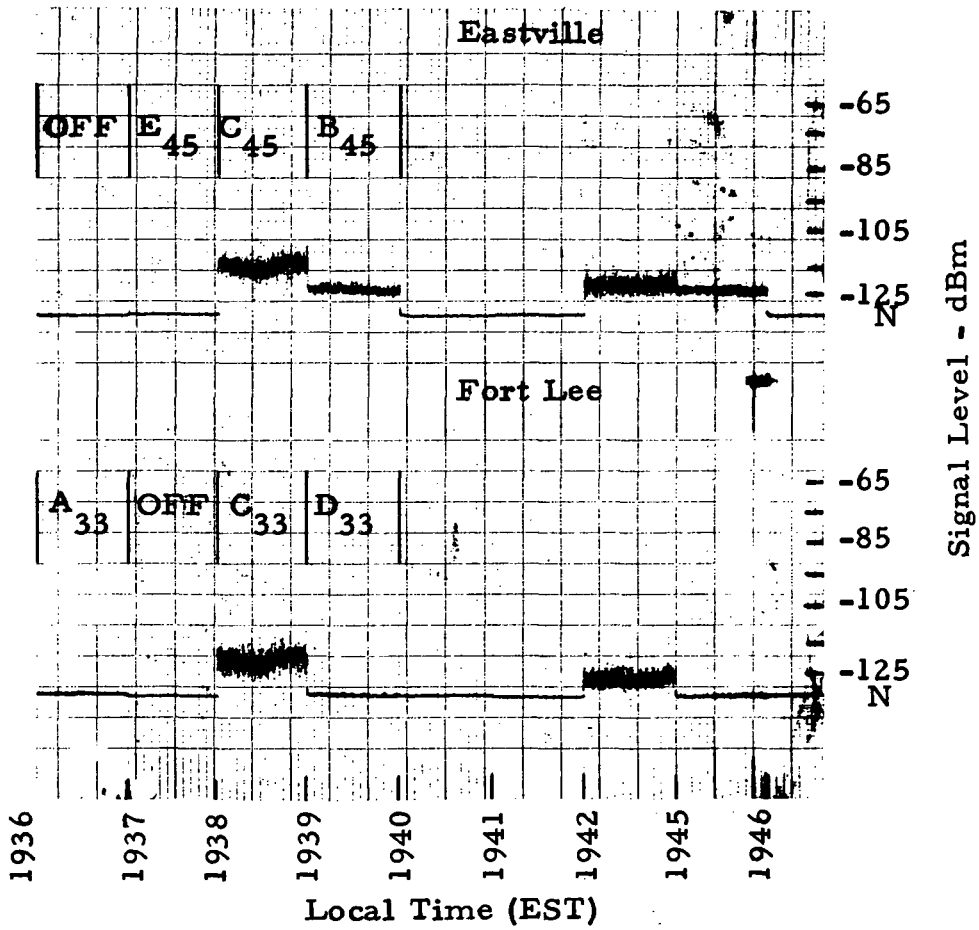

Figure 5. Sample strip chart record of signals recorded on magnetic tape at the ES from the transmitter sites at Eastville and Fort Lee.

Table 13. Factors Involved in Data Recording and Digitizing Processes

ANALOG

Record Speed	0.6 inches per second
Tape Playback Speed	15 inches per second
Speed-up Factor	25

DIGITAL

Record Length	848 characters
One Word	2 characters
One Character	6 bits
Two Characters	12 bits resolution/word
Records per file	75 records
Sampling Rate	16, 000 samples/second

MULTIPLEX

$$\frac{\text{Sampling Rate}}{\text{Speed-up factor x no. of variables}} = \frac{16000}{25 \times 8}$$

$$= 80 \text{ channel-samples/second}$$

The digitized experimental data were processed in a large scale digital computer (CDC 3800), and the detailed analysis of each event period began with the output of the computer processing. The salient functions and parameters that were derived from the computer programs were:

1. Cumulative amplitude (in dBm) distributions for each clock-minute of received signal recorded at the ES on each frequency and for each interference transmitter

path (including great-circle propagation into the ES sidelobes).

2. Computation of the mean signal level in dBm, and the standard deviation of the clock-minute signal about the mean value.
3. A count of the number of times the clock-minute signal crosses the median value in a positive direction during the minute.
4. A tabulation of all clock-minute signal mean values, medians, and other deciles from the distribution of 1 above was made from the computer analysis and recorded on a digital magnetic output tape for further computer processing outlined below.

At the time of this report, a total of 70 analog magnetic tapes have been processed which encompasses all of the significant data recorded between the period of September 27, 1970, through January 31, 1971. The digital processing of these tapes has produced 116 archive data files in which the accumulated data are recorded on digital magnetic tape and stored. Calibration data were digitized directly from the analog magnetic tapes in the same manner as the radio signals. An example of the calibration data as stored on the digital archives tape is shown in table 14, which is a page of computer print-out for a typical calibration tabulation. The table illustrates the book-keeping chores performed in the data archives as each of the eight calibration levels for each data channel was recorded on the tape. It should be noted that the tabulated levels are listed in computer units and not units of a physical quantity.

Following each calibration entry, the data from the distribution analysis were archived onto a digital tape. These records are those for each

Table 14. Calibration Data

```
00000000     319  HOUR    1140  1100     0      0      0      0 FROM TAPE UNIT NUMBER  20
 THERE ARE       0  FILES TO BE SKIPPED
      INPUT FIRST RECORD FROM FILE LL 20
 INPUT EOF FROM 20


NUMBER OF DATA POINTS EACH CHANNEL=  2106
  THIS SAMPLE  OF  81  PHYSICAL RECORDS IN THE LAST MINUTE OF DA
  NTPS WAS EXTENDED IN LEVEL   1
  NTPS=  211
  NTPS WAS EXTENDED IN LEVEL   2
  NTPS=  501
  NTPS WAS EXTENDED IN LEVEL   3
  NTPS=  791
  NTPS WAS EXTENDED IN LEVEL   4
  NTPS= 1081
  NTPS WAS EXTENDED IN LEVEL   5
  NTPS= 1371
  NTPS WAS EXTENDED IN LEVEL   6
  NTPS= 1661
  NTPS WAS EXTENDED IN LEVEL   7
  NTPS= 1951
  NTPS WAS EXTENDED IN LEVEL   8

CALIBRATION SEARCH FAILED TO FIND A VALUE AT LEVEL  8   CHANNEL  8     75
  NTPS= 2241

   PRE CALIBRATION DATA
  CALIBRATION LEVELS     CHANNEL     1104.26   699.70   303.73  -169.06  -671.92 -1121.16 -1469.92 -1584.90
  CALIBRATION LEVELS     CHANNEL     1926.74  1383.81   866.23   244.39  -421.27 -1032.29 -1461.91 -1556.20
  CALIBRATION LEVELS     CHANNEL     1445.95   979.32   594.50   143.27  -399.28  -944.62 -1346.88 -1503.78
  CALIBRATION LEVELS     CHANNEL     1450.44   921.50   540.86    55.13  -545.59 -1023.94 -1393.07 -1545.67
  CALIBRATION LEVELS     CHANNEL     1414.13   979.82   507.44    15.28  -500.92  -956.82 -1347.27 -1505.19
  CALIBRATION LEVELS     CHANNEL     1125.85   699.93   305.02  -172.87  -740.45 -1183.68 -1379.51 -1379.51
  CALIBRATION LEVELS     CHANNEL     1461.20  1038.82   569.01   127.88  -460.47  -941.49 -1199.20 -1235.99
  CALIBRATION LEVELS     CHANNEL     1189.74   789.12   381.95   -51.96  -579.03 -1062.79 -1288.90 -1296.59
      INPUT FIRST RECORD FROM FILE LL 20
 INPUT EOF FROM 20

 HEADER DATA WITH   2  WORDS.

03241480021000000   IFLAG=   0
```

minute of data from each channel of recording on the analog tape, and are cumulative values determined from 21 levels established over the spread of the amplitude values. A sample tabulation of these data for a single clock-minute is shown in table 15. In addition to the complete tabulation, several percentiles for each distribution are listed separately, as well as the mean and standard deviation values. These detailed descriptors of the clock-minute signals were computed and archived for comparison and distinction between other possible interference mechanisms, as noted earlier in this report. All signals, including those recorded during periods of no precipitation, were reduced and analyzed in the same manner to aid in mechanism recognition and separation processes when required. Values in table 15 are again in computer units, and the listings are presented only to illustrate the processing, computational, and archiving details. When the appropriate calibrations are applied to these data, a tabulation of the clock-minute distribution percentiles (or the complete distribution) can be made directly in power units (dBm). An example of such a listing is presented in table 16, in which the data are identified for several of the 32 possible time sequenced antenna/site/frequency combinations in the experiment configuration, including noise (N). The data presented in table 16 were taken from a period of general stratiform rain which occurred for approximately 5 hours on November 20, 1970. The minutes which contain significant data (i. e., mean values above minimum detectable levels given in section 2. 2) are indicated in the table. They are seen to be signals received from several great-circle paths and off-path beams, as well as common volume scatter data. This particular example serves to illustrate the compilation of data performed by the computer, and the read-out format from which significant clock-minutes of data can be recognized.

Table 15. Clock-minute Distribution Data

```
  DAY      324  HOUR    1400  1400     0     0     0     0 FROM TAPE UNIT NUMBER  20
 THERE ARE       0 FILES TO BE SKIPPED
      INPUT FIRST RECORD FROM FILE LU 20
 INPUT EOF FROM 20

NUMBER OF DATA POINTS EACH CHANNEL=   600
  THIS SAMPLE  OF  60  PHYSICIAL RECORDS IN THE LAST PIKLTE OF DATA

   NUMBER OF POINTS PER TRACE=     600     60690


CHANNEL 1   PERCENTILES    99TH -1651.00   90TH -1634.00   PEC -1612.00   10TH -1586.00   01TH -1547.00
CHANNEL 2   PERCENTILES    99TH -1559.00   90TH -1537.00   PEC -1510.00   10TH -1479.00   01TH -1462.00
CHANNEL 3   PERCENTILES    99TH -1564.00   90TH -1545.00   PEC -1521.00   10TH -1495.00   01TH -1472.00
CHANNEL 4   PERCENTILES    99TH -1614.00   90TH -1585.00   PEC -1566.00   10TH -1541.00   01TH -1517.00
CHANNEL 5   PERCENTILES    99TH -1576.00   90TH -1554.00   PEC -1531.00   10TH -1501.00   01TH -1476.00
CHANNEL 6   PERCENTILES    99TH -1471.00   90TH -1437.00   PEC -1399.00   10TH -1361.00   01TH -1326.00
CHANNEL 7   PERCENTILES    99TH -1323.00   90TH -1278.00   PEC -1217.00   10TH -1159.00   01TH -1103.00
CHANNEL 8   PERCENTILES    99TH -1391.00   90TH -1353.00   PEC -1297.00   10TH -1234.00   01TH -1186.00


CHANNEL 1 MEAN IS -1610.43  MEDIAN IS   -1612.00  STANDARD DEVIATION IS     19.4
CHANNEL 2 MEAN IS -1508.70  MEDIAN IS   -1510.00  STANDARD DEVIATION IS     22.8
CHANNEL 3 MEAN IS -1520.41  MEDIAN IS   -1521.00  STANDARD DEVIATION IS     18.8
CHANNEL 4 MEAN IS -1565.25  MEDIAN IS   -1566.00  STANDARD DEVIATION IS     18.9
CHANNEL 5 MEAN IS -1529.49  MEDIAN IS   -1531.00  STANDARD DEVIATION IS     21.0
CHANNEL 6 MEAN IS -1399.38  MEDIAN IS   -1399.00  STANDARD DEVIATION IS     29.6
CHANNEL 7 MEAN IS -1217.42  MEDIAN IS   -1217.00  STANDARD DEVIATION IS     45.0
CHANNEL 8 MEAN IS -1294.77  MEDIAN IS   -1297.00  STANDARD DEVIATION IS     45.6


CHANNEL 1 LEVELS      -1660.00 -1662.83 -1657.01 -1651.19 -1645.36 -1639.54 -1633.72 -1627.85 -1622.07 -1616.25 -1610.43
                      -1604.60 -1598.78 -1592.96 -1587.13 -1581.31 -1575.49 -1569.67 -1563.84 -1558.02 -1552.20
CHANNEL 2 LEVELS      -1577.00 -1570.22 -1563.39 -1556.59 -1549.76 -1542.98 -1536.35 -1529.21 -1522.37 -1515.54 -1508.70
                      -1501.87 -1495.03 -1488.20 -1481.36 -1474.52 -1467.69 -1460.85 -1454.02 -1447.18 -1440.35
CHANNEL 3 LEVELS      -1576.77 -1571.13 -1565.50 -1559.86 -1554.23 -1548.59 -1542.95 -1537.32 -1531.68 -1526.04 -1520.41
                      -1514.77 -1509.14 -1503.50 -1497.86 -1492.23 -1486.59 -1480.96 -1475.32 -1469.68 -1464.05
CHANNEL 4 LEVELS      -1622.08 -1616.38 -1610.69 -1605.01 -1599.33 -1593.66 -1587.99 -1582.31 -1576.64 -1570.97 -1565.29
                      -1559.62 -1553.95 -1548.27 -1542.60 -1536.93 -1531.25 -1525.58 -1519.91 -1514.24 -1508.56
CHANNEL 5 LEVELS      -1592.21 -1586.21 -1579.90 -1573.60 -1567.30 -1561.00 -1554.70 -1548.40 -1542.10 -1535.80 -1529.49
                      -1523.19 -1516.89 -1510.59 -1504.29 -1497.99 -1491.69 -1485.38 -1479.08 -1472.78 -1466.48
CHANNEL 6 LEVELS      -1480.25 -1479.36 -1470.48 -1461.59 -1452.70 -1443.81 -1434.93 -1426.04 -1417.15 -1408.26 -1399.38
                      -1390.49 -1381.60 -1372.71 -1363.83 -1354.94 -1346.05 -1337.16 -1328.28 -1319.39 -1310.50
CHANNEL 7 LEVELS      -1355.46 -1341.65 -1327.85 -1314.05 -1300.24 -1286.44 -1272.64 -1258.83 -1245.03 -1231.23 -1217.42
                      -1203.62 -1189.82 -1176.02 -1162.21 -1148.41 -1134.61 -1120.80 -1107.00 -1093.20 -1079.39
CHANNEL 8 LEVELS      -1431.49 -1417.78 -1404.11 -1390.44 -1376.78 -1363.11 -1349.44 -1335.77 -1322.10 -1308.44 -1294.77
                      -1281.10 -1267.43 -1253.76 -1240.10 -1226.43 -1212.76 -1199.09 -1185.42 -1171.76 -1158.09
```

Table 16. Clock-minute Data Tabulation for Day 324. Levels are dBm.

ANT	HOUR	MEAN	1%	10%	MEDIAN	90%	95%	MED CROSS	SIGMA	IN DB
• A_{11}	1440	-121.99	-113.16	-116.92	-122.32	-126.55	-128.20	188	122.8	3.63
• C_{22}	1440	-107.78	-98.61	-102.84	-107.85	-112.73	-117.95	194	252.9	3.67
A_{33}	1440	-127.74	-126.41	-127.13	-127.75	-128.35	-128.77	181	19.7	0.39
A_{44}	1440	-127.17	-125.51	-126.37	-127.18	-127.94	-128.48	211	24.2	0.48
(N)	1440	-128.42	-127.10	-127.76	-128.49	-129.12	-129.59	191	40.0	0.80
• A_{16}	1440	-115.16	-107.93	-111.04	-116.51	-124.23	-127.09	201	119.0	2.70
• A_{37}	1440	-124.72	-119.82	-122.16	-124.81	-127.19	-129.57	198	45.7	2.02
E_{11}	1441	-127.60	-126.21	-126.92	-127.63	-128.22	-128.61	215	17.7	0.35
• F_{22}	1441	-123.52	-118.16	-121.14	-123.90	-125.51	-126.54	159	79.5	2.10
(N)	1441	-127.89	-126.63	-127.30	-127.92	-128.44	-128.84	173	18.6	0.37
• C_{33}	1442	-120.90	-112.33	-115.44	-121.27	-126.06	-127.67	194	161.5	4.00
• C_{37}	1442	-114.36	-106.43	-110.40	-114.59	-121.56	-125.52	193	145.6	2.99
• B_{45}	1443	-123.64	-117.88	-120.57	-123.77	-126.40	-127.88	190	85.2	2.24

• Denotes significant data

In the processing of these data, a pre- and post-calibration was generally used with each data file. The calibration data were archived onto the digital tapes as noted previously. When applied to the data files, linear interpolation between the pre- and post-calibration was used whenever the particular file spanned at least half of the time between the two calibrations. In cases when the data file was short compared to the time between calibration data, the nearest calibration only was applied to these files. Interpolation improves the accuracy of the data by calibrating out system drifts and other instabilities. It is felt, however, that use of the nearest calibration will provide the best accuracy for short data files.

The digital archives tapes were used to develop the statistical summaries of the tabulated clock-minute signal values as the analysis progressed. A second CDC-3800 program was implemented to compute the cumulative distributions of median signal levels for all of the great-circle and precipitation scatter data. The program searches the archived data tapes and selects all clock-minute median values that exceed an established threshold (such as 3 dB above noise level). These values were then tabulated for any or all of the 32 path combinations selected in program software. Any median signal level which exceeds the above threshold is identified with the minute at which it occurred and the path over which it was received. An example of a short tabulation of these data is given in table 17, where only C_{33} and C_{37} data were selected. These data may be selected from any single data file or group of files as requested in the computer program.

Table 17. Clock-minute Median Tabulation

			DAY	270	HOUR	1900	
ANT	IS C33	MIN IS	1902	MEDIAN VALUE	-121.22		
ANT	IS C37	MIN IS	1902	MEDIAN VALUE	-112.86		
ANT	IS C33	MIN IS	1906	MEDIAN VALUE	-123.22		
ANT	IS C37	MIN IS	1906	MEDIAN VALUE	-117.41		
ANT	IS C33	MIN IS	1910	MEDIAN VALUE	-125.07		
ANT	IS C37	MIN IS	1910	MEDIAN VALUE	-119.66		
ANT	IS C33	MIN IS	1914	MEDIAN VALUE	-123.81		
ANT	IS C37	MIN IS	1914	MEDIAN VALUE	-116.40		
ANT	IS C33	MIN IS	1918	MEDIAN VALUE	-125.32		
ANT	IS C37	MIN IS	1918	MEDIAN VALUE	-118.99		
ANT	IS C37	MIN IS	1922	MEDIAN VALUE	-120.89		
ANT	IS C33	MIN IS	1926	MEDIAN VALUE	-125.57		
ANT	IS C37	MIN IS	1926	MEDIAN VALUE	-119.48		
ANT	IS C37	MIN IS	1930	MEDIAN VALUE	-120.67		
ANT	IS C37	MIN IS	1934	MEDIAN VALUE	-118.85		
ANT	IS C37	MIN IS	1938	MEDIAN VALUE	-120.86		
ANT	IS C37	MIN IS	1946	MEDIAN VALUE	-122.81		
ANT	IS C37	MIN IS	1958	MEDIAN VALUE	-121.62		
ANT	IS C37	MIN IS	2002	MEDIAN VALUE	-121.44		
ANT	IS C37	MIN IS	2006	MEDIAN VALUE	-122.90		
ANT	IS C37	MIN IS	2010	MEDIAN VALUE	-121.18		
ANT	IS C37	MIN IS	2014	MEDIAN VALUE	-122.95		
ANT	IS C37	MIN IS	2026	MEDIAN VALUE	-122.81		
ANT	IS C37	MIN IS	2030	MEDIAN VALUE	-119.37		
ANT	IS C33	MIN IS	2034	MEDIAN VALUE	-124.27		
ANT	IS C37	MIN IS	2034	MEDIAN VALUE	-115.45		
ANT	IS C33	MIN IS	2038	MEDIAN VALUE	-123.62		
ANT	IS C37	MIN IS	2038	MEDIAN VALUE	-114.39		
ANT	IS C33	MIN IS	2042	MEDIAN VALUE	-123.36		
ANT	IS C37	MIN IS	2042	MEDIAN VALUE	-114.39		

The program formats these selected clock-minute values into cumulative distributions for each path selected, based on the percentage of minutes for each file or group of files. The latter can be a particular storm period in which the bistatic interference data were accumulated total of all storm periods, or a period of non-precipitation in which other interference mechanisms may be prevalent. Following the listing of table 17, the program provides a listing of the number of clock-minutes of data selected for each path from each data file and a similar listing for all previous files processed in a given run. In this manner,

the cumulative distributions for individual data files, particular storms, and/or total distributions of all previously entered data may be derived. The cumulative distribution functions generated in this program were plotted in a computer routine that uses a cathode ray tube (CRT) output. The data plots were recorded from the CRT on microfilm. An example of these function plots is shown in figure 6, printed directly from a frame of film. For each function, the date, starting data minute, and the total number of clock-minute median signal values accumulated in the distribution are recorded at the top of the plot. For long-term accumulative data, the computer also keeps a record of the last minute of data compiled in the function plots, and all of these bookkeeping notations are tabulated in the computer printout. They were used in later analyses to convert the percent-time scale as in figure 6 to total minutes or hours (see section 5).

The procedures discussed above were the primary data processing functions. Other parameters such as the standard deviation and the number of positive going median crossings within each minute were used when required to help distinguish and separate non-precipitation scatter signals. In addition, data were processed for this purpose in a small time series analysis system (TD-100) noted in figure 3. Probability distributions, correlation functions, and special analyses were performed in this system through hard-wired programs. Output was in the form of direct analog plots or photos from an internal CRT display, and digital magnetic tape. The latter were processed in the CDC-3800 system as noted in figure 3. These procedures are not described in detail as they were used only occasionally to augment the primary processing routines. The TD-100 was also used to monitor overall system gain and drift performance of the fixed-beam configurations through long-term analysis of noise levels and calibration data.

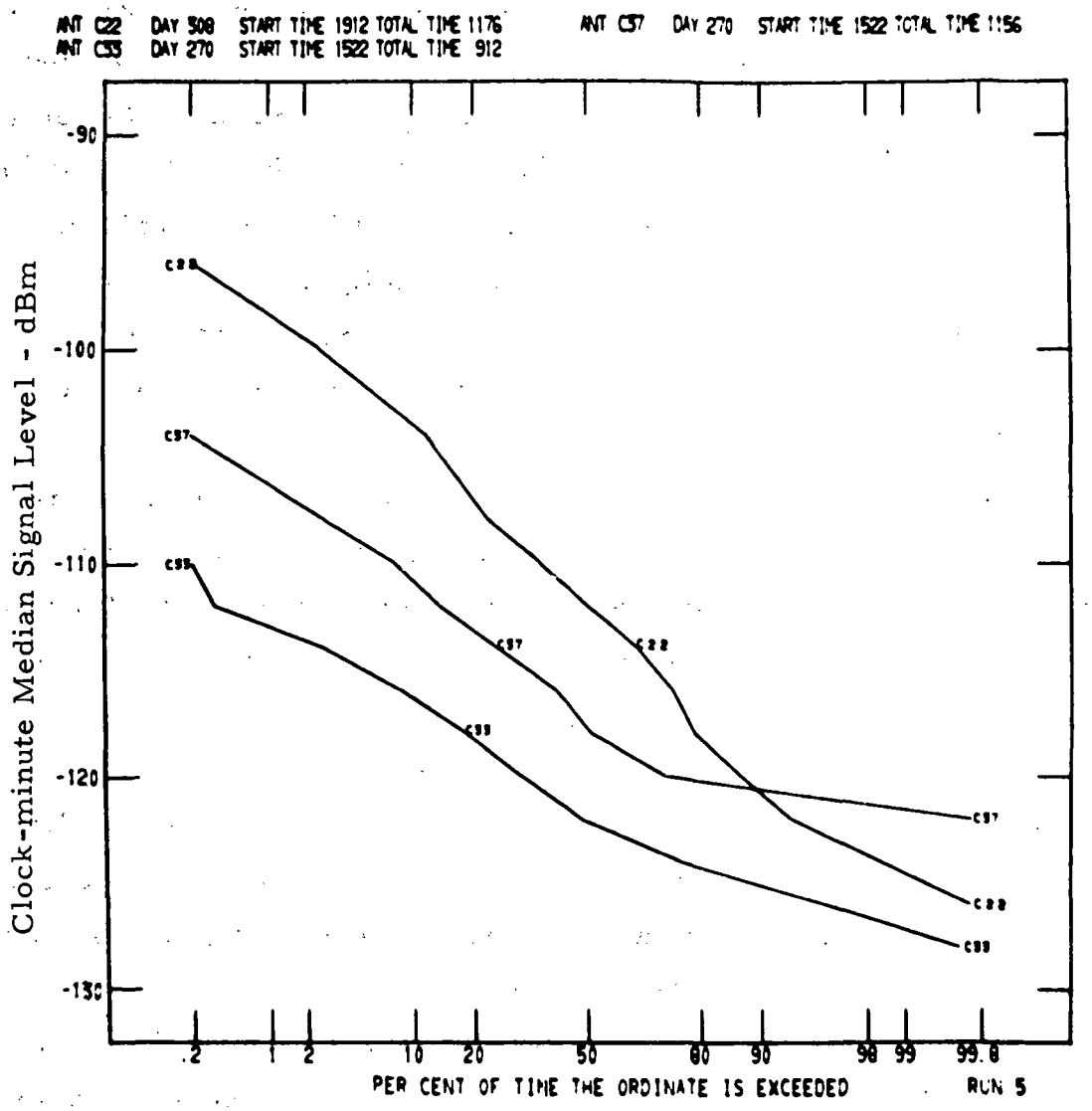

Figure 6. Cumulative distribution functions of radio clock-minute median signal levels for three path configurations and frequencies.

4.2 Rain Gauge and Meteorological Data

Meteorological data processing consisted of two distinct phases: processing of the rain gauge data to obtain rain-rate data for comparison with the radio interference data, and processing of other meteorological data for a synoptic description of the area weather system. These two phases are discussed separately.

The rain gauge recorder charts were read manually with an optical comparator (a ruled-reticle equipped magnifier) yielding a history of the time intervals over which amounts of rain varying from 0.01 inch to 0.1 inch were accumulated by the rain gauge; the resolution obtainable is inversely proportional to the rain-rate, so that at rates over about 50 mm/hr the record was read for every 0.1 inch accumulated.

The manually reduced rainfall record was processed with an XDS-940 computer program that yields both a time history of the rainfall rates as recorded and a cumulative distribution of rain-rates; the distribution is listed by both cumulative minutes and percent of time for the rainfall event being reduced. An example of the program output is shown in table 18 in which the rain-rate (R) is converted to dB in the 16 log (R) column, as shown in equation (12).

Individual rainfall events were separated into convective and non-convective storms (the convective class includes but is not limited to thunderstorms), and overall cumulative distributions were prepared for each type of rainfall for the entire data-taking period available. Cumulative distributions for all rainfall rates throughout the total experimental period were also prepared. In this report the total period examined is from September 24, 1970, through January 31, 1971, inclusive.

Table 18. Example of Computer-Reduced Rain Gauge Data

10, 000 ft. Subpoint, 10 Sept. 1970, 2209-2229 EDT.

Sequential Data			Cumulative Data		
Precip. Rate (R) mm/hr.	Time Int. min.	16 log(R) dB	Precip. Rate (R) mm/hr.	Cumul. Time min.	Per-cent
16.9	0.90	19.7	38.5	1.98	9.9
12.7	1.20	17.7	30.8	3.96	19.9
21.2	1.44	21.3	24.2	5.22	26.2
38.5	1.98	25.4	21.2	6.66	33.4
30.8	1.98	23.8	16.9	7.56	38.0
13.4	1.14	18.1	13.4	8.70	43.7
24.2	1.26	22.2	12.7	9.90	49.7
7.5	2.04	14.0	8.2	11.76	59.0
2.5	6.12	6.4	2.5	19.92	100.0

Total Precip. = 0.19 inch

Max. Rate = 38.5 mm/hr

The majority of the other meteorological data, such as daily weather maps, radar summary maps, weather radar PPI photographs, and monthly weather summaries, were not processed in a routine sense. They were used instead as synoptic information in the separation or identification of mechanisms, and required analytical analysis using expert meteorological judgment to arrive at a conclusion.

The radiosonde data received daily by teletype (TTY) were processed through an XDS-940 computer program to obtain radio refractive index vertical profiles, from which significant super-refractive or

subrefractive layers were identified and recorded in the meteorological log book.

More detailed refractive index profiles were obtained for days during which significant radio interference signals were logged by obtaining copies of original radiosonde recorder charts. These charts were read manually and then processed through an XDS-940 computer program to obtain pressure, temperature, and humidity at various levels. This output was then processed through the same program used on the TTY data to obtain a more detailed radio refractive index profile.

The meteorographs yield records of pressure, temperature, and humidity for one-week periods. These records were evaluated manually at least twice daily at the times of minimum and maximum temperature, and were processed with an XDS-940 computer program to obtain the radio refractive index at the transmitter sites. This is a valuable indicator of radio micro-climate.

5. SUMMARY OF EXPERIMENTAL DATA FOR A PARTIAL YEAR

Data from the fixed-beam experiment were collected continuously, beginning in late September 1970. The period of analysis covered in this report is from September 27, 1970, through January 31, 1971; approximately one-third of a year. This four-month period involved slightly more than 3000 hours of experiment time, with a total precipitation period of 157 hours. The latter is the time of measurable precipitation above 0.1 mm/hr rates as recorded by the 10,000-ft subpoint rain gauge. These data and the radio interference* data recorded during the precipitation periods are summarized in this section.

*The term "interference" used here is intended to imply an unwanted signal from the terrestrial transmitter sites at the satellite receiver terminal. The degree of interference which such a signal will cause depends on many parameters of the satellite link, such as modulation, level of desired signal, etc.

The analysis discussed in this section is not considered to be conclusive, but it is useful to indicate trends that are observable for the period, and to illustrate the format of final results from the experiment. As noted in section 2, a one-year measurement period was considered to be the minimum required to obtain an adequate statistical data base from this experiment. The results presented below are the first cumulative summary of data that are useful to determine trends, and it must be empahsized again that these data represent only one-third of the desired year. At the time of this analysis, the experiment had not yet been operating during the highest rainy (thunderstorm) season of the year for the southern Virginia region, i.e., the summer months.

During the precipitation period from September 27, 1970, through January 31, 1971, rain scatter interference data were observed from the two lower common volume intersections, i.e., 5000 ft and 10,000 ft, during nearly all periods when surface precipitation was recorded. Radio scatter data at the common volume intersections of 20,000 ft and 30,000 ft were observed only on rare occasions from the forward transmitter sites. For example, only one clock-minute of measureable interference data was observed at 20,000 ft from the cross-path site at Ft. Lee (path D_{33}). This was an S-band signal that occurred during a 4-hour stratiform rain period in the early morning hours of January 23, 1971. On path D_{44} (Eastville - 20,000 ft) a total of 3 clock-minutes of measurable data were recorded, 2 minutes occurring during a short convective interval of a long storm on November 10-11, 1970. It was also during this short interval that the only interference data at the 30,000 ft common volume were measured; namely 1 minute of data on path E_{11} and 9 minutes on E_{48}. Obviously these data samples

are not sufficient to provide a statistically meaningful example; consequently, this report does not contain data summaries for common volumes above 10,000 ft. It is anticipated that the rainy season during the summer months in Virginia will yield data for the common volume intersections above 10,000 ft [Crane, 1972].

5.1 Comparison of Rain Scatter Data

The experiment configuration was planned to provide redundant coverage of the common volumes in both path and frequency. The redundant measurements provide high data reliability for the 10,000 and 20,000 ft common volumes, real-time data comparisons for evaluating system performance during the experiment, and a direct comparison of results between the S-band and X-band frequencies.

As an example of the real-time data comparisons possible, we note from the switching matrix of table 7 that the 10,000 ft common volume was illuminated from both the Ft. Lee and Eastville sites at both the S- and X-band frequencies during the same minute of the switching sequence. This permits a direct comparison of data to be made on a minute-by-minute basis between paths such as C_{33} and C_{45}, C_{37} and C_{48}, and between frequencies as C_{33} vs. C_{37}. Similarly, data may be compared from the 5000 ft common volume between the two frequencies, i.e., paths B_{45} and B_{48}. Scatter diagram plots of these data comparisons for several typical intervals are shown in figures 7 through 11. Figure 7 shows a comparison of data for paths C_{33} and C_{45}, taken from data intervals recorded on October 16, 1970. Note that the diagonal line for one-to-one correspondence of these data (solid line) has been adjusted by 1 dB to account for the path loss difference given by the constants in table 1. The dashed line is a manual best fit to these data and indicates that the C_{33} data samples are consistently on the order of 6.5 dB lower than C_{45} data for this date. Figure 8 shows a comparison of these data for a storm on January 5, 1971, indicating that the C_{33} data samples are on the order of 4 dB low for this period.

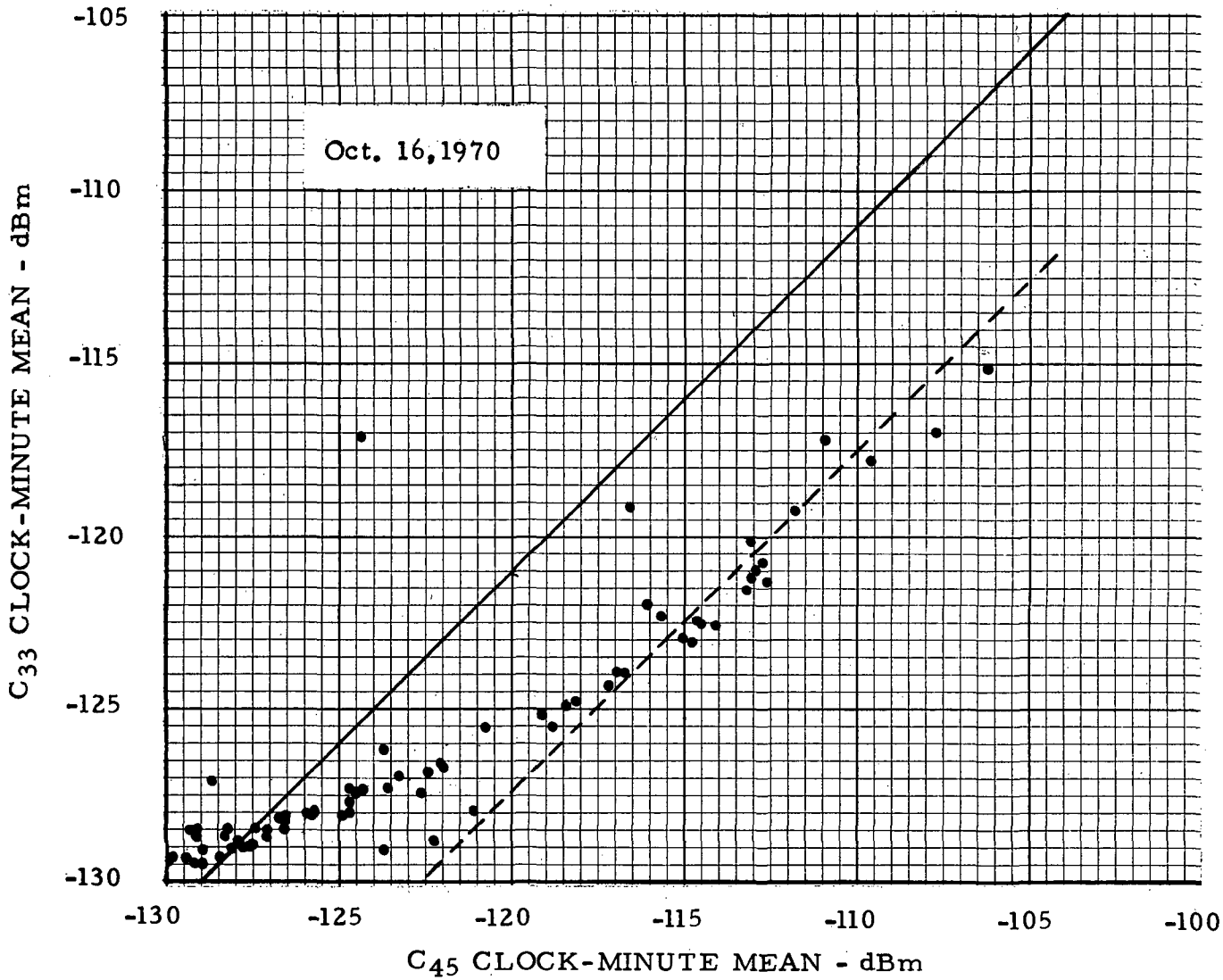

Figure 7. Clock-minute data comparison between Ft. Lee and Eastville from 10,000 ft. common volume (S-band).

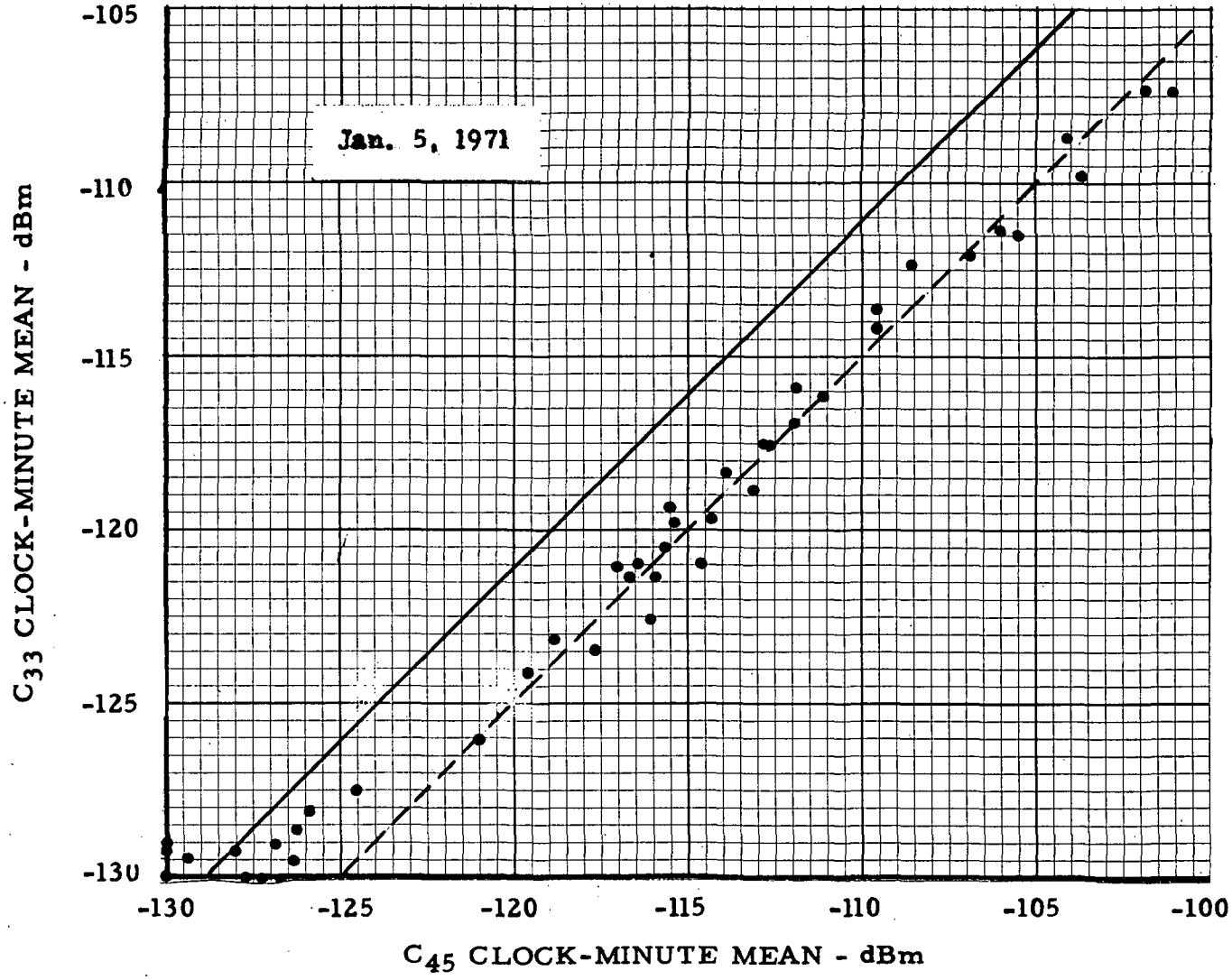

Figure 8. Clock-minute data comparison between Ft. Lee and Eastville from 10,000 ft. common volume (S-band).

However, if these two storms are combined for a minute-by-minute comparison of the data, the results are shown in figure 9. The regression in this figure indicates a data discrepancy on the order of 4.5 dB. The variance of these values is within the measurement accuracy of the experiment, which is estimated to be about ±5 dB. Individual storm comparisons are useful in the analysis for detecting equipment or other experimental problems, which will be seen in a later example. However, it is difficult to assess the long-range conduct of the experiment on the basis of such comparisons. When minute-by-minute comparisons are made, they cannot be conclusive because of the unknown factors such as storm cell size, distribution of rain within the storm, and the question of partial or complete filling of common volumes during each minute. These factors, as well as antenna orientation and system calibration errors, are involved in the variations found between the data comparisons such as figures 7 and 8. The combination of events into larger statistical samples will tend to average these effects, and provide a better statistical norm as illustrated by the average regression in figure 9.

Since the overall objective of the experiment is based upon statistical sampling of a long duration, it was felt that the best comparison of data could be based on the total cumulative samples. Experimental error will be averaged over the longer sample, and with assurance that there are no events with an extreme error, the cumulative data will provide a basis for meaningful data comparison. Thus, the scatter type analysis on a minute-by-minute basis was used only to verify reasonable agreement between experiment measurement and rain scatter theory. The conclusive comparison of the data on the basis of cumulative results is presented later in this section.

In the course of examining these data on a minute-by-minute basis, an interesting comparison was found for a storm which occurred

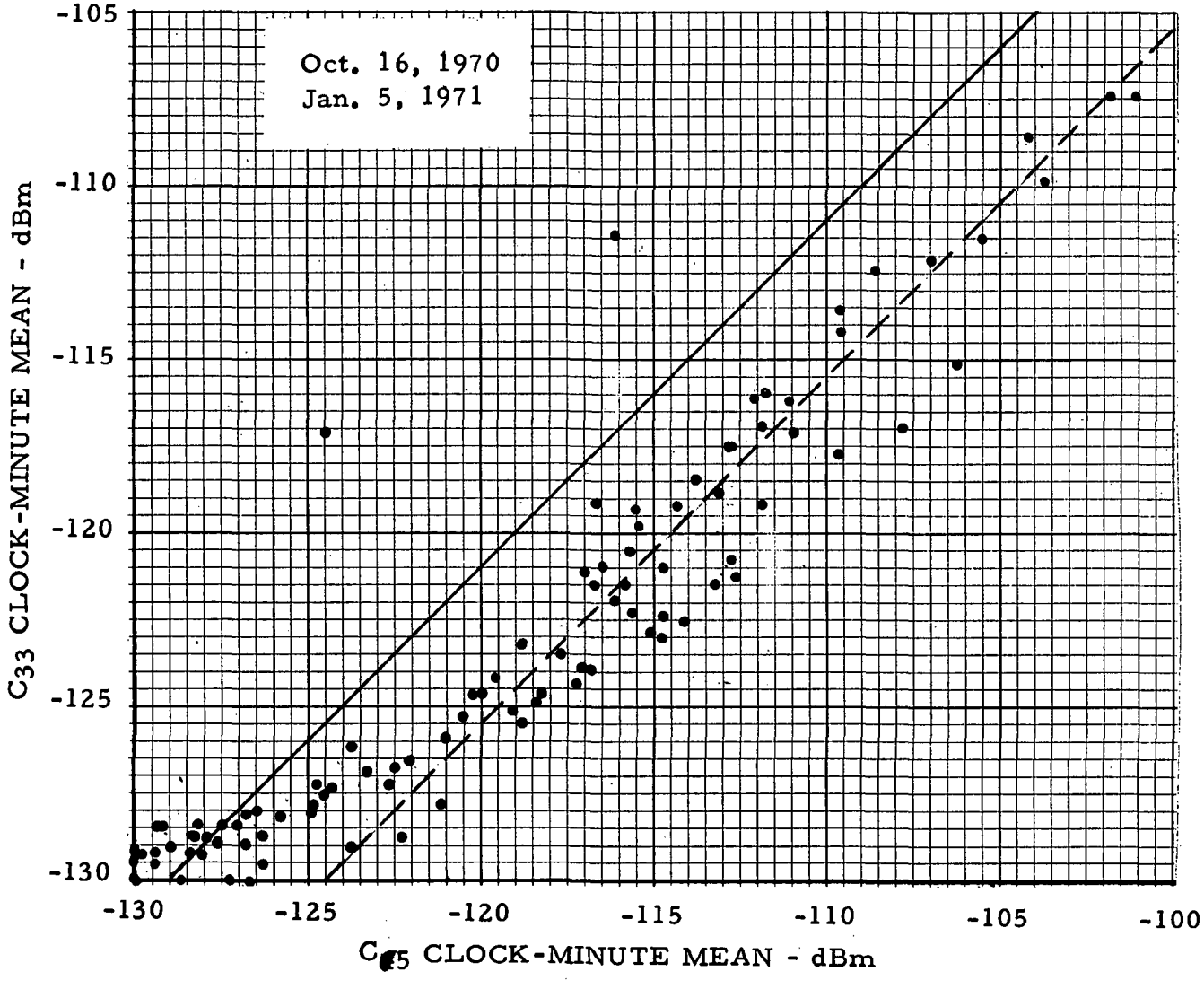

Figure 9. Clock-minute data comparison between Ft. Lee and Eastville from 10,000 ft common volume (S-band).

on December 16, 1970. A plot of the 10,000 ft common volume data for C_{33} and C_{45} is shown in figure 10. We note a rather significant number of clock-minute means for which there is a strong signal present on path C_{45}, while the C_{33} signal is near noise level. Regression of the remaining data points, however, agrees with that found in figure 9. The majority of the minutes during which a signal was observed for C_{45} and not for C_{33} occurred during the morning hours, beginning around 0900 EST and persisting until 1300 EST, in the afternoon. A few isolated minutes were observed between 1400 and 1700 EST, followed by the normal precipitation scatter pattern until the end of the storm at approximately 2130 EST. This storm represents the only event during the reporting period in which a serious discrepancy in the minute-by-minute comparisons was observed. The storm period was analyzed for other propagation modes based on meteorological observations and data, and is discussed in some detail in Appendix C. The probability for a super-refractive propagation mode was found to be high on the Eastville side of the experiment configuration, and somewhat subrefractive on the Ft. Lee side. However, these conditions were not deemed adequate to permit the diffractive mode to explain the uncorrelated, high signal level minutes from the Eastville site. The transmitter antenna elevation angle was greater than 3° at this site. Because of the elevation angle and side-lobe gain considerations, superrefraction was ruled out. Similarly, subrefractive conditions could cause an upward bend in transmissions from the Ft. Lee site. Again, the elevation angle of approximately 2° for this antenna would not produce sufficient bending to explain the data on this basis.

System status for the period was carefully considered, to make sure the data were not due to a malfunction in a transmitter or ES receiver. A comparison of the minute-by-minute data at the X-band frequency was made (C_{37} vs. C_{48}), and is shown in figure 11. It is

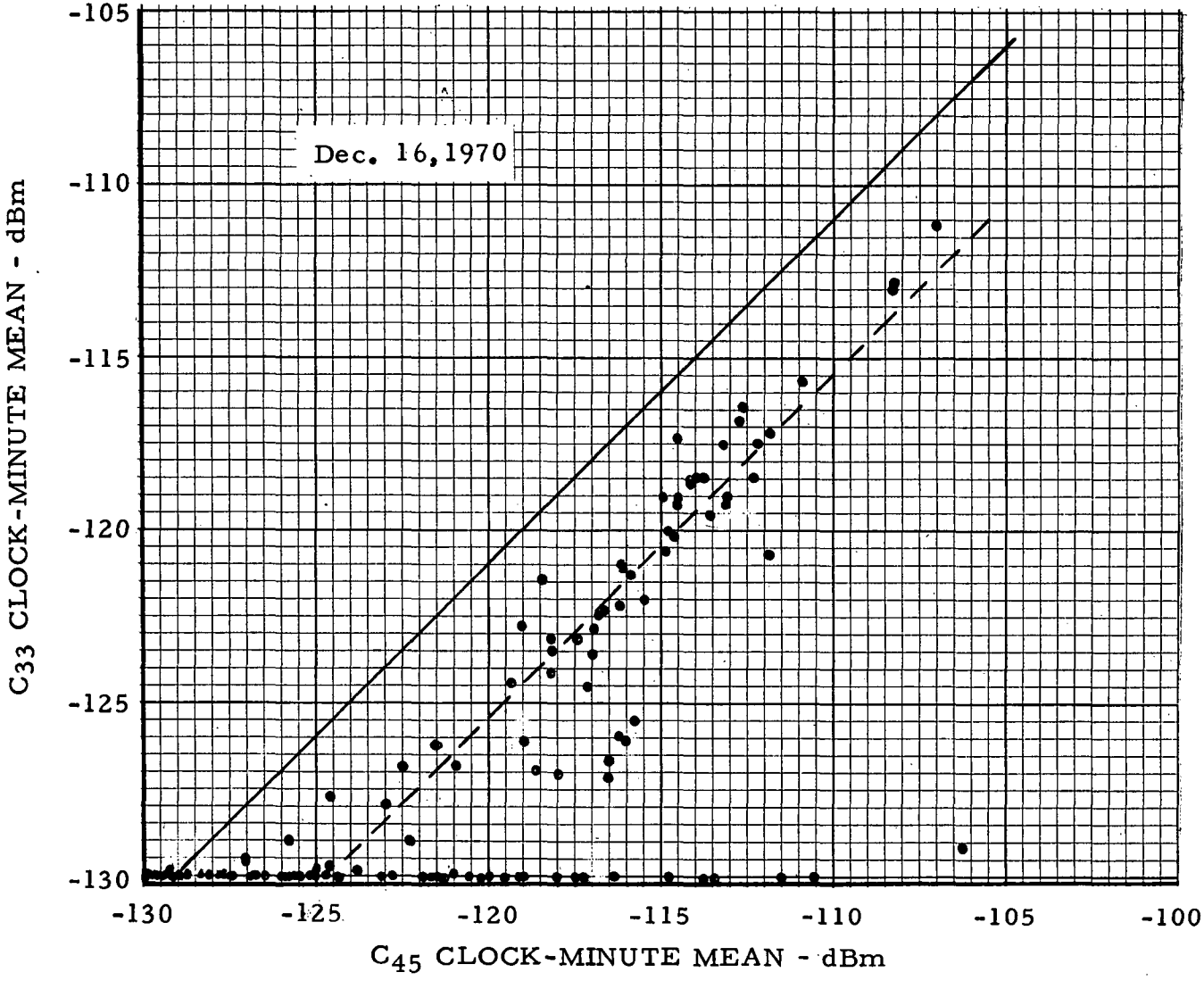

Figure 10. Clock-minute data comparison between Ft. Lee and Eastville from 10,000 ft common volume (S-band).

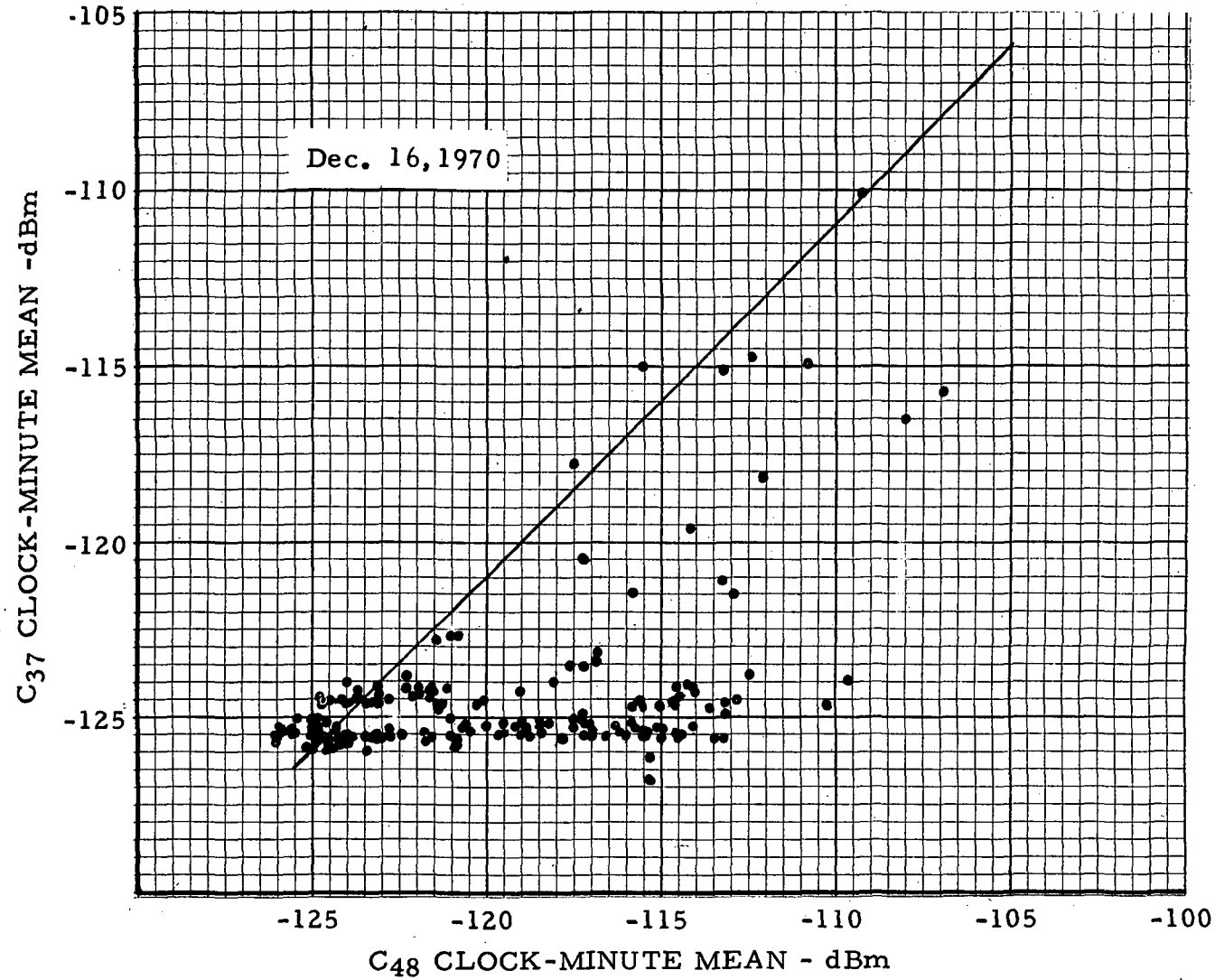

Figure 11. Clock-minute data comparison between Ft. Lee and Eastville from 10,000 ft common volume (X-band).

noted that the X-band behavior was quite similar to that of the S-band in figure 10, with more variance in the correlated minutes. These data tend to confirm an anomaly in the configuration or propagation conditions rather than a system problem, as the S- and X-band systems were essentially independent.

Several causes for the observed anomaly during this storm are possible. The combination of antenna pointing angle errors and the size and distribution of cells within the storm could produce the observed results. For example, the Ft. Lee and Eastville transmitters may not have been illuminating the exact same common volume. In addition, slight bending due to the cited refractive conditions would compound this problem, and minute-by-minute correlation could be destroyed. A second likely cause to be considered is the position of a possible "bright band" during the storm. If the bright band should envelop more of one common volume than the other (assuming that one was actually higher in elevation than the other), the reflectivity for the two paths could be significantly different. The analysis of the storm in Appendix C indicates that the bright band at noon (at Wallops Island) was slightly above 5000 ft. However, there are not sufficient data to confirm this altitude in the Langley vicinity. Analysis of the distribution and variance of the signals within the minute for the uncorrelated data from Eastville, indicates that these signals have the characteristics of rain scatter. Thus, these data were included in the total analysis, and it is assumed that the illuminated 10, 000-ft common volumes were not identical during this storm.

As stated previously, the primary data comparisons were made on the basis of cumulative data for the total 4 month period analyzed for this report. For example, the comparison noted earlier between such transmission paths as C_{33} and C_{37} was made on the basis of the cumulative distribution data. These computer-derived distributions

are presented in figure 6. Note that the separation of these distribution curves is on the order of 4-5 dB; a value that agrees quite well with the theoretical value computed from the path constants and given in table 1 (i.e., $K_s - K_x = -124.1 + 119.5 = -4.6$ dB). This difference indicates that the clock-minute mean signal level should be 4.6 dB higher for the X-band (C_{37}) than for the S-band (C_{33}) data, and is verified by figure 6. Similar comparisons were made for other path combinations using the cumulative distribution data presented in Appendix A. All of these results are summarized in the following observations:

1) Data from path C_{33} appear to be low in clock-minute mean value by 4.5 dB in comparison with C_{45} (which agrees also with figure 9).
2) Data from paths C_{33} and C_{37} agree extremely well, as noted above.
3) From observations 1) and 2), we conclude that C_{37} data are low in value by 4.5 dB.
4) C_{45} and C_{48} data agree well with theoretical difference of 4.6 dB.
5) Data from path B_{48} are nominally 7 dB higher than those from B_{45}. The theoretical value is 4.5 dB from table 1. Thus, if B_{48} data are correct, the B_{45} data are approximately 2.5 dB low in value.
6) A redundant path either from Ft. Lee (TS-3) or at another frequency is not available for comparison directly with B_{48} data. Thus, in order to evaluate these data in a theoretical sense, they were compared with C_{48}. The two path constants (table 1) are the same, and it is seen from Appendix A that these data distributions agree very well. We conclude that B_{48} data are correct, and the low value for B_{45} data noted in 5) above should be assumed.

7) Theoretical distributions of C_{22} and C_{45} data should show C_{22} generally 10.5 dB higher than C_{45}. The cumulative data show C_{22} high by only 8 dB (see Appendix A), indicating that the C_{22} data are low on the order of 2.5 dB.

These observations from the cumulative data for the 5000 and 10,000 ft common volumes show very good agreement between the measurements and the simplified bistatic radar scatter theory. The largest discrepancies are seen in the 5000 ft data from Eastville (B_{45}) and the two 10,000 ft data sets from Ft. Lee (C_{33} and C_{37}). These discrepancies can be directly attributed to a partial blockage of the transmitting antennas by trees at the respective sites. This problem is illustrated and discussed in Appendix B. It is not clear why the foreground blockage appears to be 2.5 dB higher for the S-band data (B_{45}) from Eastville than the corresponding X-band (B_{48}) data. However, as noted in 6) above, a redundant comparison with B_{48} data was not possible, and the comparison with C_{48} data assumes no height dependence. This may not be an absolute assumption. The 2.5 dB difference in these data is, however, within the probable experimental error, and thus cannot be explained conclusively.

Data from common volumes above 10,000 ft were observed only sparsely during the four month period. Specific occurrences of contiguous samples of observed rain scatter at the higher altitudes were noted in the preceding section. However, isolated minutes of data throughout the total period were accumulated for the 20,000 and 30,000 ft common volumes as well as the off-path scattered signals. The cumulative distribution functions for some of these data are included in Appendix A, even though, in most instances, the number of minutes in each distribution is much too small for an adequate sample. For instance, on the cumulative time scale in percent, a total of at

least 500 minutes must be accumulated before the 0.2% probability level is equivalent to one clock-minute of data. Thus, the only distribution found to be somewhat significant above 10,000 ft is that for the D_{16} path, which is an "on path" common volume illuminated from the Quantico (TS-1) site.

The overall accuracy of the clock-minute median signal levels measured in the bistatic radio system has been estimated to be $\pm$ 5 dB or less for all path configurations. This estimate is based upon a comprehensive consideration of the precision and accuracy of individual system components, and the physical accuracies involved with antenna alignments. In addition, the estimate includes those system effects that reflect in the use of the simplified bistatic radar equation. The analyses performed in arriving at this value were quite extensive in both aspects, and are completely outlined by Levine, et al. [1972] for the instrumentation, and by Crane [1972] for the bistatic radar and raindrop distribution models.

It should be noted that the accuracy estimate is relative to any one specific clock-minute of data. The dynamic error on a minute-by-minute basis will approach a mean-zero value within this estimated bound. The total experiment error however, when averaged over the long-term cumulative analyses presented in this section, will be an rms value of the minute-by-minute errors, and thus considerably smaller than the $\pm$ 5 dB bound.

5.2 Comparison of Radio and Surface Rain Rate Data

Sections 2.1 and 2.2 have outlined the methods of comparing data in the Virginia experiment. It was noted that equations (15) and (16) can be used directly to compare measured values of interference with computed values where the surface rain rate (R_s) is substituted for the unknown rate (R_v) in the common volume. Also, equation (17) can be used to compute an effective rain rate (R_e) from the measured values of interference power (P_r) over any path. Both of these methods have been applied to the experimental data, and the results are presented in this section.

The analysis involving equations (15) and (16) begins with the distribution of surface rain-rates measured in the experiment. These distributions for the entire period from September 24, 1970, through January 31, 1971, are given in Appendix A. They include the distributions of the total rain measured at the 10,000, 20,000, and 30,000 ft subpoint gauges. The convective rain-rates measured at the 10,000 ft gauge are generally higher and longer in duration than those measured at the other points in the configuration. Appendix A also shows cumulative distribution curves (figure A-4) that combine the measurements from all three subpoint gauges, together with a summary table for all rainfall measured in the region of the experiment. The highest rate of 120 mm/hr noted in these distributions was measured prior to September 27, 1970, at which time the precipitation scatter measurements were begun. Thus, in the comparative analysis presented below, the rain-rate data used do not include the period prior to September 27, 1970. The highest rate recorded during the bistatic radio measurements, is on the order of 90 mm/hr, as seen later in this section.

Data from the bistatic CW radio system have been analyzed for each clock-minute in terms of median signal level. However, the mean signal power should be used in the bistatic radar equation. Thus, before the data were plotted in the comparisons between computed and observed values, the median signal level was converted to a mean power value for each clock-minute. The conversion was made as follows:

1) In detailed analysis, the distribution of the received signal within the minute (as recorded from the ES receiver) was found to be nearly Gaussian in dBm [Hull et al., 1970]*.

2) The normal distribution in dBm at the receiver output means that the power in the input signal is distributed as a log-normal variable. The mean power of the log-normal input signal can then be computed from [Beckmann, 1967],

$$\bar{p} = \exp\left[\frac{1}{2}\left(\frac{\sigma^2}{c}\right) + \frac{P_m}{c}\right], \tag{23}$$

where $\bar{p}$ = the mean power of the log-normal signal in mw

P_m = median power of the normal distribution in dBm

σ = standard deviation of the normal distribution in dB

c = constant = $10 \log_{10} e = 4.3429$

Converting (23) to dB, we have

$$\bar{P} = 10 \log \bar{p} = \sigma^2 / 2 + P_m$$

$$\approx P_m + 1.5 \text{ dB} \tag{24}$$

*Hull, J.A., P.L. Rice, R.W. Hubbard, and G.D. Thayer [1970], An experiment for the study of earth station-terrestrial station interference, Pt. 1 - Interference model for rain scatter and fixed-beam experiment, Telecommunications Tech. Memo. OT/ITSTM 14, unpublished report.

where the 1.5 dB is estimated from the average variance observed for the normal distribution of rain-scatter signals within the minute. The ES receiver process included a linear-log detector and a low-pass filter at the data output. This processing of a signal log normally distributed in power, results in a slight reduction in signal power at the receiver output. This reduction is estimated to be 1 dB for the ES receiving system used. Therefore, in all of the data plots presented in this section, each clock-minute median value has been corrected by +2.5 dB in order to report clock-minute mean power levels. This same correction factor has been used by Crane [1972], but is derived in a more rigorous fashion, starting with the premise that bistatic radar data are Rayleigh distributed.

In the analyses of these data, the measured surface rain-rate was converted to an effective or predicted received power level, using either equation (15) or (16) and the constants in table 1. A direct comparison of the converted rain-rate statistics with those measured in the bistatic CW radio system at S- and X-band frequencies is shown in figures 12 through 15 for typical path intersections at the 5000 and 10,000 ft common volumes. In each case, the 10,000 ft subpoint rain gauge data were used as noted above, deleting rain data for those periods of time when the radio signals were lost due to equipment or power failures. The total data sample (approximately 4 months) has not been sufficient to determine how well the bistatic radio data will relate to surface values at the higher rain-rates. However, significant trends may be observed in these data presentations, and in the following analyses.

For most engineering purposes, the intercomparison of rain-rate and bistatic radio data (as seen in figures 12-15) indicates that an adequate prediction of the probability of precipitation scatter can be made from the distribution of surface rain-rates for common volumes up to at least 10,000 ft altitude. This is particularly true if adjustments

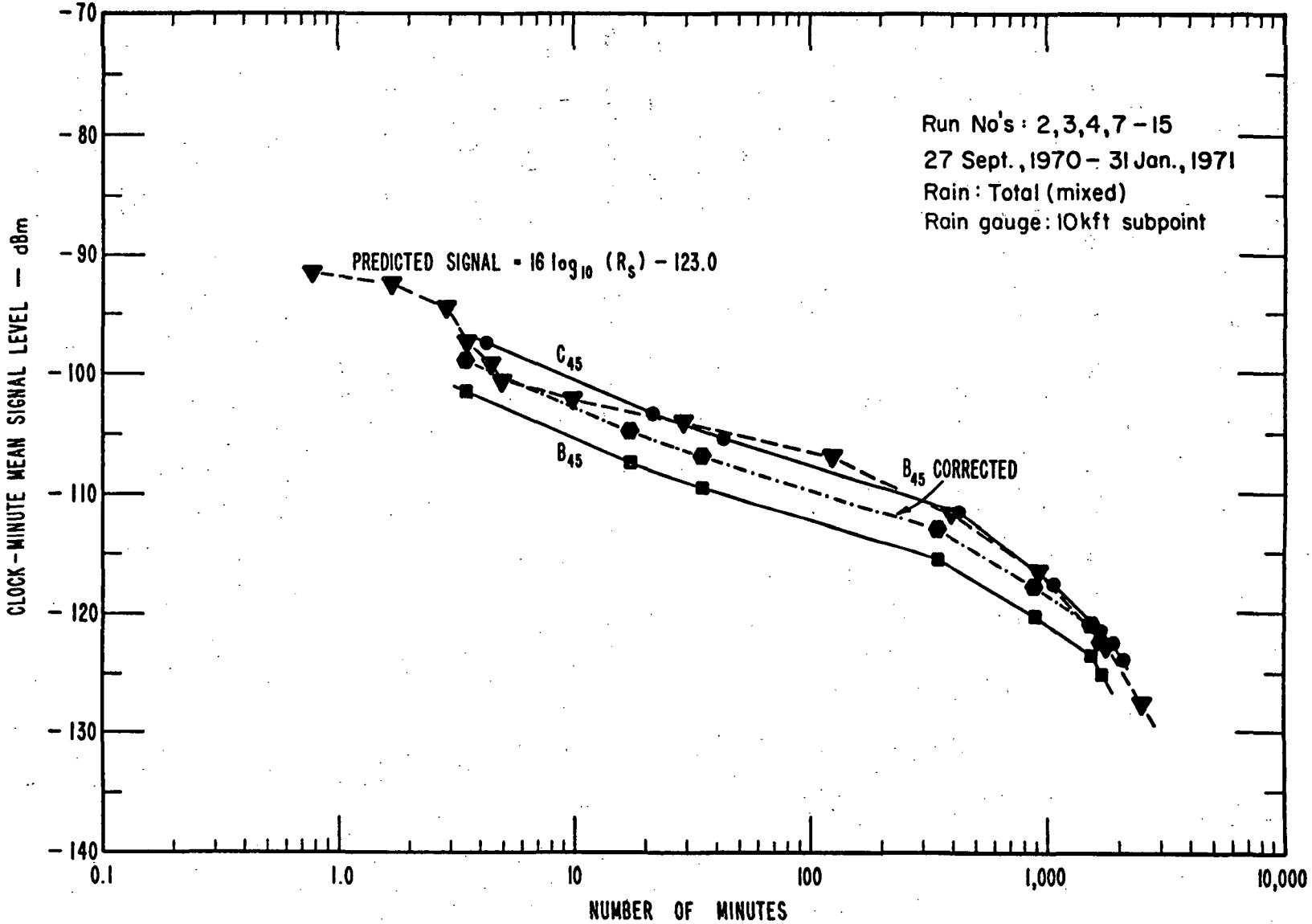

Figure 12. Intercomparison of data from Eastville (TS-4) for the 5000 ft and 10,000 ft common volumes (S-band data).

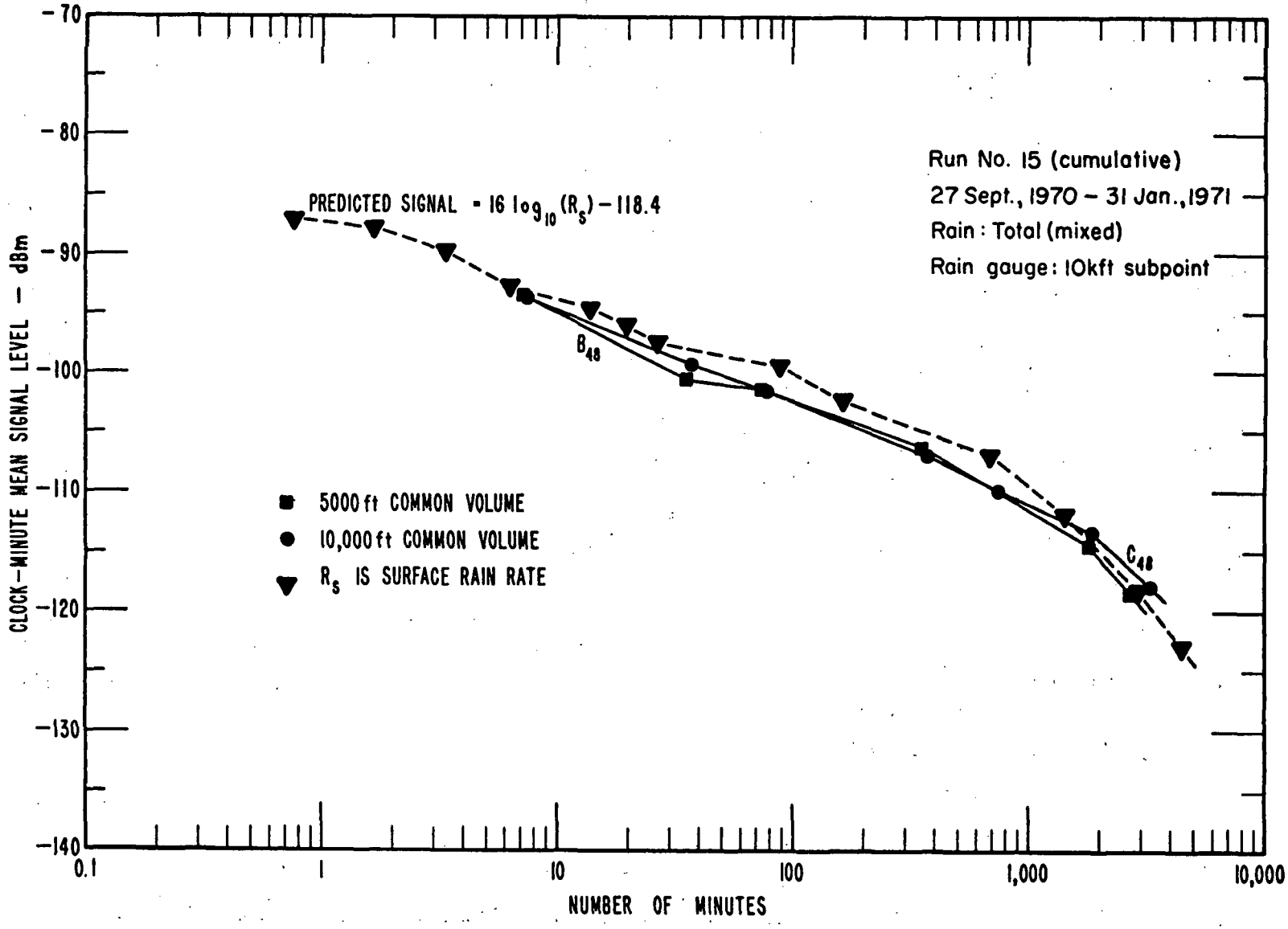

Figure 13. Intercomparison of data from Eastville (TS-4) for the 5000 ft and 10,000 ft common volumes (X-band data).

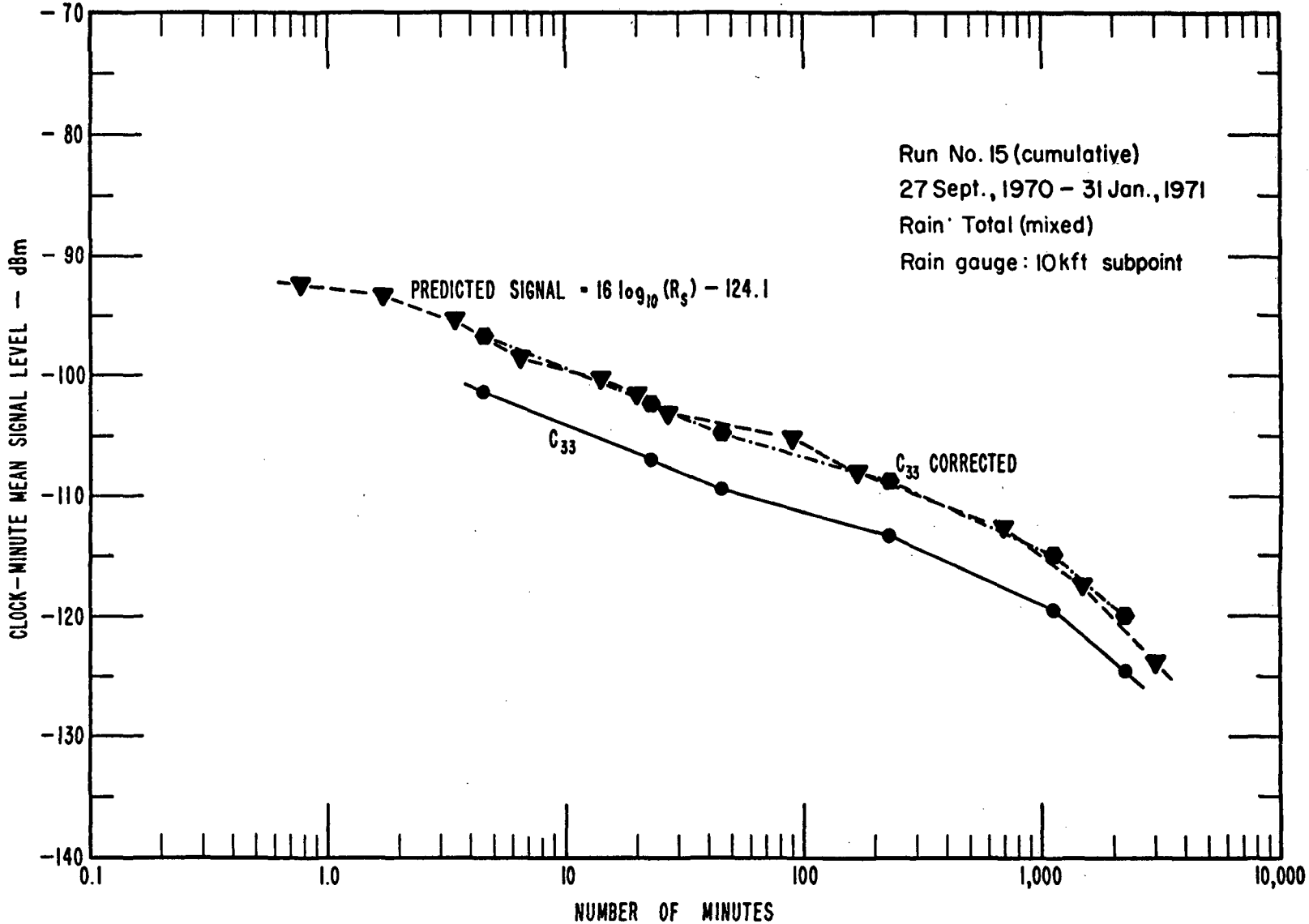

Figure 14. Intercomparison of data from Ft. Lee (TS-3) for the 10,000 ft common volume (S-band data).

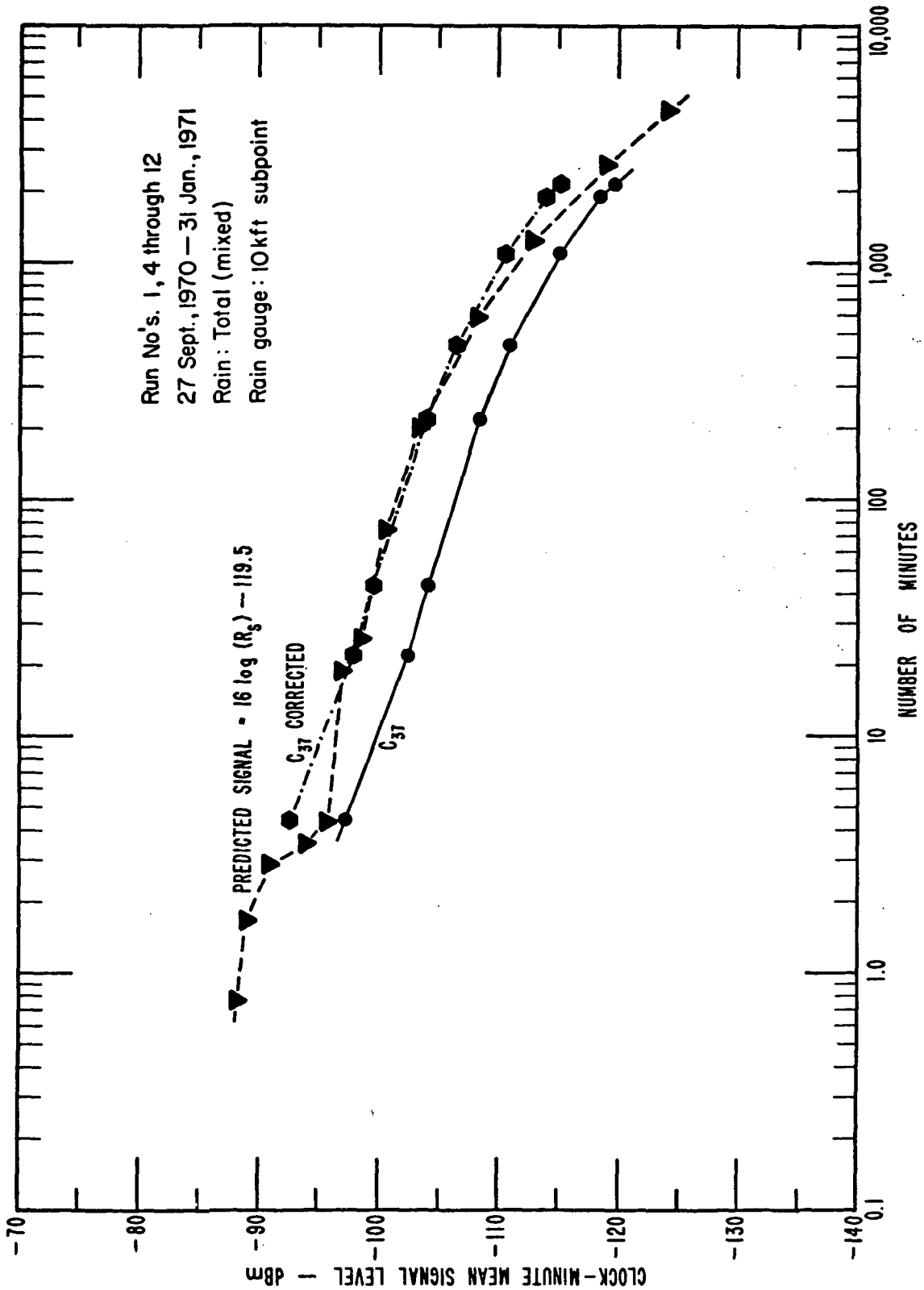

Figure 15. Intercomparison of data from Ft. Lee (TS-3) for the 10,000 ft common volume (X-band data).

to the data for paths B_{45} (figure 12), C_{33} (figure 14), and C_{37} (figure 15) are made in accord with the observations in section 5.1 for the antenna foreground blockage at the transmitter sites. For example, the data in the solid curves in these figures have not been adjusted. However, the noted foreground factors have been applied to the above three paths, and the corrected rain-scatter distributions are shown by the broken-line curves. The latter are seen to be very close to the predicted distribution based on the surface rain measurements.

These data plots are displayed in dBm, and are therefore relatively insensitive at the higher rain-rates because of the logarithmic scale. A more sensitive data comparison can be made by using (17), in which an effective rain-rate, R_e, is calculated from the measured interference power and compared with the surface value, R_s, on a linear scale. To illustrate the sensitivity of these calculations, the following analyses were made. First, we wished to observe the data for a single storm. Figure 16 is an analysis of a typical stratiform rain period which occurred on November 10-11, 1970. It can be seen that the radio data used to calculate an effective rain-rate, R_e, for this period were at best only a gross indication of the measured surface value, R_s. In addition, the highest measured rain-rate at the surface was not observed in the radio data, since it was measured for only 1 minute at the surface. There is no minute-by-minute guarantee that a surface rate will be observed in any given common volume aloft. A typical short convective storm was also analyzed which lasted for a period of about 105 minutes. It was found (data not presented) that the radio data were fairly accurate in predicting the observed rain-rates below about 22 mm/hr, but data were lacking for comparison above this rate to the maximum of 90 mm/hr which lasted less than a minute. These results are considered typical for short duration storms, particularly where the

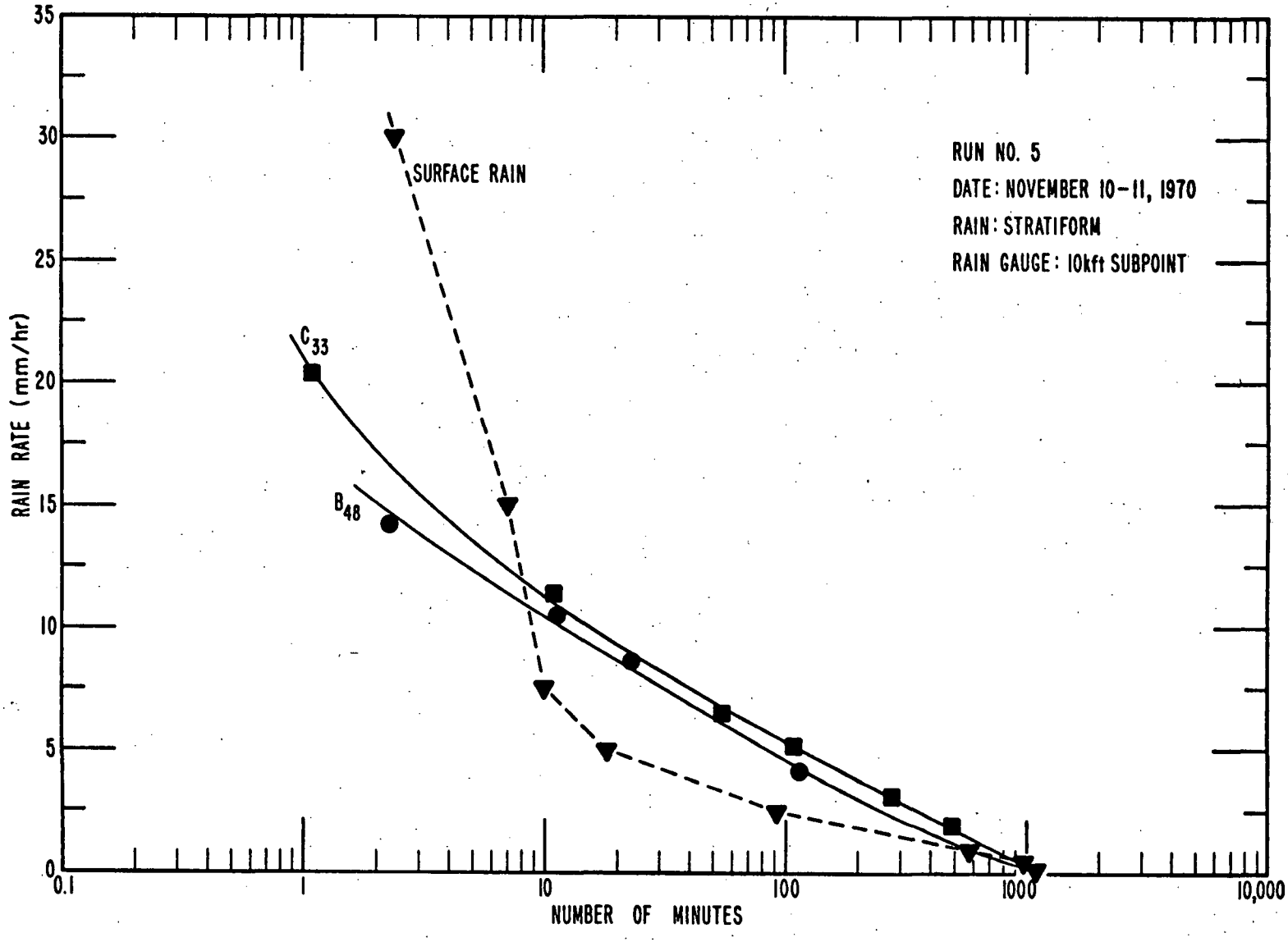

Figure 16. Comparison of measured and calculated rain-rates for a single stratiform rainstorm.

radio data are not collected continuously on any one path.

The primary reason for only partial agreement in these data calculations is the relatively small sample size of a single storm and the possible resolution of the rain measurement and the bistatic radio data. Better agreement is expected between R_s and R_e when comparisons are made over longer statistical samples, from which the radio data may be resolved to relatively lower intervals of time. Examples of such comparisons are shown in figures 17, 18, and 19, which cover all of the accumulated data for the period through January 31, 1971. The data presented in figure 17 are complete for the entire period, while those plotted in figures 18 and 19 are complete except for short periods of data during the run numbers that are omitted in the figures. The missing data were lost due to transmitter failures and a station power failure at the Eastville site (TS-4) during a storm in September 1970. The rain-rate distribution has been computed accordingly in these figures, by deleting the storm periods corresponding to the noted missing data. As in the previous figures, the data from paths with an antenna foreground blockage have been plotted directly as measured, and for corrected values based on the factors given in section 5.1.

Figures 17, 18, and 19 demonstrate that for cumulative data over many storms, better agreement between the surface and effective rain-rates is achieved. They also indicate that the R_e curves will depict the higher rain-rates aloft more accurately over longer periods of time. The total data sample reported is small relative to the year-long statistics sought in the total experiment, but results of this four month phase have been found to be informative. It is perhaps possible to detect in these data some height dependence between the 5000 ft and 10,000 ft common volumes. For example, note in both figures 17 and 18 that the 5000 ft data are lower than the 10,000 ft data as the curves approach the high rain-rates. If this trend persists in later accumulations, it could

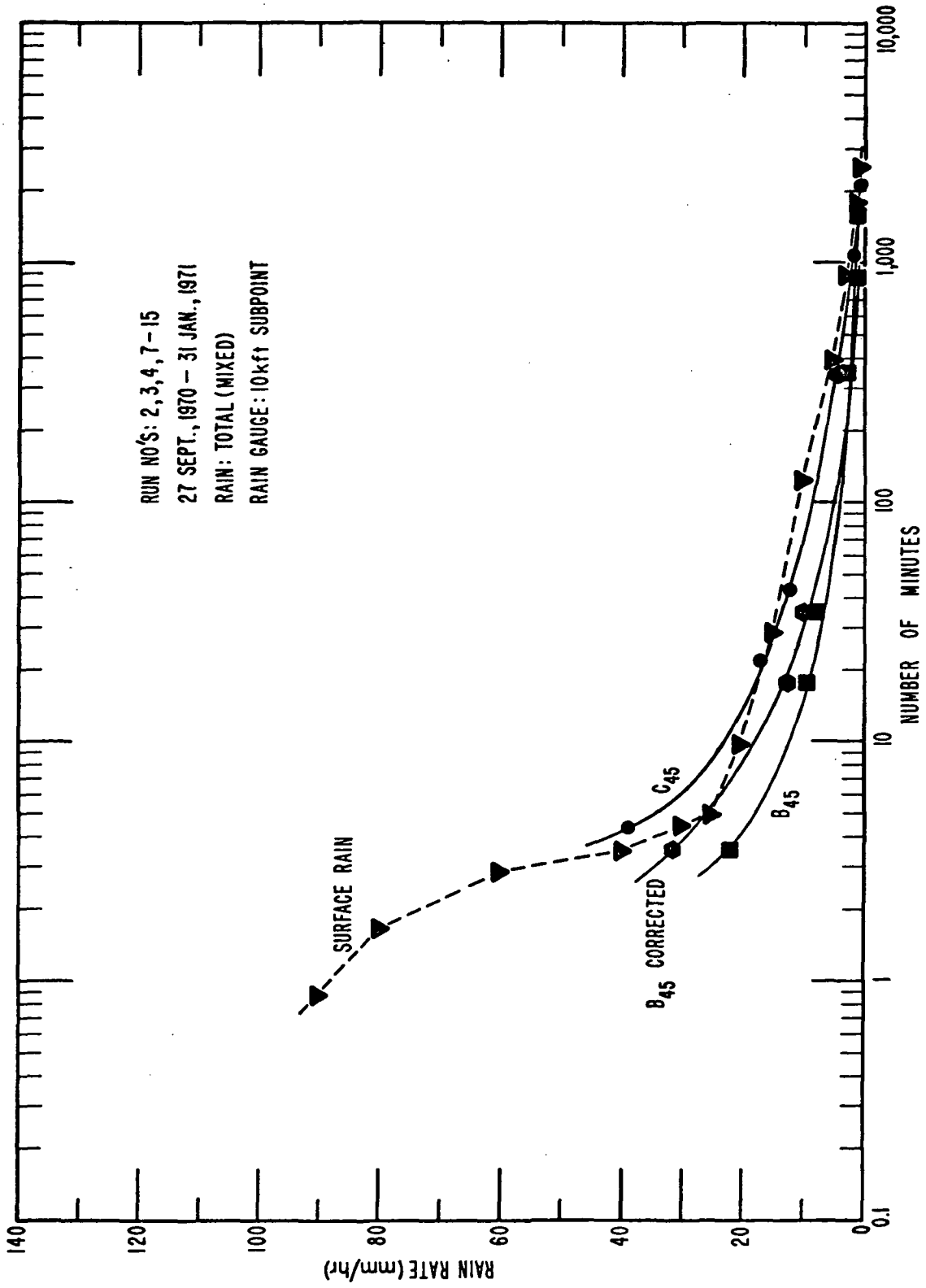

Figure 17. Comparison of measured and calculated rain-rates for total cumulative rainfall.

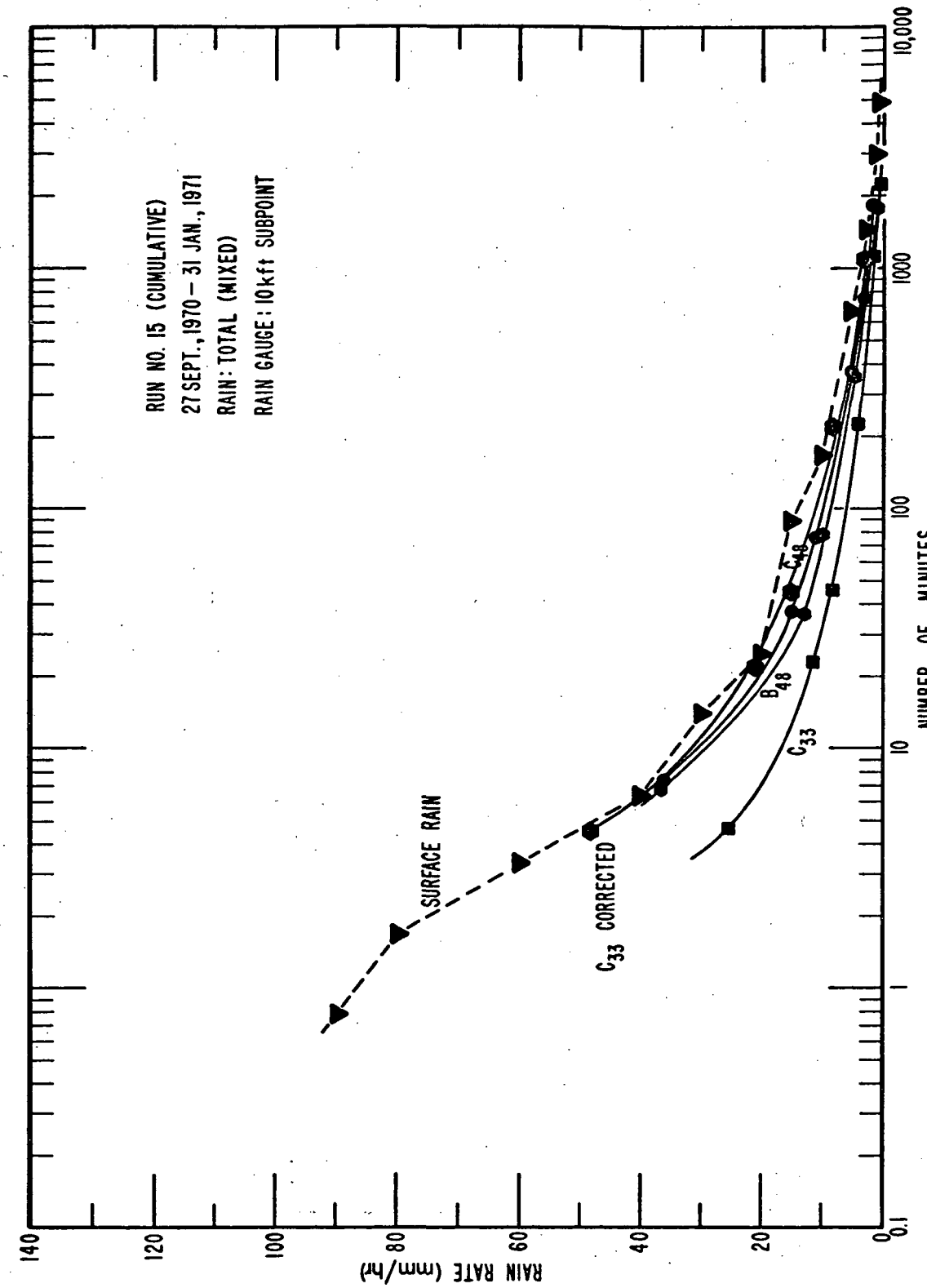

Figure 18. Comparison of measured and calculated rain-rates for total cumulative rainfall.

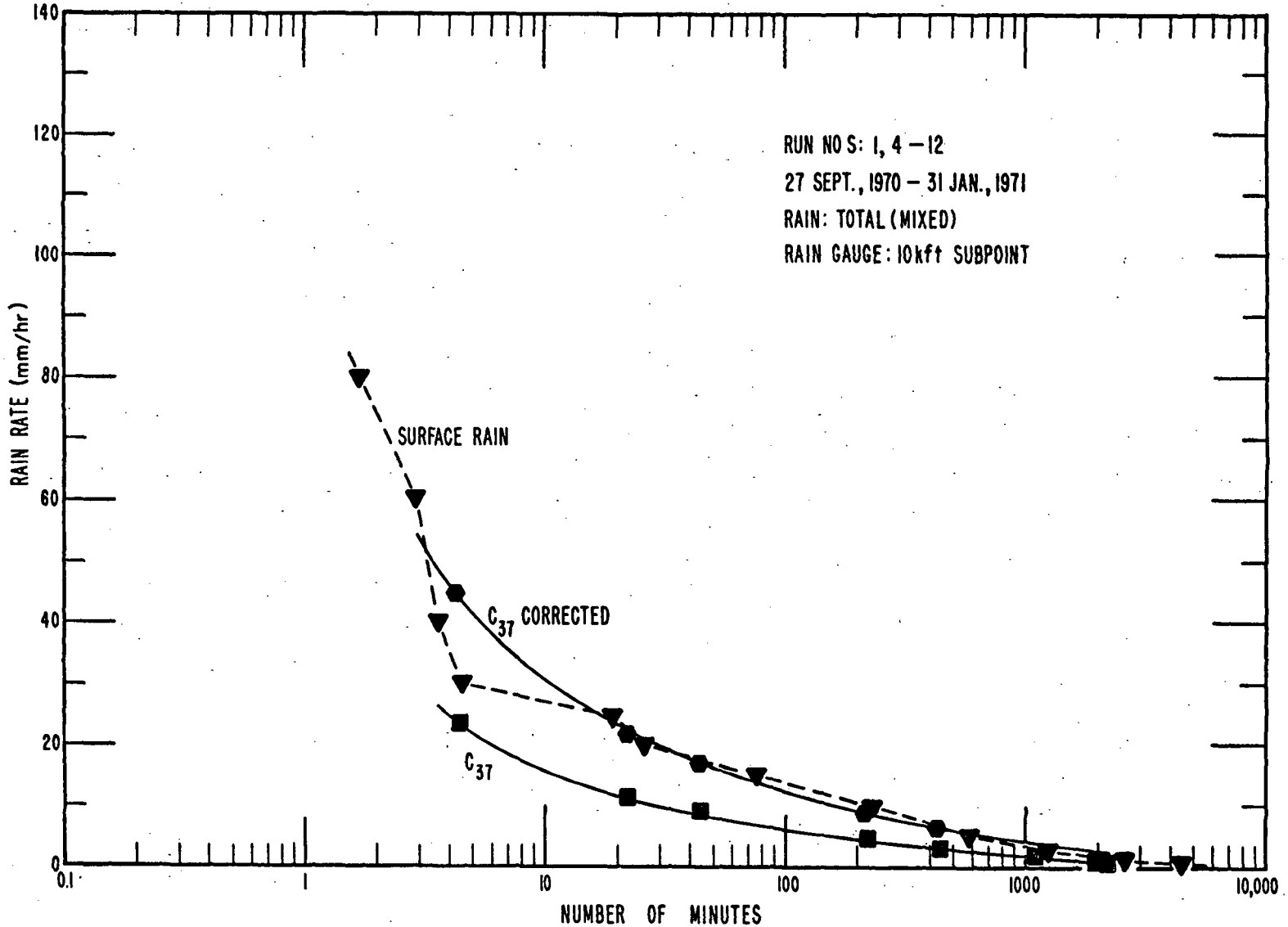

Figure 19. Comparison of measured and calculated rain-rates for total cumulative rainfall.

imply that the heavier rain is more dispersive in nature at 5000 ft as compared with rain at higher altitudes. This conjecture does not seem too improbable based on a study of highly convective thunderstorms [Culnan et al., 1965], but current data such as those in figures 17 and 18 are certainly inconclusive. Some empirical check on height dependence of this type, particularly above 10,000 ft, is expected as a final result of the fixed-beam experiment [Crane, 1972].

In all of the comparative analysis presented in this section, the clock-minute median signal levels and the number of accumulated minutes have been determined from the computer-derived cumulative distribution functions mentioned previously. As the data were processed, two distribution functions were compiled and plotted on the CRT at the end of each run. These were the distributions for the current run and a total cumulative plot for this and all previous runs. Fifteen computer runs were made for the analysis presented here, and the complete cumulative plots for the data analyzed are given in Appendix A. The starting day and minute at which data were first assimilated, and the total number of minutes accumulated for the plot are printed at the top of each computer printout. This information was compiled by the computer for each path, and was written automatically on the CRT plots. The total minute count was used to convert the percentage scale on the abscissa to total minutes as seen in the data plots in this section. The computer counts do not reflect calibration periods, however, and some adjustment was necessary in the analysis. For example, the calibration period was 15 minutes (usuall every two hours) during which time data were not recorded. These minutes were accounted for manually in the analysis to determine the total minutes for each distribution, using the following criteria. If data were observed both before and after a calibration period, the 15 minutes of calibration time was added to the computer count assuming that data would have been recorded. If data were observed only before or after a

calibration, the calibration minutes were not added to the computer count. A good agreement between total number of rainy minutes and the bistatic radio clock-minutes has been found using this procedure. Evidence of this agreement is seen in the data plots in this section.

The total number of bistatic radio clock-minutes compiled in the cumulative data given in Appendix A were calculated in accordance with the switching sequence given in table 7. Note from this table that, in most instances, the data were sampled for only one minute out of each four-minute time block. Thus, the total number of minutes of radio data used for comparative purposes in this section was derived by multiplying the number of accumulated minutes by 4. This, of course, assumes that the distribution for each unobserved minute within the block would have been essentially the same as the observed minute. As a check on this assumption, the data for path C_{22} are informative. This path was monitored on the first and third minute of each four-minute block. The data for the first and third minute were accumulated separately in the computer routine, and, as can be seen from the cumulative functions in Appendix A, the two distributions are nearly identical. This provides reasonable assurance that the sampling rate for the radio clock-minute data was adequate.

5.3 Relationship to Rainfall Statistics Model

The statistical model of surface rainfall rates developed by Rice and Holmberg [1972] is based upon the sum of individual exponential modes of rainfall rates, each with a characteristic average rate, $\bar{R}$. The temporal statistical data used in developing this model were taken from a great many rain gauge stations and for periods spanning many years of data. The data have shown that the average rainfall rate for each of the modes is fairly constant, but the coefficients that represent the total number of rainy t-minute periods for each mode are relatively more variable from year to year and station to station or climatic region. According to the descriptive analysis proposed for summarizing the cumulative time statistics of surface rainfall rates at a point,

$$\text{Rainfall} = \text{Mode 1 rain} + \text{Mode 2 rain}, \tag{25}$$

where the exponential distribution chosen to describe "Mode 1 rain" corresponds to a physical analysis of thunderstorms, while "Mode 2 rain", represented by the sum of two exponential distributions, is simply "all other rain".

The average annual total rainfall depth, M, is the sum of the contributions of the two modes, M_1 and M_2;

$$M = M_1 + M_2 \ \text{mm}, \tag{26}$$

and the ratio of "thunderstorm rain", M_1, to total rain, M, is

$$\beta \equiv M_1 / M. \tag{27}$$

The number of hours of rainy t-minute periods for which a surface point rainfall rate R is exceeded is the sum of contributions from the two discrete modes:

$$T_t(R) = T_{1t}\, q_{1t}(R) + T_{2t}\, q_{2t}(R) \text{ hours}, \tag{28}$$

where

$$T_{1t} = M_1/\overline{R}_{1t} = \beta\, M/\overline{R}_{1t} \text{ hours}, \tag{29}$$

$$T_{2t} = M_2/\overline{R}_{2t} = (1-\beta)\, M/\overline{R}_{2t} \text{ hours}, \tag{30}$$

and

$$q_{1t}(R) = \exp(-R/\overline{R}_{1t}), \tag{31}$$

$$q_{2t}(R) = 0.35 \exp(-0.453074\, R/\overline{R}_{2t}) + 0.65 \exp(-2.857143\, R/\overline{R}_{2t}), \tag{32}$$

The quantities $\overline{R}_{1t}$ and $\overline{R}_{2t}$ are average annual Mode 1 and Mode 2 rainfall rates. For t = 1, the parameter R represents clock-minute rates, and the values from the model are $\overline{R}_{11} = 100/3$ mm/hr, and $\overline{R}_{21} = 1.75505$ mm/hr. Therefore, for clock-minute rates, $T_1(R)$ may be written as

$$T_1(R) = M\left\{0.03\,\beta \exp(-0.03R) + 0.2(1-\beta)\left[\exp(-0.258R) + 1.86\exp(-1.63R)\right]\right\} \text{ hours} \tag{33}$$

Figure 20 shows $T_1(R)/M$ plotted versus R and the parameter β, and Figure 21 and 22 are world maps of M and β, respectively.

In general, $\overline{R}_{1t}$ and $\overline{R}_{2t}$ are functions not only of t, but also of M and the number of rainy days, D/24, in an average year. Figure 23 shows average-year cumulative distributions $T_t(R)$ versus R for t = 1, 5, 30, 60, 360, and 1440 minutes (1 day) for M = 1000 mm (40 inches),

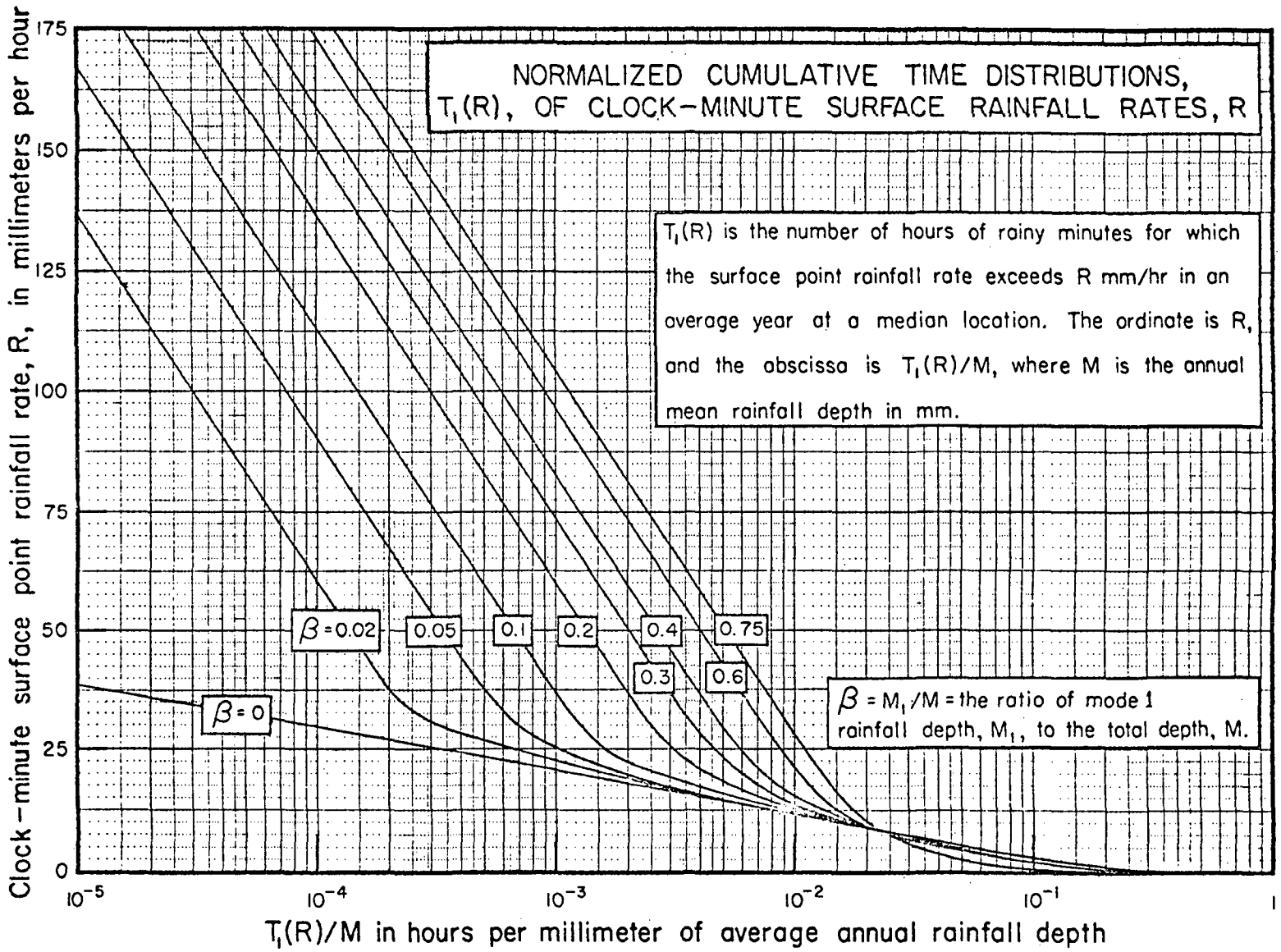

Figure 20. Normalized cumulative time distributions of clock-minute surface rainfall rates.

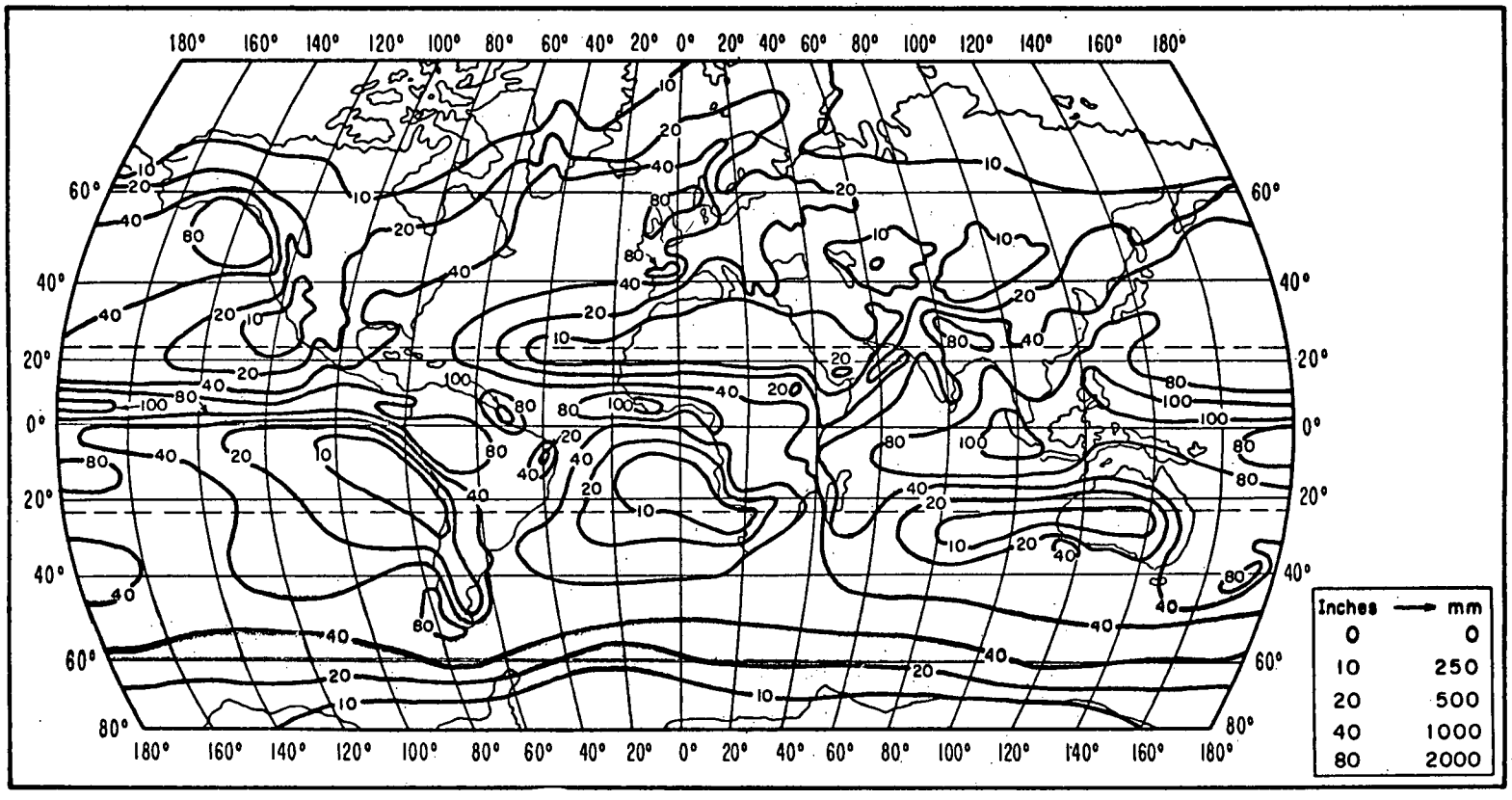

Figure 21. World contour map of mean annual depth of precipitation, M.

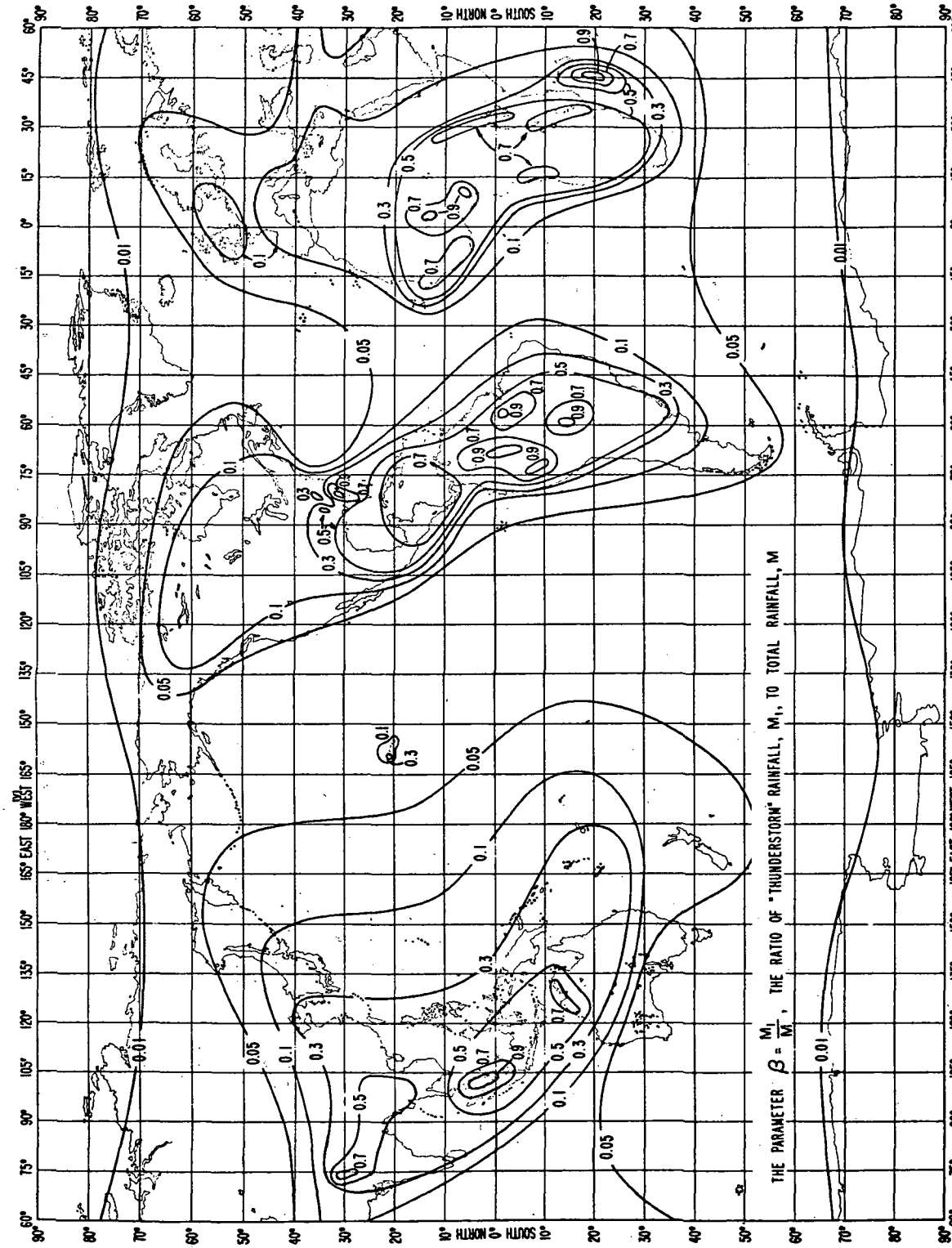

Figure 22. World contour map of the ratio of "thunderstorm" rainfall to total rainfall depth, β.

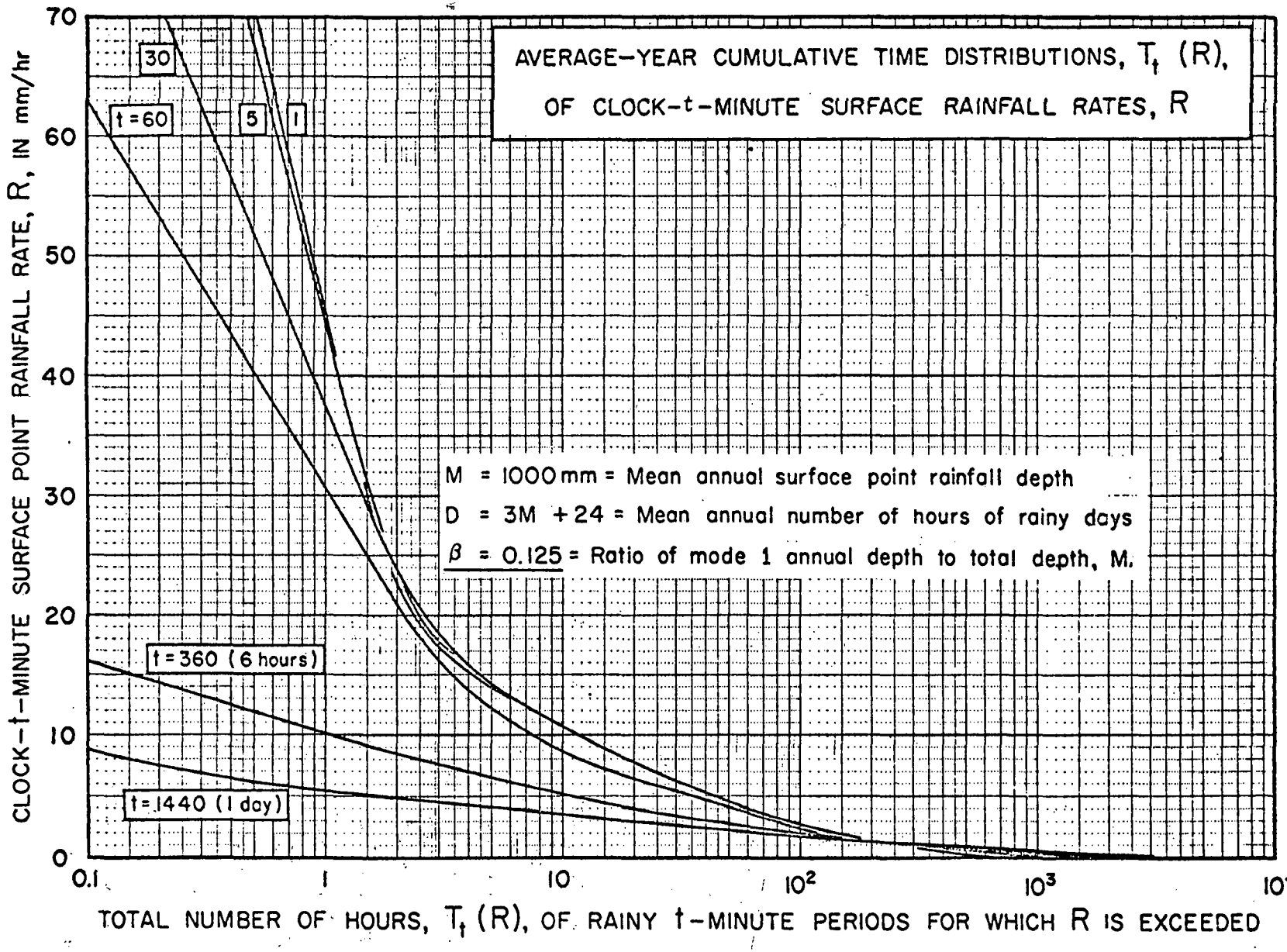

Figure 23. Average-year cumulative time distributions of clock-t-minute surface rainfall rates.

$D = 3M + 24$ hours (a good average for U.S. stations), and $\beta = 0.125$. For $t = 60$ minutes, Figure 24 shows similar estimates for Norfolk, Va., compared with the average of observed clock-hour rate durations $T_{60}(R)$ for the period 1951-1960. The cumulative distribution is shown for both $R(T_{60})$ and $16 \log_{10} R(T_{60})$.

The data upon which this model is based include: (1) average-year cumulative distributions of clock-hour rates (mostly for the years 1951-1960), for a total of 63 stations, 49 in the continental U.S.; (2) distributions for all 15-year averages with $t/60 = 6$, 12, and 24 hours for 22 of these stations; (3) short-duration excessive precipitation storm data with $t = 5$, 10, 15, 20, 30, 45, 60, 80, 100, 120, and 180 minutes; (4) a U. S. map of the highest 5-minute rates observed in a two year period; and (5) maximum monthly accumulations for the period 1931-1960 for 17 U. S. stations and 135 additional stations reported by the World Meteorological Organization.

The data sample that has been analyzed for this report is not adequate to make a conclusive comparison with the rain-rate model. The model is based on conditions for an average year, and the measured rain data from the experiment represents approximately 35% of the year. However, the statistical rain-rate data presented in Appendix A have been used to make a comparison with the model for a partial year in the southern Virginia region. For example, the statistical model given by (33) for this region estimates a total of 7.34 hours of rainy minutes of Mode 1, and 513.63 hours for Mode 2 in an average year. Combining the two modes, the model estimates a total of 521 hours of rainy minutes. It is not strictly correct to adjust this estimate for a partial year, as the distribution of rainfall over the year is not uniform. However, if this is done, the model would estimate the total number of hours of rainy minutes for the experiment period (35% of a year) to be 182. This compares favorably with the actual measured value of 157 hours for the 10,000 ft subpoint

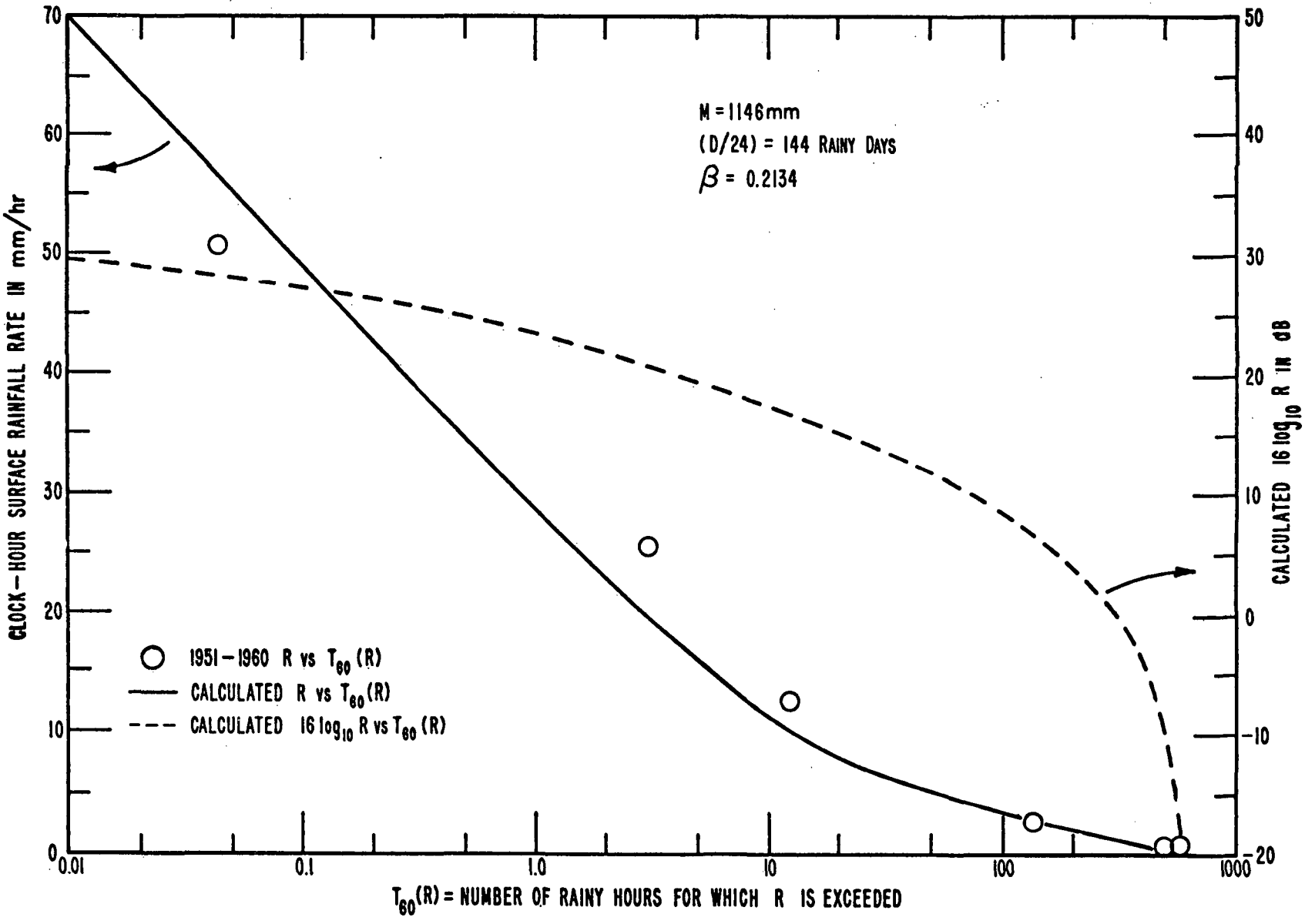

Figure 24. Average-year cumulative distribution of clock-hour surface rainfall rates for Norfolk, Virginia.

rain-gauge. The accuracy of the gauge method to resolve rain-rates of 1 mm/hr or less is, however, low. Comparing only those rates above 1 mm/hr, the model estimates 76 hours of rainy-minutes for the partial year, and the measured value is approximately 61 hours.

In these calculations from the model (33), the values of M = 1146 mm and β = 0.2134 for Norfolk, Va. have been used as shown in figure 24. The results are seen to compare quite well, and provide the only point check possible for the Rice and Holmberg model at this time.

6. SUMMARY

This report has described an experiment designed to obtain a statistical measure of bistatic radio interference between a simulated satellite receiver and terrestrial microwave communication systems. The measurements were made in the 4 and 8 GHz frequency bands which these services share in assignment. One of the basic objectives of the experiment is to determine how well measurements and/or known temporal distributions of surface rainfall can be used to predict interference between these services due to precipitation scatter. Rain or other hydrometeors can cause serious interference levels by scattering energy from one antenna system into another. Such interference is more probable when hydrometeors exist in the space defined by antenna beam intersections, but can also occur when energy is scattered from one antenna main beam into the side-lobes of another.

Methods for prediction of the precipitation scatter interference are necessary to establish new coordination procedures in the planning phases for satellite and/or terrestrial microwave communication facilities. Previous recommendations of the CCIR for coordinating between these services did not include specific consideration of precipitation scatter interference. The Virginia experiment and others looking into this problem have shown that this type of interference can be significant when antenna beams are likely to intersect at altitudes below about 20,000 ft.

Results of the experiment presented in this report cover the period from mid-September, 1970, through January, 1971. This represents approximately one-third of the planned experiment year, and does not include the high-rain season for southern Virginia. The results for the period, however, have been very useful in testing the stated prediction hypothesis, and have been used by the CCIR and the World Administrative

Radio Conference (WARC) in their consideration of rain-scatter models for new coordination procedures. The separation of transmitter and receiver sites in the experiment are shown to be within or near the coordination distances previously recommended for the satellite-terrestrial services. Thus, the observed duration and levels of interference due to the precipitation scatter mechanism were found to be quite useful in developing the proposed new coordination procedures.

Measured surface rain-rates and the bistatic radio interference levels observed are directly compared in the data analysis. Temporal distributions of the surface rain-rates are converted to equivalent radio interference levels using the simplified bistatic radar theory, and a fairly standard relationship between Z (radar reflectivity) and R, the surface rain-rate. This conversion derives a predicted interference distribution curve for each common volume intersection in the experiment, and is compared directly with the distribution of the measured radio interference. The process is also reversed in the analysis, converting the bistatic interference level to an effective rain-rate distribution in the common volume. These curves are then compared with the temporal distribution of the surface rain-rate, measured by tipping-bucket gauges located at the sub-points of the common volume intersections of the antenna patterns.

The first comparison has shown that the surface rain-rate calculations could have been used to predict the clock-minute interference signal distribution to within 1 to 3 dB for the common volumes up to 10,000 ft above the surface. The data sample was insufficient to test the prediction above this altitude. The second data comparison has shown that the calculated effective rain-rate distributions in the common volumes match the measured surface distribution to within ± 5 mm/hr or better for surface rates below about 40 mm/hr. Again, the data sample and resolution of the bistatic radio data preclude a comparison

above this rate. However, the data plots indicate that the radio data will reasonably predict the higher rain-rate distribution when the data sample has been increased.

In addition to the comparison of the measured temporal statistics noted above, a cursory comparison of the experiment results with a model of the temporal rainfall statistics developed by Rice and Holmberg [1972] has been made (section 5.3). Even though the total data sample is less than the desired year, a reasonable agreement between the observation and the model has been seen. This aspect is important, as the Virginia experiment can be used as an "anchor point" in geographic area to test the Rice and Holmberg or other models of the temporal rainfall distribution. Successful comparison of the model and measurement for the Virginia region then permits the extension of the model for use in predicting interference in other geographic regions.

In summary, it is concluded that the Virginia precipitation scatter experiment has provided the first well-defined temporal data relative to the rain-scatter interference problem between satellite and terrestrial communication systems. This experiment, together with efforts to model the problem, has been instrumental in defining new coordination procedures which will enhance interference-free operation of these services.

As noted in the Foreword, the balance of data from this experiment (February through September, 1971) is on file at the ITS Laboratories. Available funding did not permit the continued computer analyses. A hand analysis has been made, however, for a limited number of paths at the S-band frequencies, and are reported by Crane (1972). His results include the high-rain season (the summer months) for Virginia, and substantiate the conclusion drawn in this report for rain-scatter statistics up to 10,000-ft altitudes. The additional data also reflect an observed height dependence of the scatter effects above 10,000 ft, as noted in section 5.2.

7. ACKNOWLEDGMENTS

This study of the scatter of radio energy by rain was a joint undertaking of the National Aeronautics and Space Administration (NASA) and the Institute for Telecommunication Sciences (ITS), with the guidance of a special committee composed of the Office of Telecommunication Management (now Office of Telecommunication Policy (OTP)), NASA, ITS, and the Federal Communications Commission. The authors wish to express their particular appreciation to the NASA Program Manager, Dr. Jerome Eckerman, and to the Project Technical Officer, Mr. Francis X. Downey.

Within ITS, many individuals (too numerous to name them all) contributed to this project. However, the authors wish to extend their special thanks to: Mr. L. G. Hause, who was responsible for the design, installation, and testing of the bistatic radio system; Mr. D. V. Glen, who was responsible for the data recording and telemetry systems; Dr. D. R. Wortendyke, who was responsible for the surveillance radar; Mr. G. D. Thayer and Mr. C. M. Miller, who were responsible for the rain gauge and meteorological systems and for processing the meteorological data; the field operations crew, consisting of Messrs. L. G. Hause, F. G. Kimmett, D. R. Wortendyke, D. V. Glen, R. L. Ehret, J. B. Wood, R. D. Moody, W. L. Dobbin, W. L. Robinson, G. E. Evers, F. Shute and R. I. Juneau; and to those responsible for the computer reduction of the bistatic radio data, Messrs. J. A. Payne, D. V. Glen, J. B. Wood, and R. I. Juneau.

The authors also wish to thank all of the ITS personnel who helped in the preparation of the manuscript, and the technical reviewers for their many helpful suggestions.

8. REFERENCES

Altman, F. J. [1970], Prediction of hydrometeor reflectivity profiles, Computer Sciences Corporation Report No. 6012-1 and 6012-A, Falls Church, Va., 22046.

Austin, P. M. [1969], Application of radar to measurement of surface precipitation, Final Report to U. S. Army Electronics Command on Contract DAAB 07-67-C-0319, March.

Austin, P. M. [1971], Some statistics of small-scale distribution of precipitation, Dept. of Meteorology, Mass. Institute of Technology, Scientific Report No. 1 under Contract NASA/ERC 0420, February.

Beckmann, P. [1967], Probability in Communication Engineering, Harcourt, Brace & World, Inc., New York, New York.

Carey, R. B. and G. S. Kalagian [1969], Detailed analysis of FCC/USAF POPSI Project Data, URSI-Fall Meeting, Austin, Texas, December.

CCIR [1966a], Doc. IV/Part 2, Space Systems, Radioastronomy, CCIR XIth Plenary Assembly, Oslo, 1966, Report 382, 356-368.

CCIR [1966b], Models of phase-interference fading for use in connection with studies of the efficient use of radio-frequency spectrum, Documents of the XIth Plenary Assembly, ITU, Geneva, Report 415, 73-89.

CCIR [1966c], Operating noise-threshold of a radio receiving system, Documents of the XIth Plenary Assembly, ITU, Geneva, Report 413, 5-58.

CCIR [1970], Doc. V/1039-E, CCIR XIIth Plenary Assembly, New Delhi, 5 November 1969.

CCIR [1971], Report of the Special Joint Meeting of CCIR Study Groups, 4 February to 4 March, Chapter 10, Annex 1.

Crane, R. K. [1970], A comparison between monostatic and bistatic scattering from rain and thin turbulent layers, MIT Lincoln Laboratory Technical Note 1970-29.

Crane, R. K. [1972], Virginia precipitation scatter experiment--data analysis, NASA/GSFC X-750-73-55, to be published.

Critchfield, H. J. [1960], General Climatology, Prentice-Hall, Englewood Cliffs, New Jersey.

Culnan, D. E., F. O. Guiraud, and R. E. Skerjanec [1965], Radio scattering cross sections of thunderstorms, NBS Report. 8816, June.

Donaldson, R. J., Jr. [1961], Radar reflectivity profiles in thunderstorms, J. Meteor. 18, No. 3, 292-305.

Dutton, E. J., and H. T. Dougherty [1973], Modeling the effects of clouds and rain upon satellite-to-ground system performance, to be published as an Office of Telecomm. Report OTR 73-5.

Federal Communications Commission [1965], Rules and Regulations #25, Subpart C - Technical Standards, Sections 25. 201 through 25. 500.

Gusler, L. T., and D. G. Hogg [1970], Some calculations on coupling between satellite communications and terrestrial radio-relay systems due to scattering by rain, Bell Systems Tech J., Sept.

Levine, E., R.K. Crane, P.I. Wells, and F.X. Downey [1972], Virginia precipitation scatter experiment - experiment description, NASA/GSFC X-Document.

Longley, A.G., and P. L. Rice [1968], Prediction of tropospheric transmission loss over irregular terrain - A computer method, ESSA Technical Report No. ERL 79-ITS 67, July.

Rice, P.L., A.G. Longley, K.A. Norton, and A.P. Barsis [1967], Transmission loss predictions for tropospheric communication circuits, NBS Technical Note 101, Vol. I and II, Revised. (NTIS Access Nos. AD 687820 and AD 687821)

Rice, P.L. [1970], Modeling radar reflectivity statistics, Draft Report to CCIR Study Groups 4/1080, 5/17, December.

Rice, P.L., W.I. Thompson, III, and J.L. Noble [1970], Idealized pencil-beam antenna patterns for use in interference studies, IEEE Trans. on Comm. Tech., COM-18, No. 1, February.

Rice, P.L., and N.R. Holmberg [1973], Cumulative time statistics of surface rainfall rates, a paper presented at the 1972 Fall Meeting, URSI, Williamsburg Conference Center and College of William and Mary, Williamsburg, Va., Dec. 12-15 (to be published).

Rinehart, R.E., D.W. Staggs, and S.A. Changnon, Jr. [1968], Identification of hail and no-hail echoes, 13th AMS Radar Conference, McGill University, Montreal, Canada, 20-23 August, pp. 422-427.

APPENDIX A

Total Cumulative Distribution Plots of Surface Rain-Rate and Bistatic Radio Data

This appendix contains the total cumulative distribution plots of the surface rain-rate measurements, and the bistatic radio data accumulated in the computer process described in section 4.1. A complete tabulation of the cumulative rain-rates used for the data comparisons in section 5 is also given in table A-1. A total of 15 computer runs were used in analyzing the radio data. Table A-1 indicates the rain tabulation relevant to each of the computer run numbers.

Figures A-1 through A-4 present the cumulative distributions of the surface rain-rates, measured at the 10,000, 20,000, and 30,000 ft subpoint gauges.* Figures A-5 through A-15 present the cumulative distribution functions of the bistatic radio data for the 5000 and 10,000 ft common volumes used in the comparative analysis in section 5, and for other path configurations where data were accumulated.

---

* The data for the 5000 ft subpoint gauge are not included, as this gauge was out of service for an extended period due to malfunction.

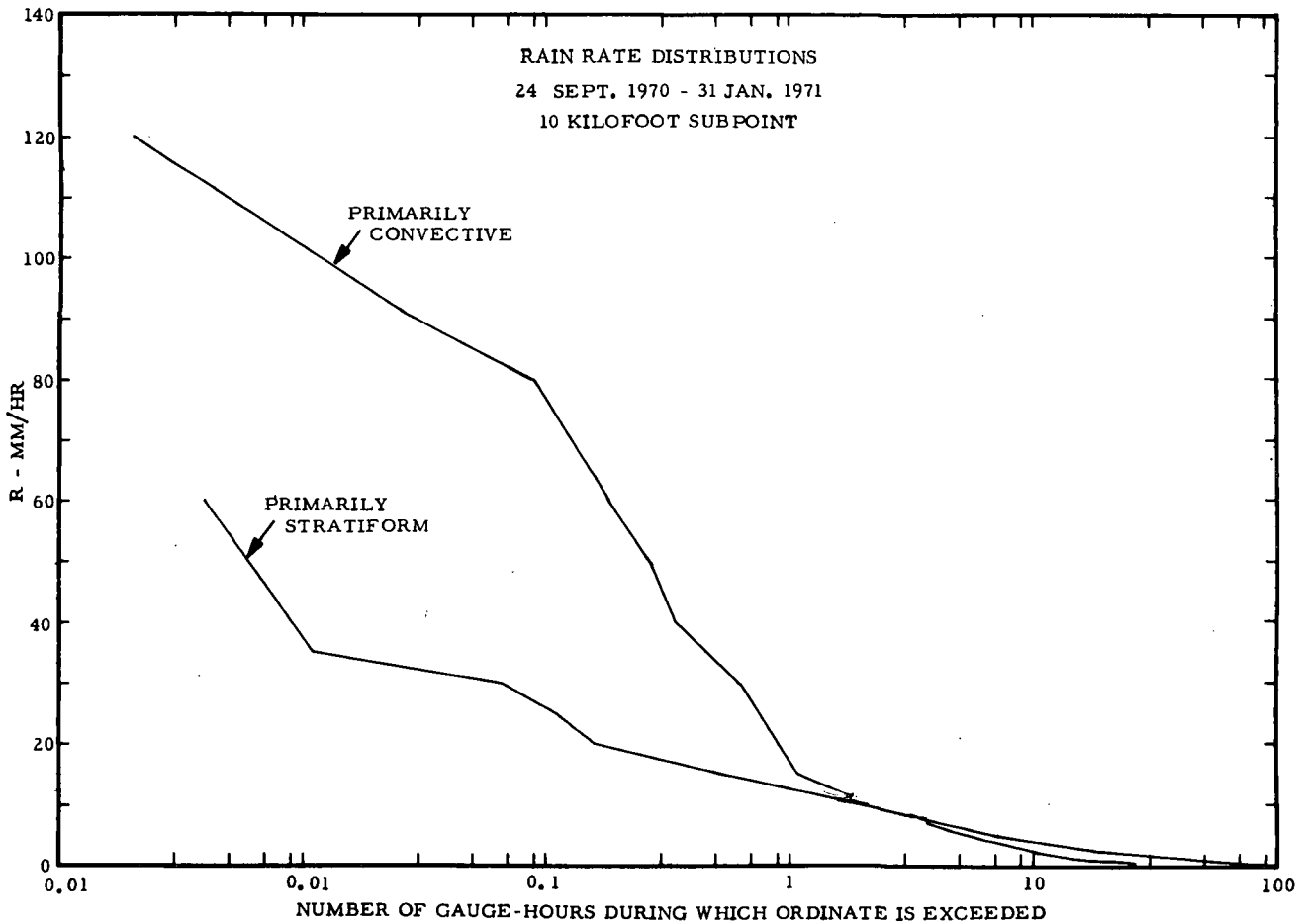

Figure A-1. Rain-rate distributions measured at the 10,000 ft subpoint gauge, Sept. 24, 1970 - Jan. 31, 1971.

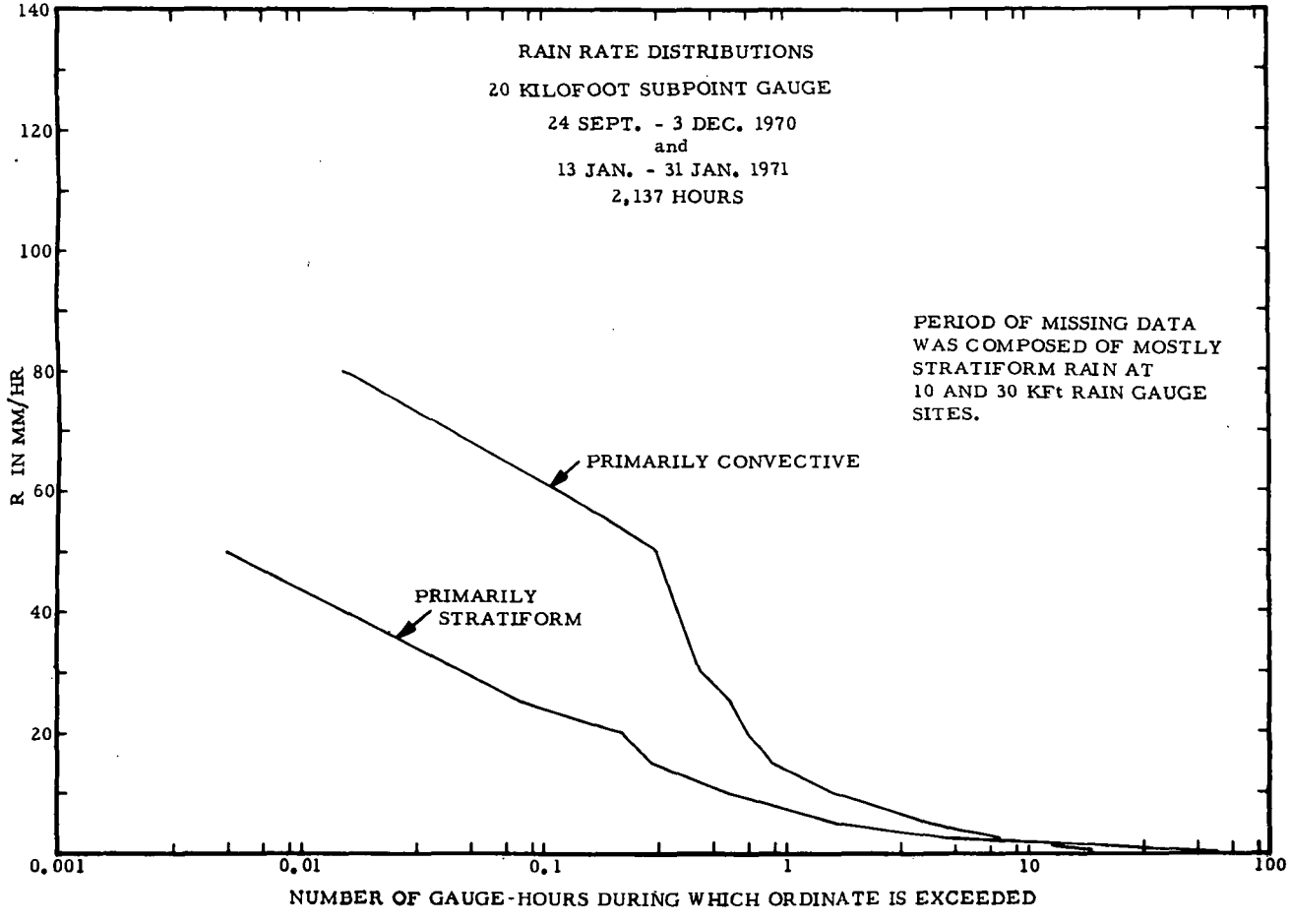

Figure A-2. Rain-rate distributions measured at the 20,000 ft subpoint gauge, Sept. 24 - Dec. 3, 1970 and Jan. 13 - Jan. 31, 1970.

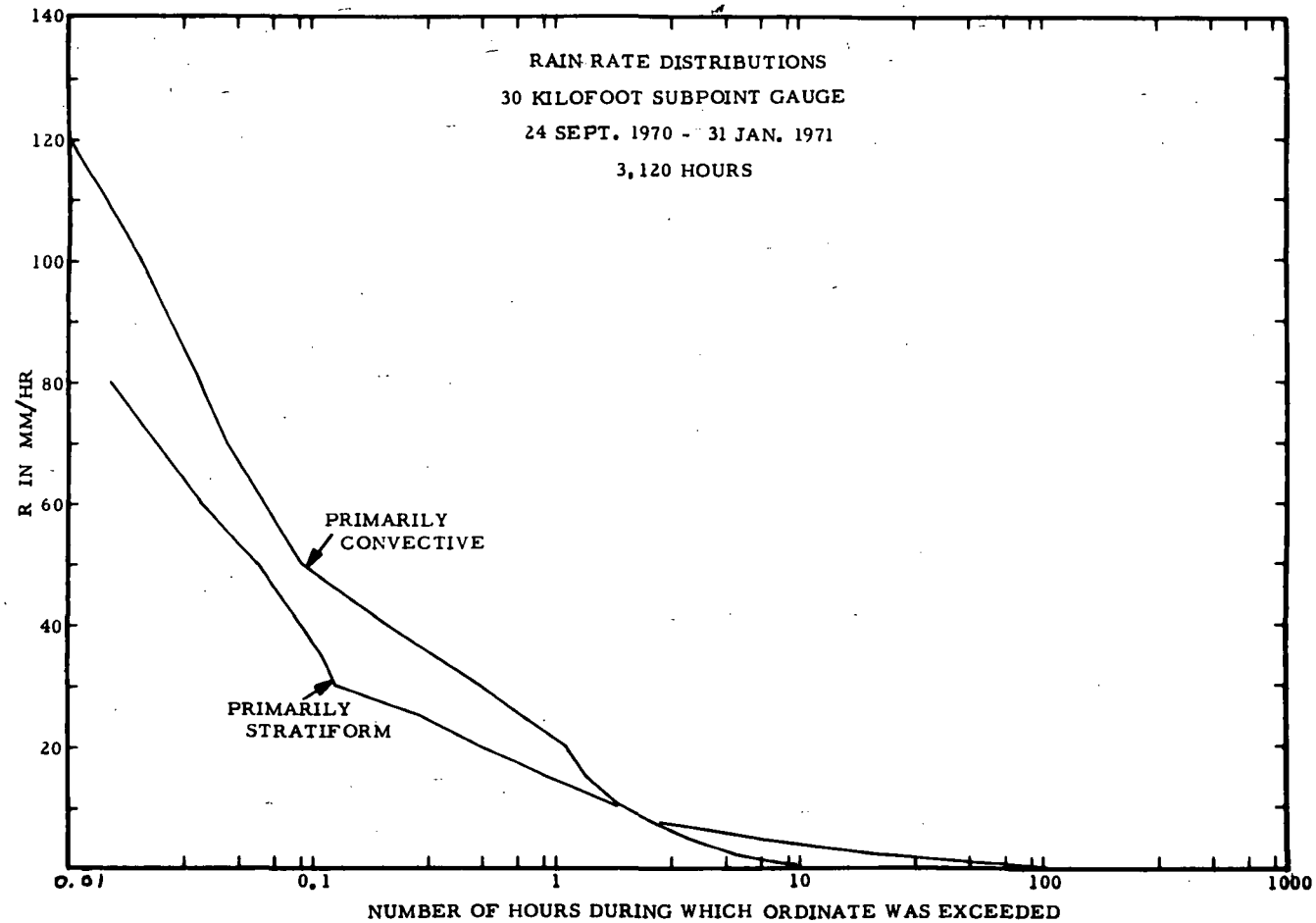

Figure A-3. Rain-rate distributions measured at the 30,000 ft subpoint gauge Sept. 24, 1970 - Jan. 31, 1971.

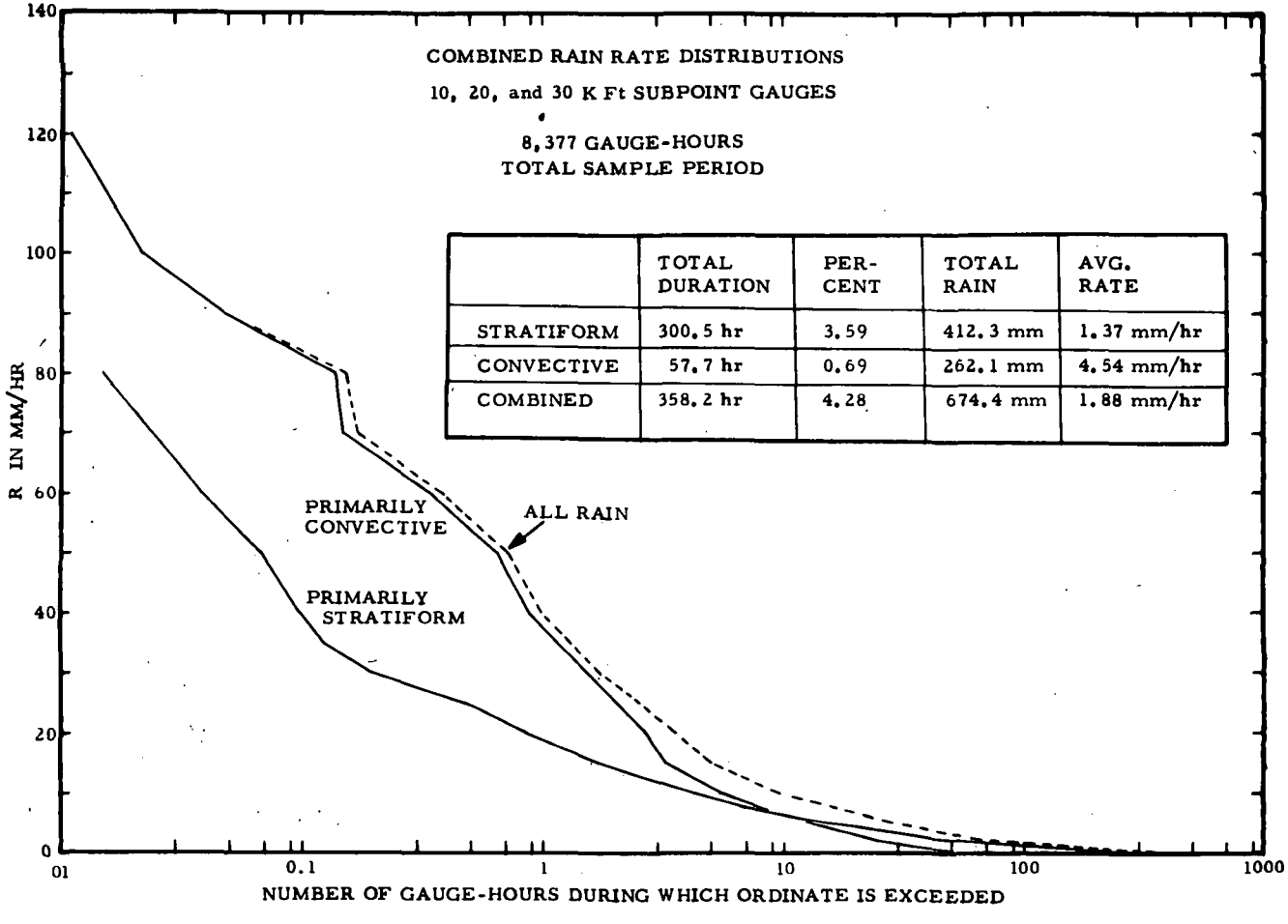

	TOTAL DURATION	PER-CENT	TOTAL RAIN	AVG. RATE
STRATIFORM	300.5 hr	3.59	412.3 mm	1.37 mm/hr
CONVECTIVE	57.7 hr	0.69	262.1 mm	4.54 mm/hr
COMBINED	358.2 hr	4.28	674.4 mm	1.88 mm/hr

Figure A-4. Combined rain-rate distributions, 10,000, 20,000, and 30,000 ft subpoint gauges.

Table A-1. Rain-Rate Data Used in Comparisons with Bistatic Radar Data

	1970															1971					
DATA RUN NO.	1	1	2	3	3	4	4	4	5	5	6	7	7	8	9	9	10	11	12	13	14	15
R/Date mm/hr	9/27 min.	9/28	10/16	10/21	10/21	10/22	11/3	11/4	11/10	11/10-11/11	11/14-11/15	11/20	12/12	12/16	12/31	1/5	1/14	1/14	1/15	1/23	1/24	1/30
120																						
110																						
100																						
90	0.78															0.78						
80	3.48															1.68						
70																						
60	7.08										0.48					2.88						
55	9.90																					
50									1.02		1.86											
45																						
40	13.50															3.54						
35												0.42										
30	26.22								4.32	2.40	2.76			0.48								
25	27.42			0.60					9.72													
20	30.30								11.64					1.20	0.72	4.20						2.94
15	33.66		1.62	10.50					16.14	6.78		2.10		9.96								
10	62.46		7.14	15.72			1.44		28.26		3.78	7.80	1.38	64.68	11.82	8.58						7.74
7.5				23.04						9.78		11.28		104.64	33.42	41.16	1.98					
5	155.76	22.08	24.60	45.24			13.20		51.54	18.06	13.38	17.04		184.20	84.60	85.50	4.68		5.16		5.34	11.46
2.5	227.88	32.76	58.62	100.44			21.00		111.84	91.98	25.80	25.02		373.86	176.52	134.34	27.06		29.16	16.14	50.52	17.40
1	303.18	76.80	110.28	239.22				72.18	145.02	571.56	36.60	56.64	43.56	556.20	202.98	155.82	86.04	12.90	72.06	72.48	191.40	
0.5	474.30	93.30	155.82	282.12	22.50	16.32		158.40	181.80	981.00		73.02	106.02	711.60	231.18		210.18	52.50	97.20	199.98	231.72	
0.2				398.40		56.22		385.80		1102.20				765.60	316.20		382.98	92.70		238.80	320.40	
0.1					191.40																	

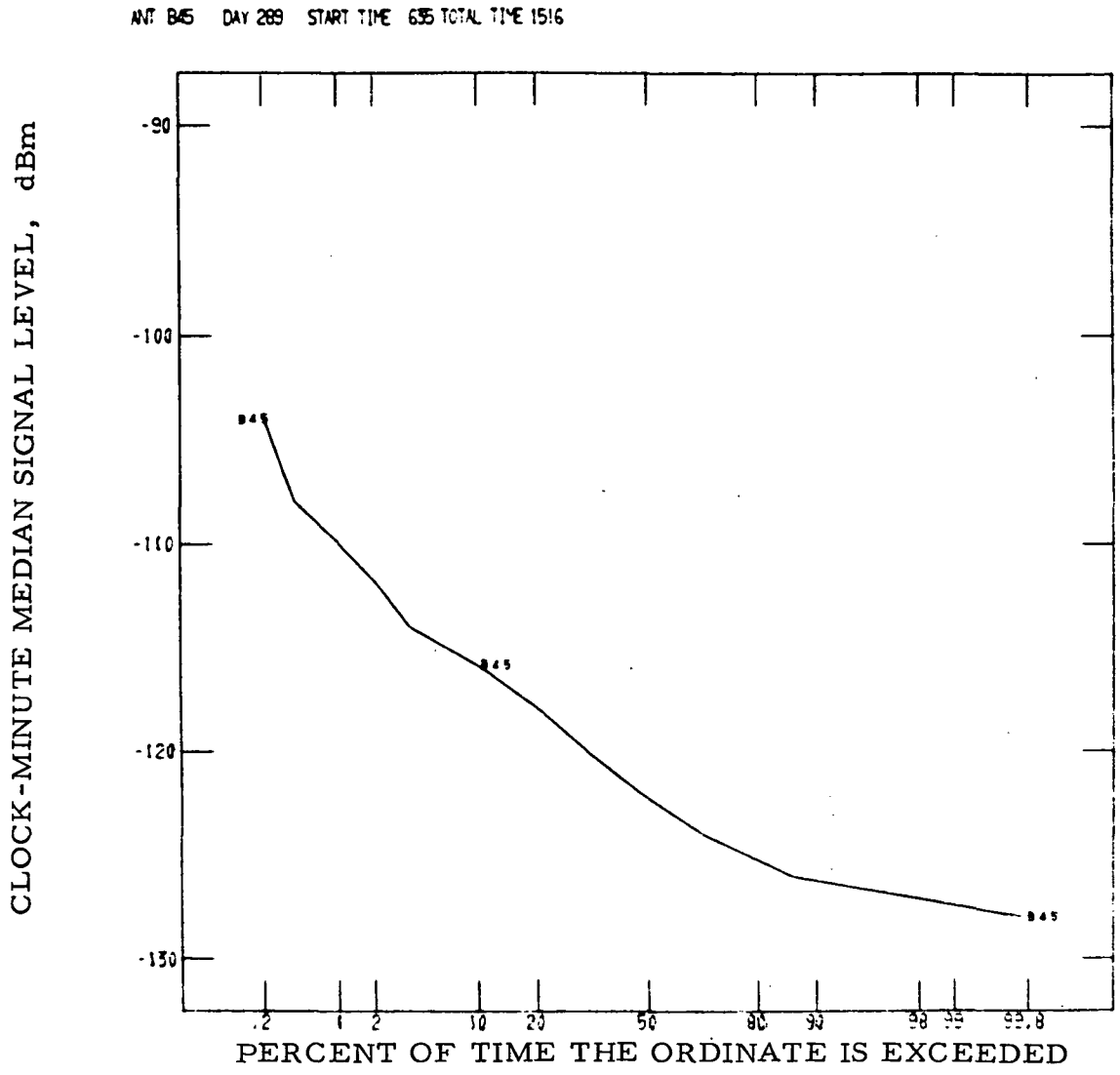

Figure A-5. Cumulative distribution of B_{45} data.

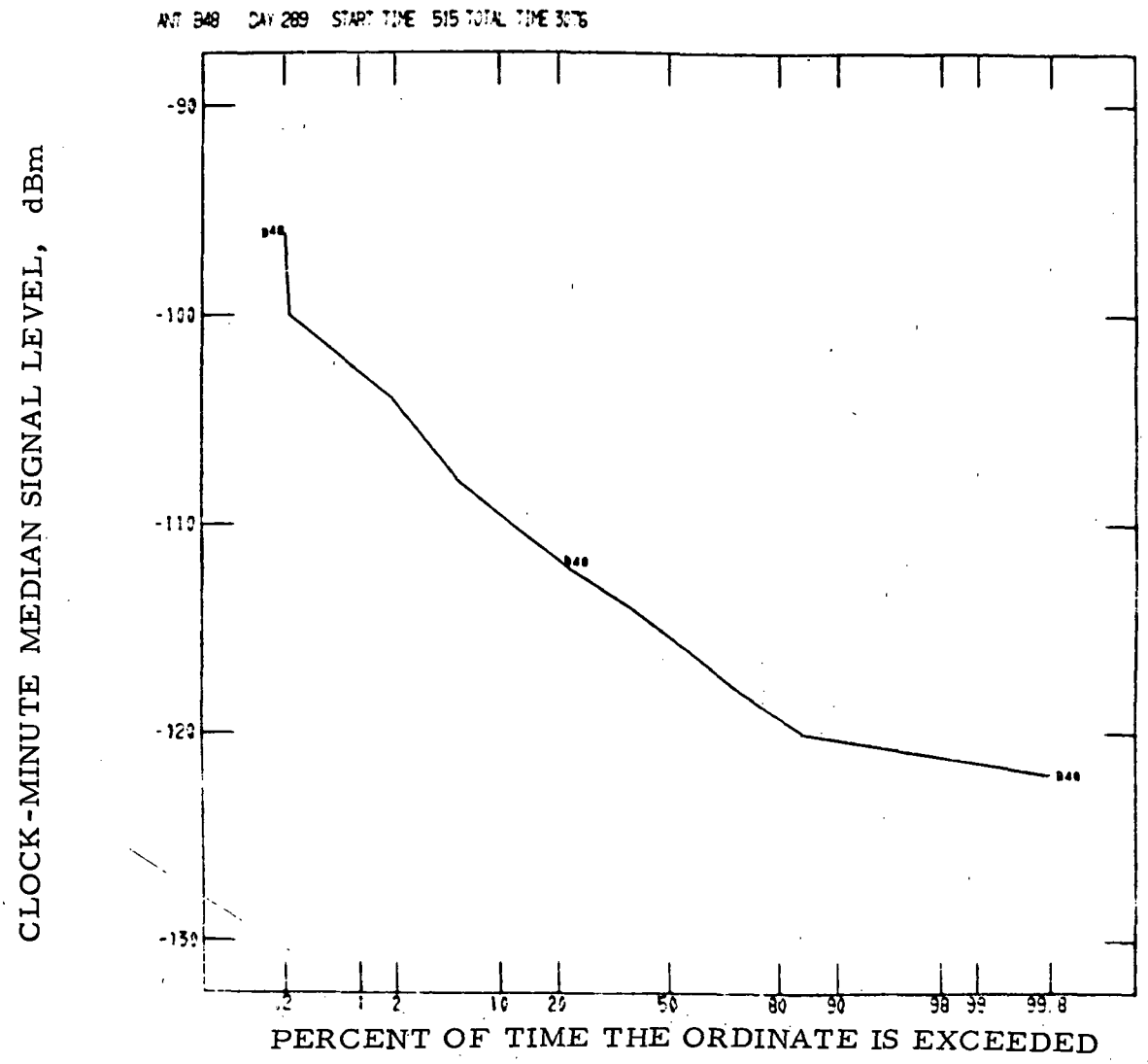

Figure A-6. Cumulative distribution of B_{48} data.

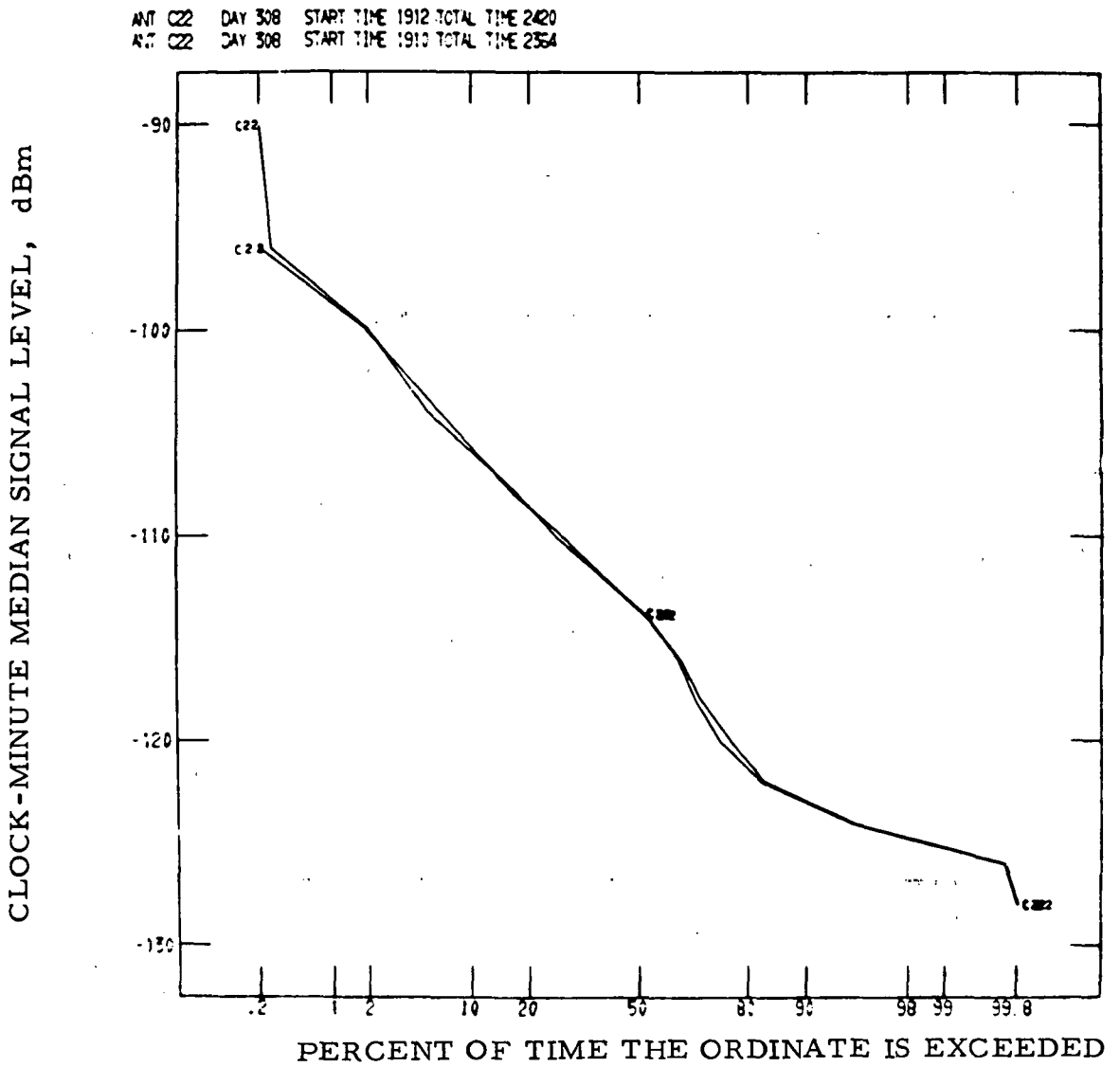

Figure A-7. Cumulative distribution of C_{22} data.

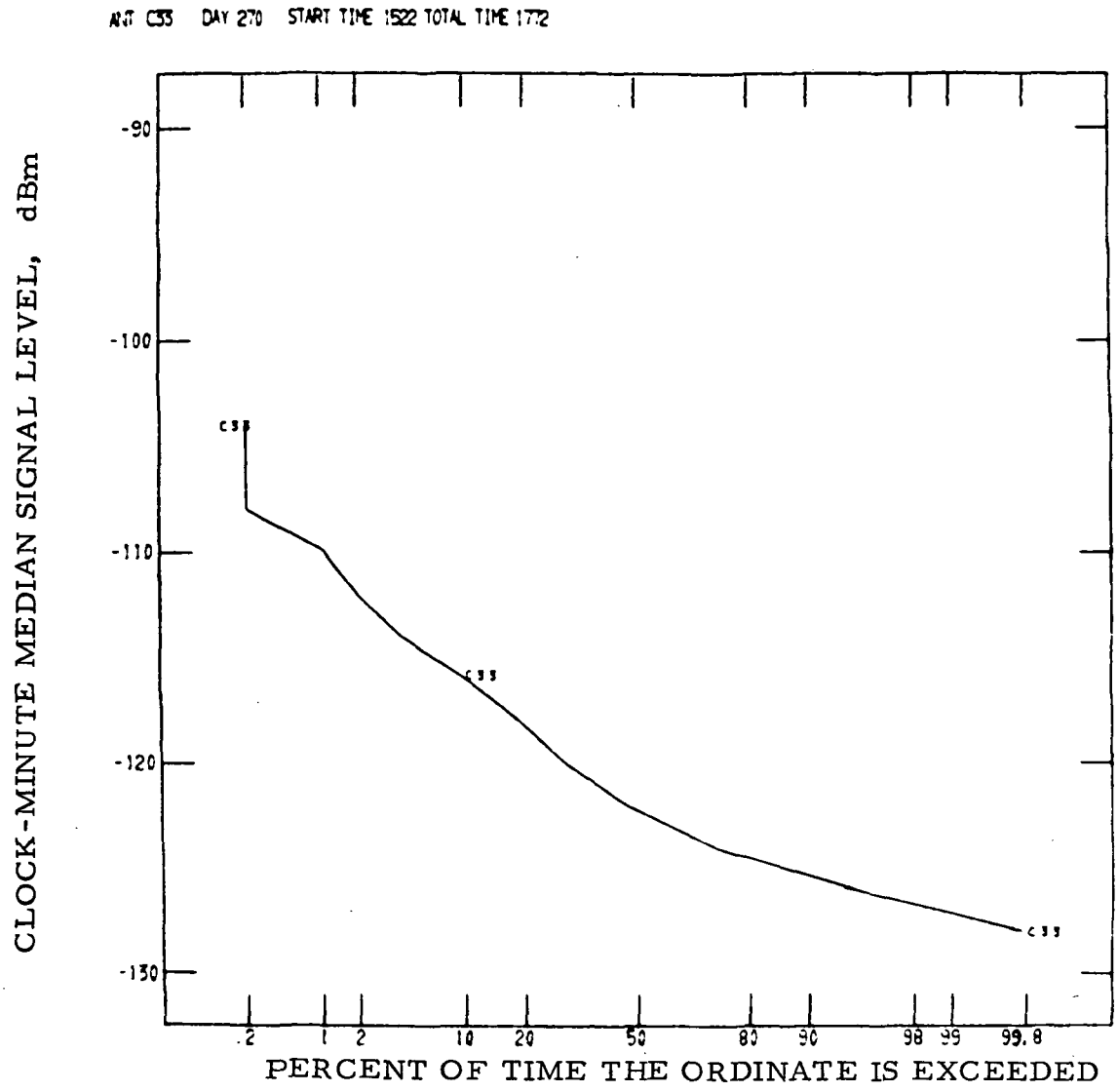

Figure A-8. Cumulative distribution of C_{33} data.

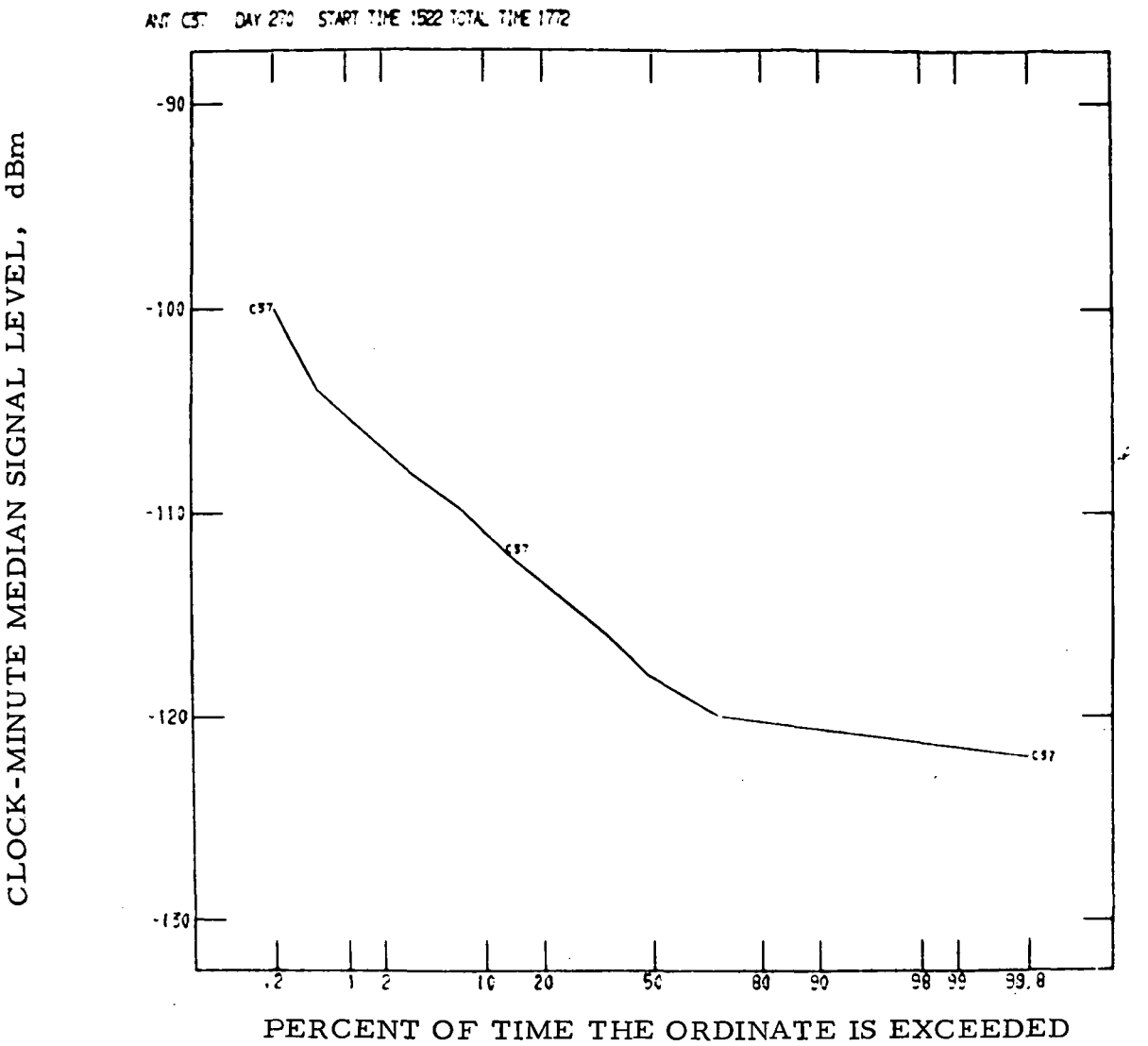

Figure A-9. Cumulative distribution of C_{37} data.

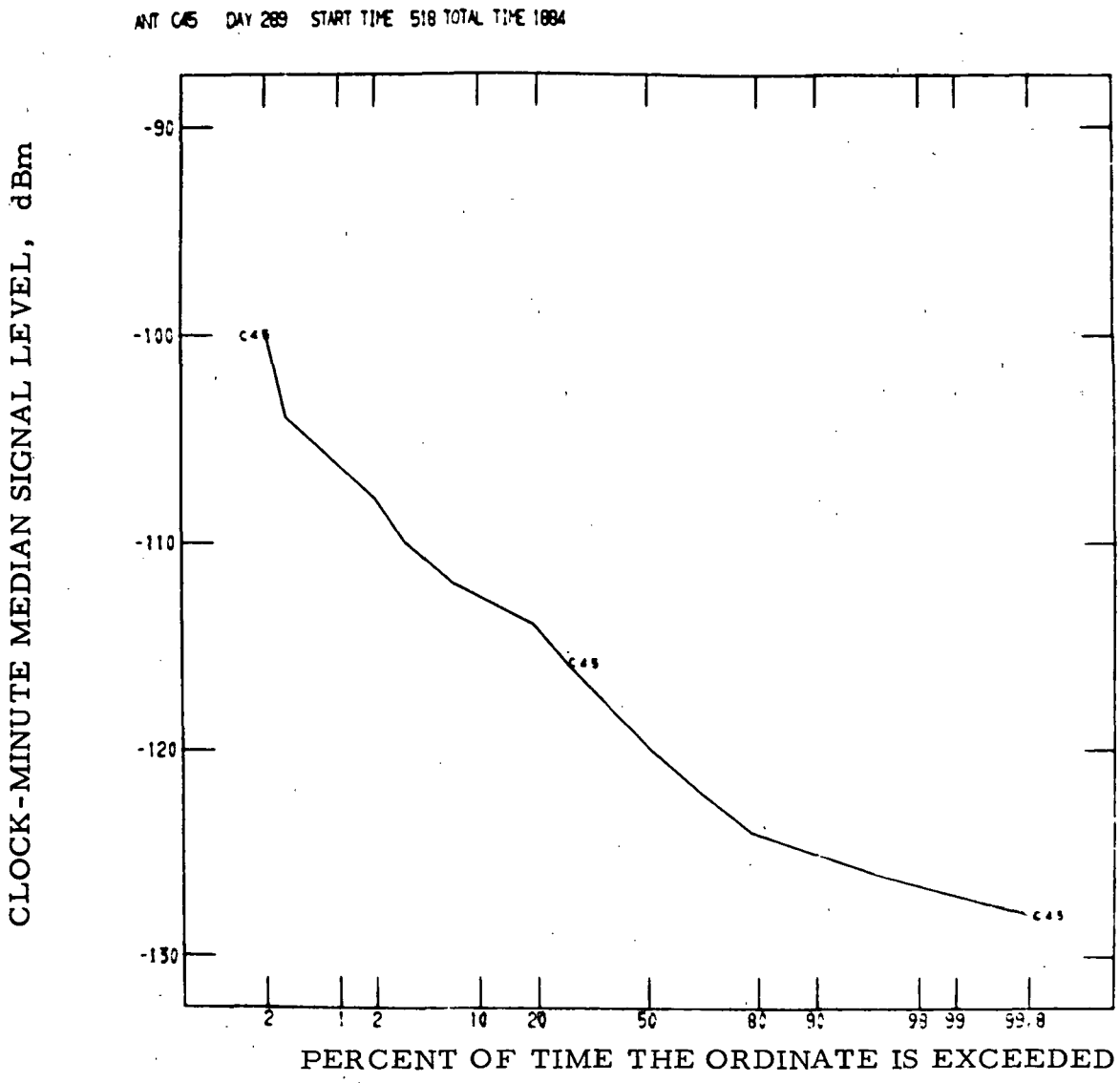

Figure A-10. Cumulative distribution of C_{45} data.

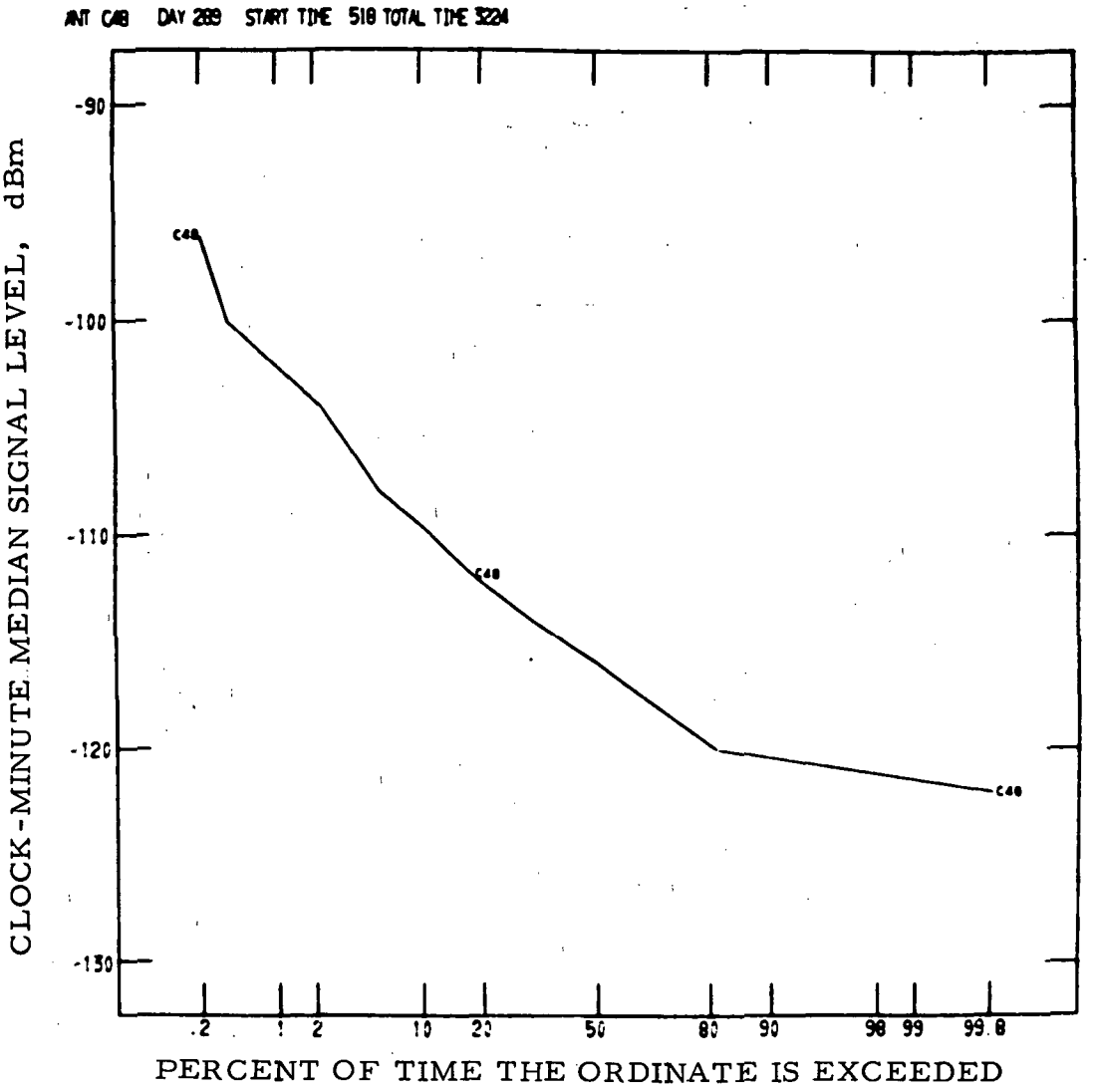

Figure A-11. Cumulative distribution of C_{48} data.

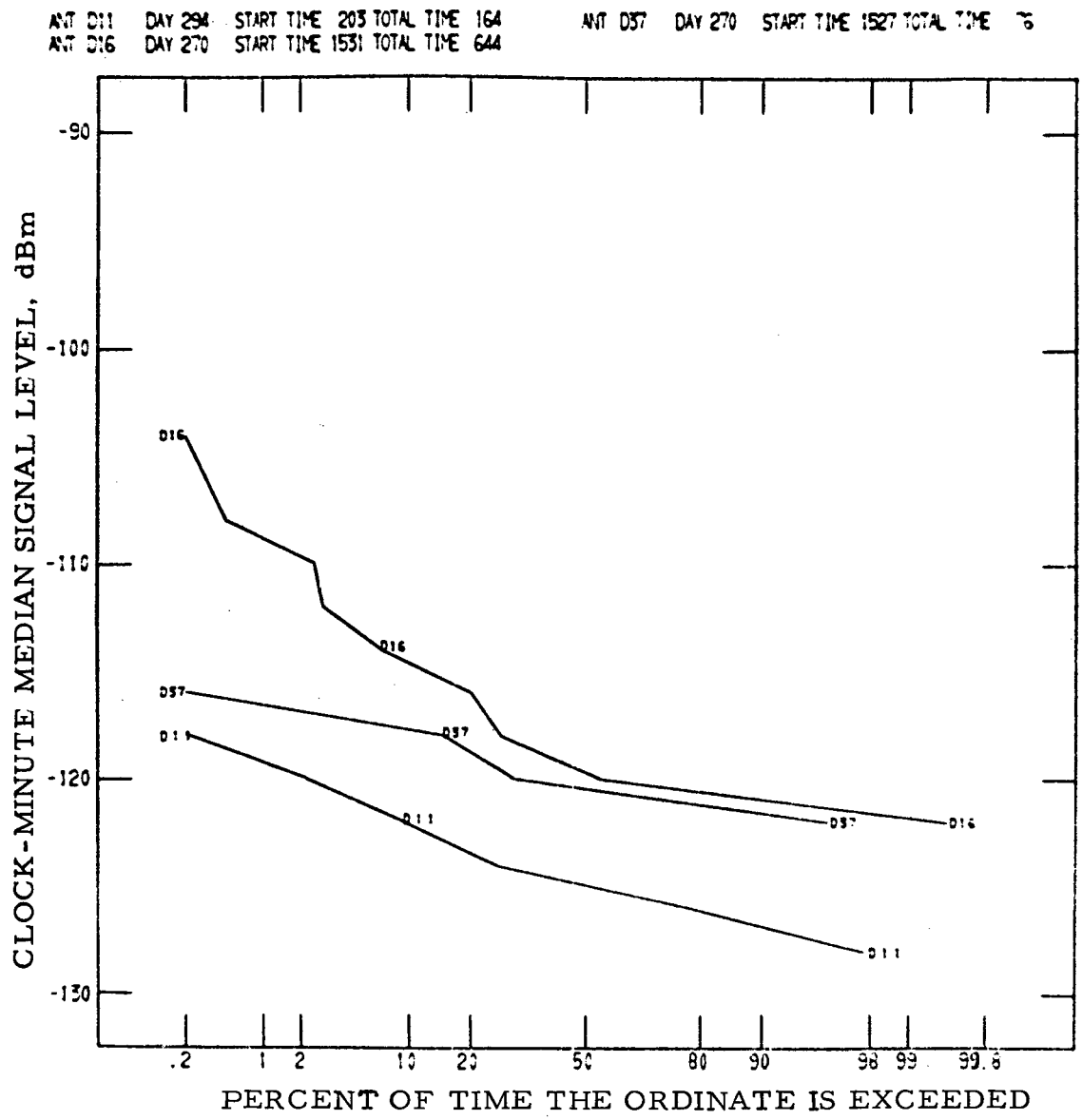

Figure A-12. Cumulative distributions for the 20,000 ft common volume data.

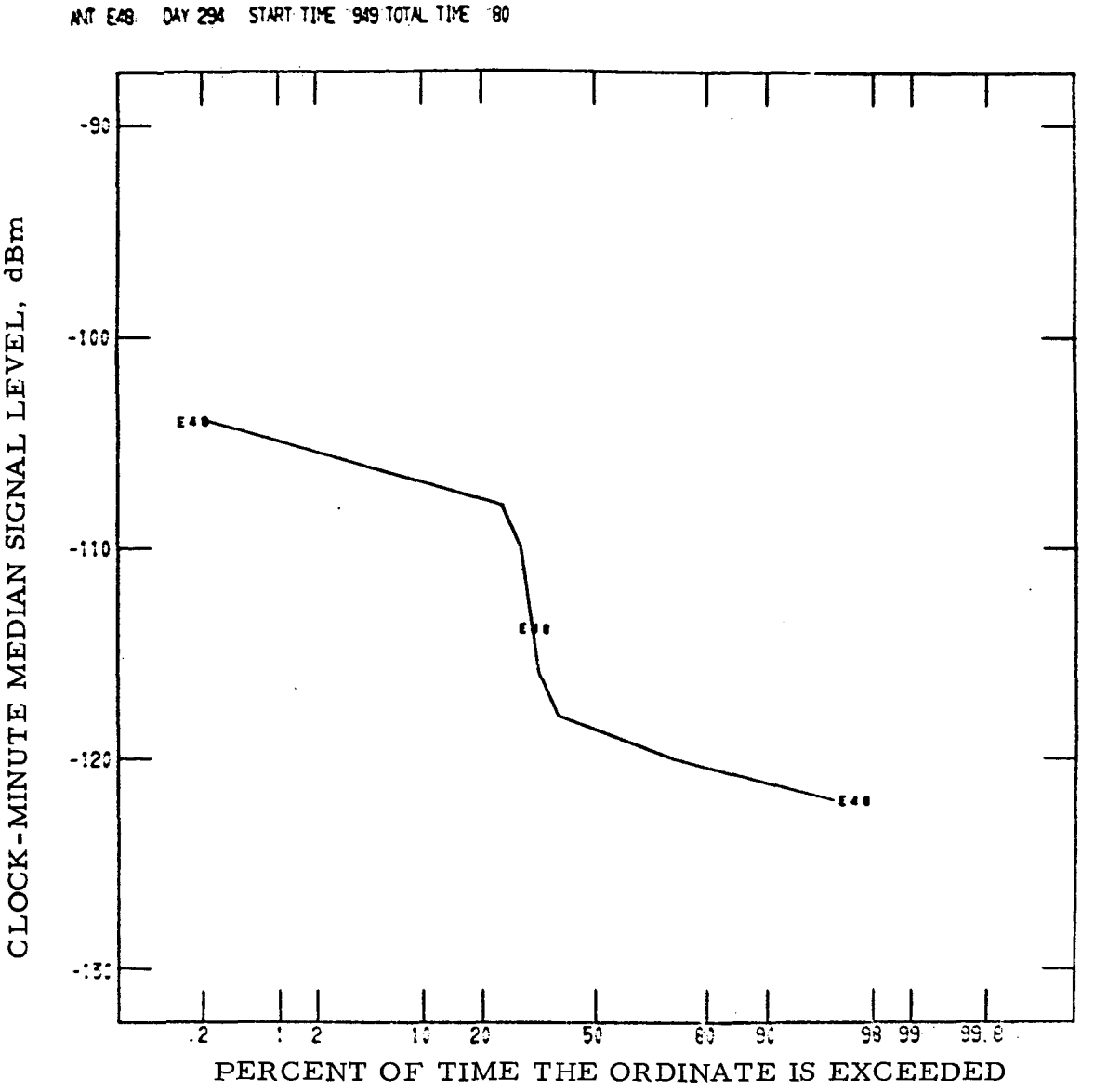

Figure A-13. Cumulative distribution of E_{48} data.

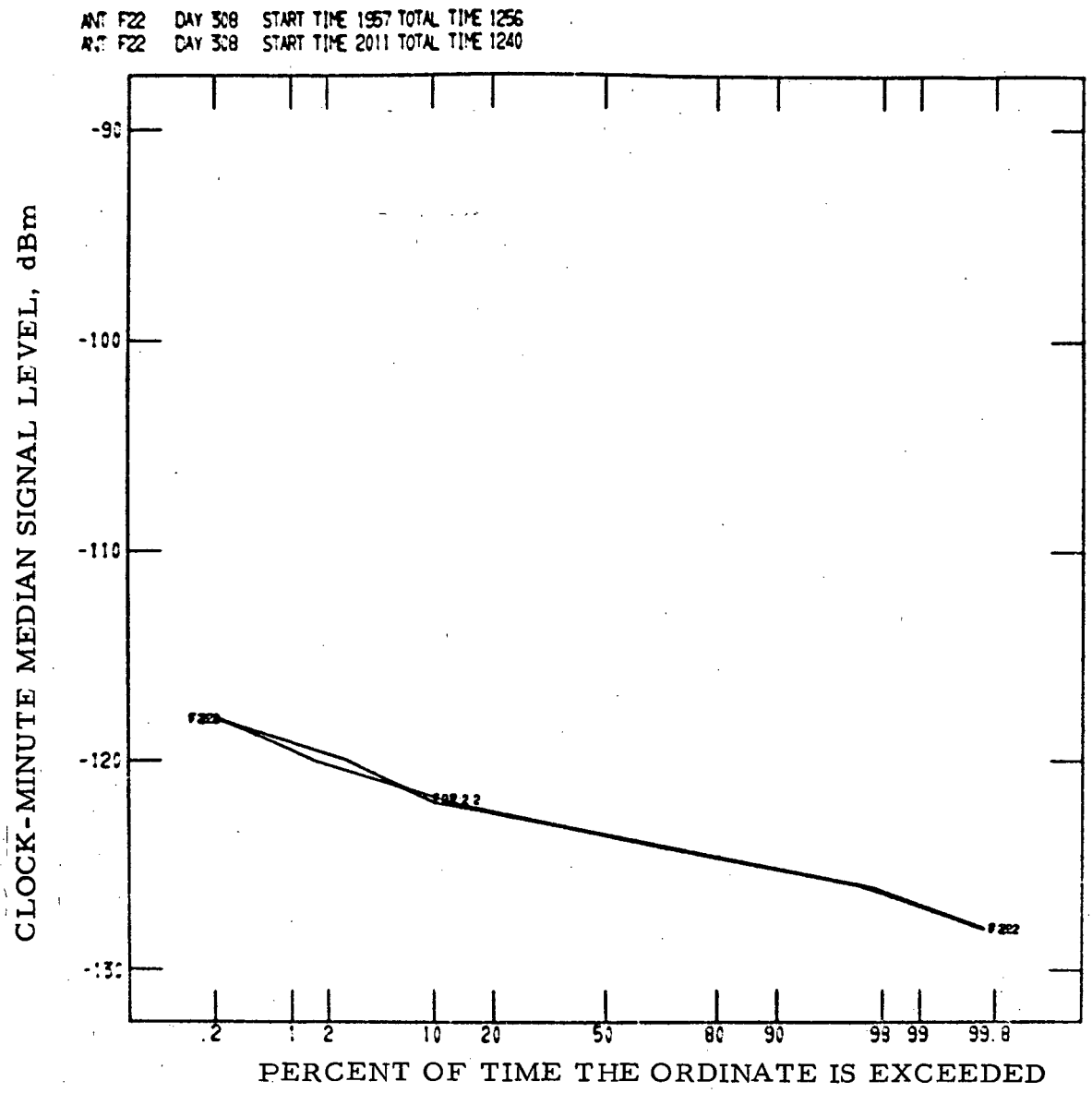

Figure A-14. Cumulative distributions for the off-path data, F_{22}.

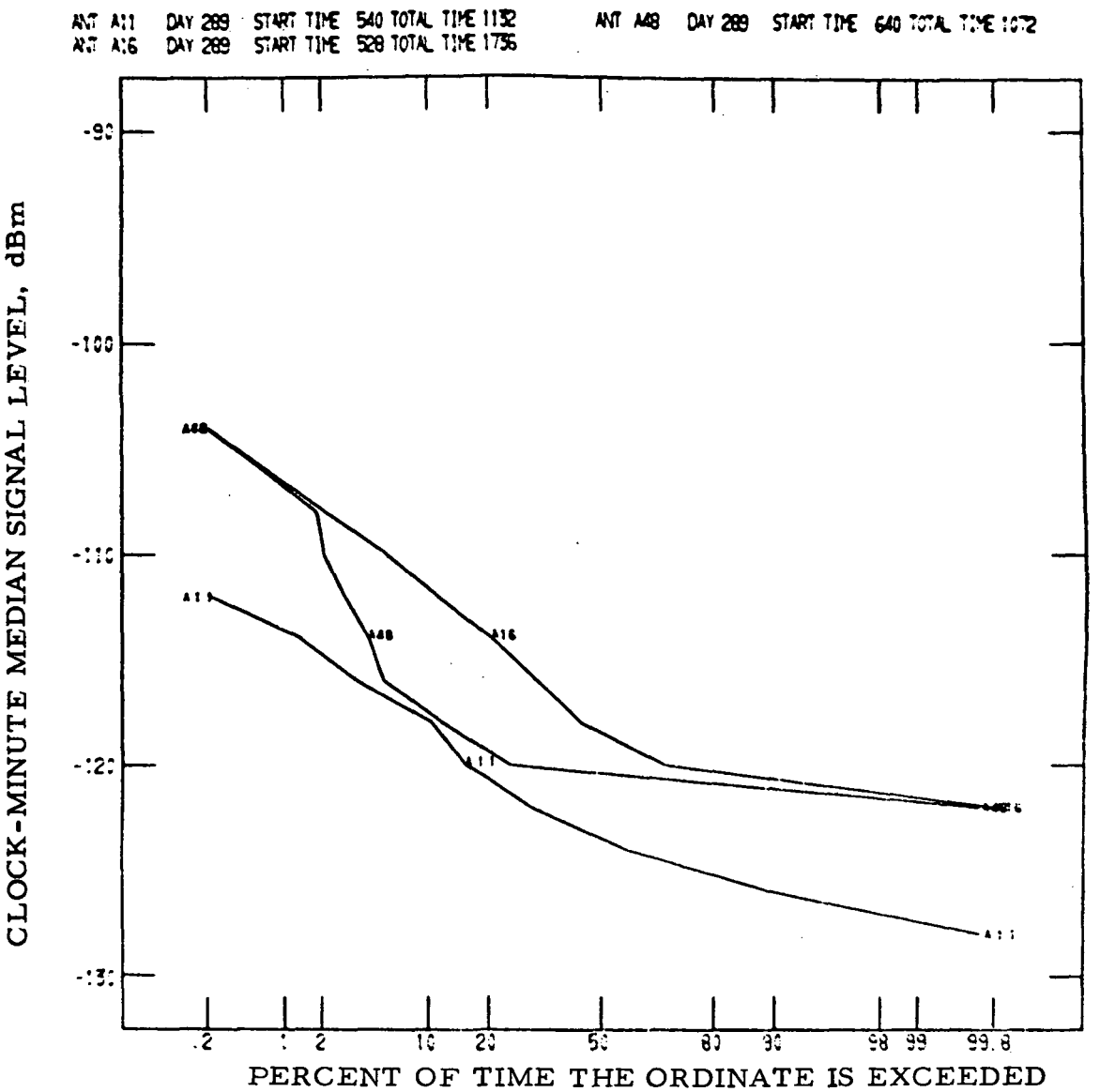

Figure A-15. Cumulative distributions of the Great Circle path data.

APPENDIX B

Transmitter Foreground and Horizon Effects

In section 5.1 it was determined that a few of the bistatic CW radio signals, based on clock-minute distributions, were lower in value than predicted by the bistatic theory. On a minute-by-minute basis the individual signal means will fluctuate around the predicted value due to variations in the actual amount of rainfall within the common volume. The calculated expected value is based upon the assumption of complete uniform filling of the common volumes by rain. Analysis of the clock-minute data for all of the common volumes and paths over the total data sample have produced the cumulative distributions in Appendix A. From the comparison of these curves, it was deduced that the data from the B_{45}, C_{33}, and C_{37} path/frequency elements of the experiment configuration were low. An antenna foreground effect at the transmitter sites was cited as the most probable explanation.

Figure B-1 is a photograph of the foreground and horizon tree-line in front of the transmitting antennas located at the Fort Lee (TS-3) site. The small crosses indicate the tops of the tree lines or the radio horizon for each path configuration, including the great circle (GC). The circles illustrate the approximate location and size of the transmitter beam pattern at the horizon for the S-band system. It can be seen that a shielding effect did exist on the 10,000 ft orientation, as the lower portion of the transmitted beam directed to this common volume was in the horizon tree-line. It was seen in section 5.2 that a correction of 4.5 dB brings the C_{33} and C_{37} data into line with the other data.

It is noted from figure B-1 that the great circle data from Ft. Lee was also affected by trees in the foreground.

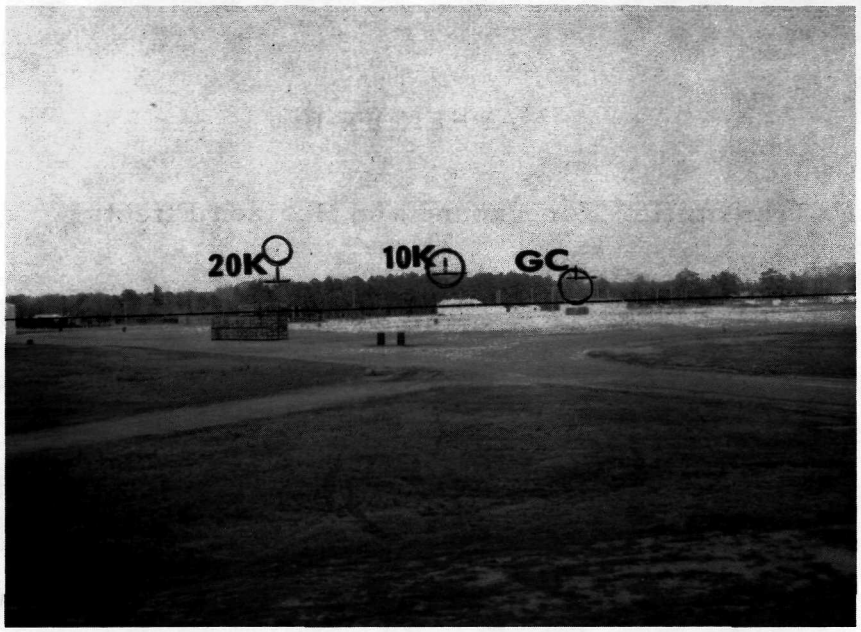

Figure B-1. Foreground and horizon for Ft. Lee transmitter site (TS-3).

The other configurations from the site, however, did not require allowances for the foreground. The methods available for calculating the average foreground effects provide estimates consistent with those observed, but cannot be conclusive without supporting field measurements to provide good estimates for individual cases.

Figure B-2 presents two photographs taken at the Eastville (TS-4) transmitter site. Here we note that a significant foreground effect was possible for the 5000 ft common volume orientation, which is seen in the data for paths B_{45} and B_{48} as noted in section 5.1.

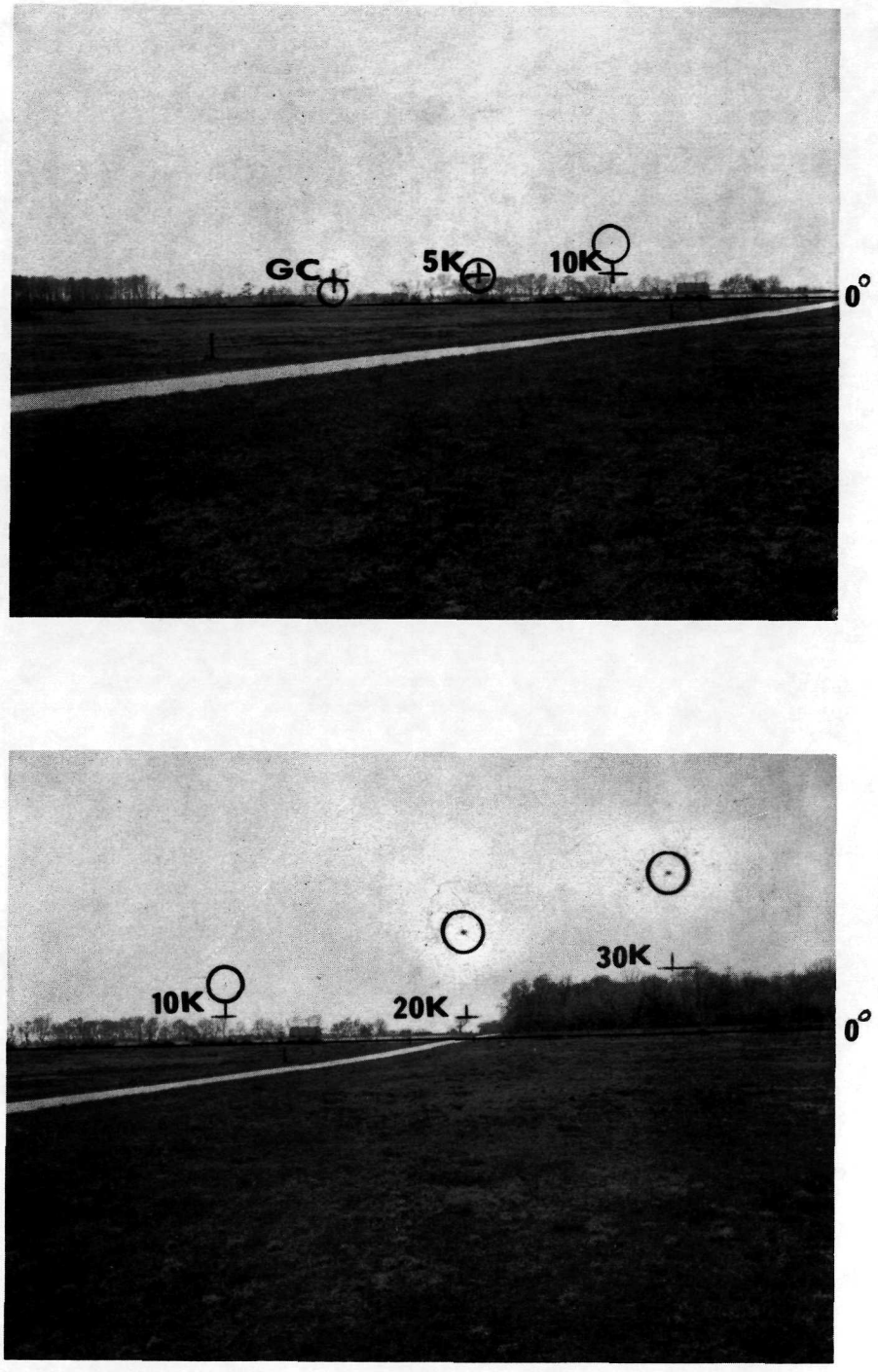

Figure B-2. Foreground and horizon of the Eastville transmitter site (TS-4).

APPENDIX C

Example of Meteorological Analysis

The following synopsis of a storm that occurred in the experiment area on December 16, 1970, is presented as an example of the general weather and meteorological analysis applied in the Virginia experiment. This particular storm was selected to help explain the anomalous data noted in section 5.1.

At 0700 EST, a low pressure system was centered over Cairo, Ill., with an occluded front extending to SE Alabama. From this point, a cold front extended SW into the Gulf of Mexico, and a warm front extended ENE to the Atlantic coast near Charleston, S.C., and SE into the Atlantic ocean. A shield of light to moderate rain covered most of the SE states, with thunderstorms along the cold front. This storm and its associated frontal system moved rapidly to the ENE, the low pressure center reaching a point over New York City by 0700 EST on the 17th.

Widespread warm-frontal, stratiform type rain occurred with this system over the experimental area from about 0900 EST on the 16th until passage of the cold (occluded) front through the area at approximately 2130 EST. The surface maps for these two dates are shown in figures C-1 and C-2.

Cloud tops associated with this frontal system were detected by weather radar and found to be generally between 16,000 and 24,000 ft over the experiment area. Rainfall began at about 0800 EST on December 16 in southern Virginia and about 1100 to 1200 EST in northern Virginia, generally ending at 2300 EST as reported by National Weather Service stations in the area. Rainfall was fairly uniform, averaging 1.24 inches at 6 stations in the experiment area and ranging from 0.98 inch at Dulles International Airport (Sterling, Va.) to 1.76 inches at

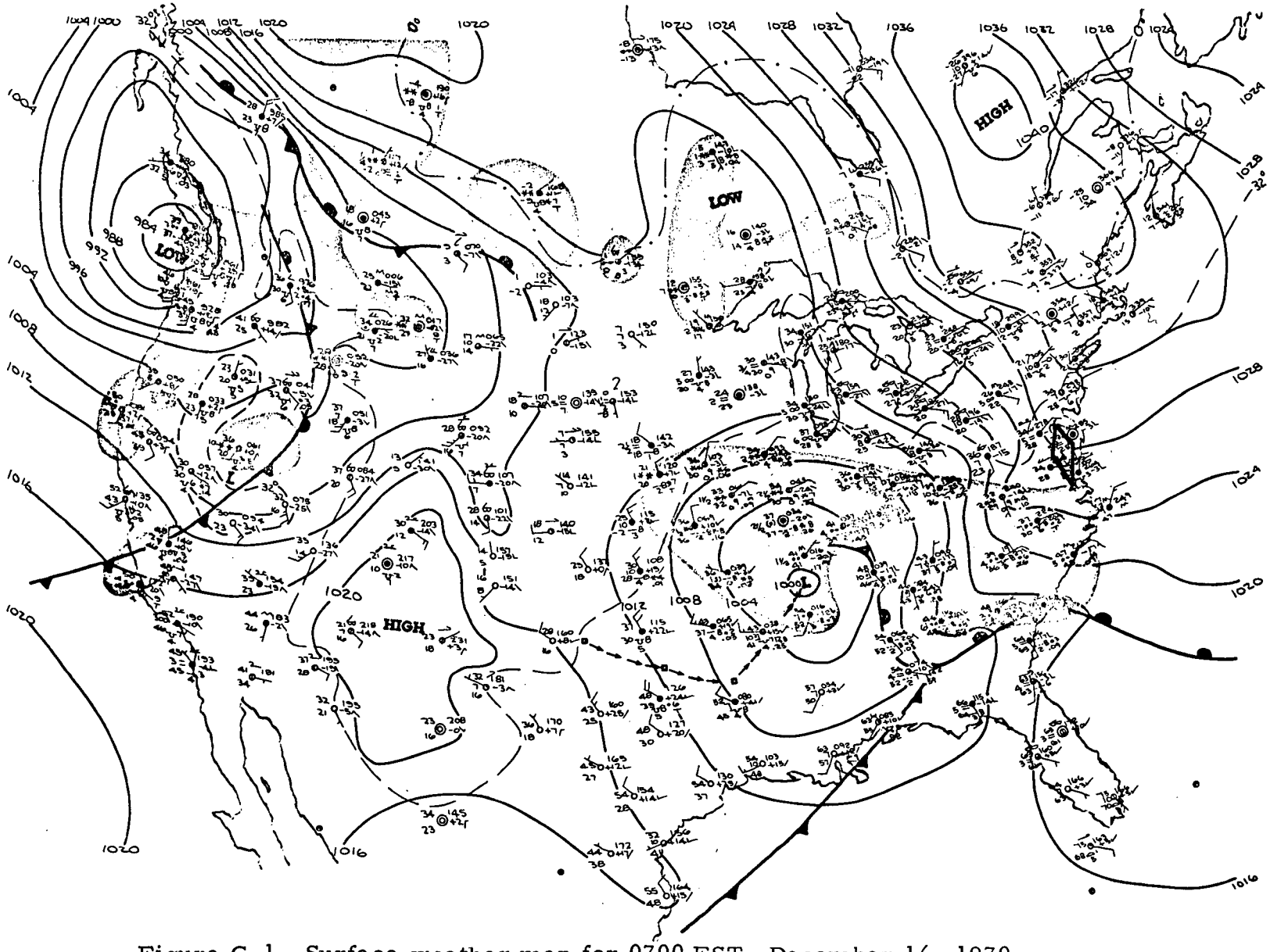

Figure C-1. Surface weather map for 0700 EST, December 16, 1970.

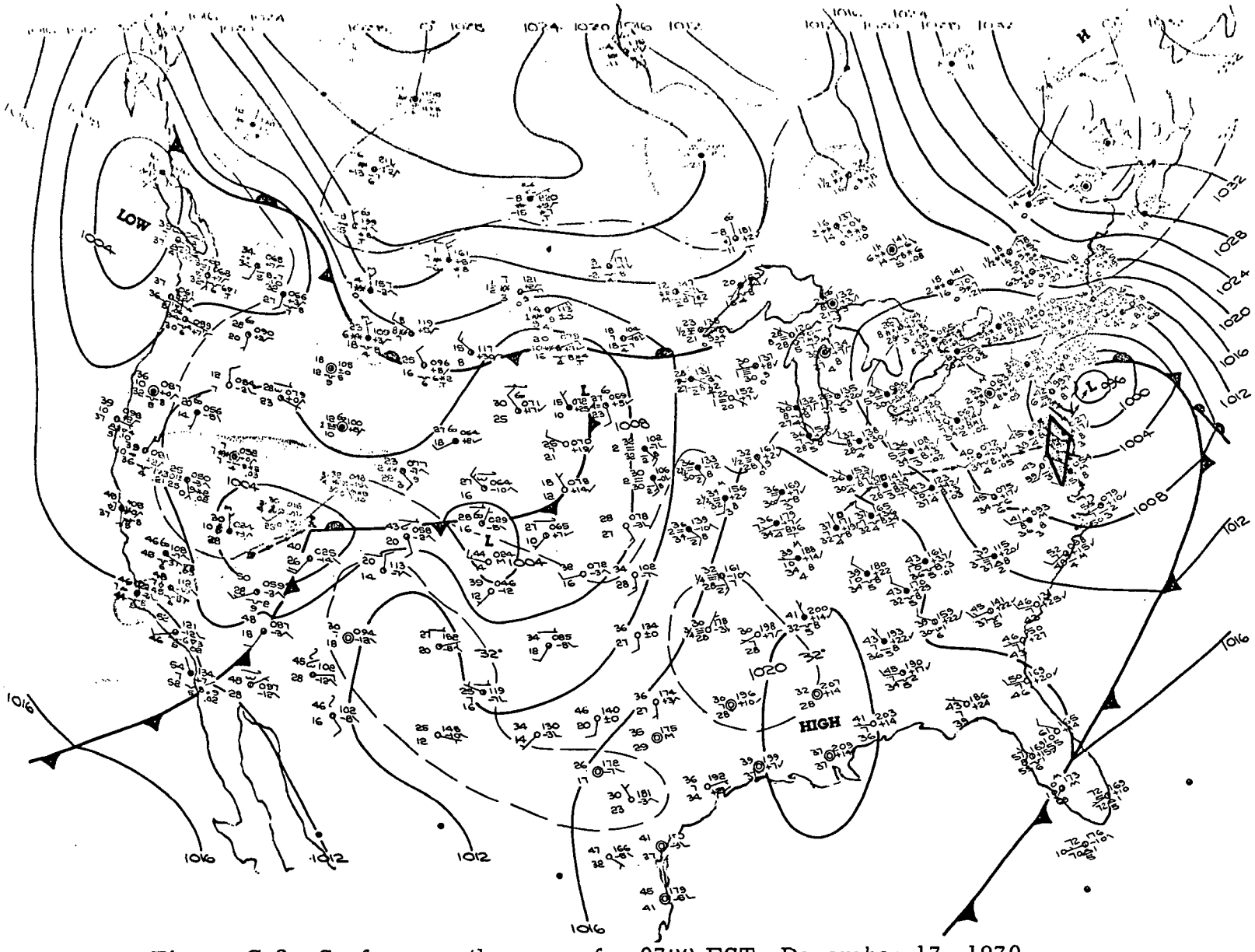

Figure C-2. Surface weather map for 0700 EST, December 17, 1970.

Norfolk, Va. Maximum hourly amounts averaged 0. 30 inch (7. 6 mm/hr) and ranged from 0. 24 inch at Wallops Island, Va. and Washington National Airport, to 0. 39 inch at Norfolk, Va. The rain gauge network in the experiment reported average rainfall of 1. 57 inches, ranging from 1. 43 inches at the 5000 ft subpoint to 1. 79 inches at the 10, 000 ft subpoint. Maximum hourly amounts (not clock-hours as the National Weather Service stations report) averaged 0. 42 inch, ranging from 0. 32 inch at the 5000 ft subpoint to 0. 50 inch at the 30, 000 ft subpoint. The reported rainfall and maximum hourly amounts from the experiment network compare favorably with the NWS report for Norfolk, Va., the closest reporting station.

The meteorological network indicated that cold frontal passage occurred from a WSW direction at approximately 2000 EST at Ft. Lee, 2100 EST at Quantico, 2145 at Poquoson, and 2230 at Eastville.

A brief heavy shower, apparently of convective origin due to lifting just prior to passage of the cold front, occurred at the 30, 000 ft subpoint at approximately 2100 EST. Duration of this shower, which was imbedded in stratiform rain, was 4. 8 minutes, during which time 0. 20 inch of rain was recorded - a rate of 65 mm/hr. The maximum one-minute rain-rate with this shower was 85 mm/hr.

The PPI display of the VERLORT radar located at the Langley site was photographed between 0915 EST and 2250 EST on the 16th. During this time the radar indicated widespread rainfall of varying intensity throughout the experiment area in patterns consistent with stratiform rain. Especially strong echoes were photographed between 1900 EST and 2200 EST. The frontal passage was indicated to have occurred between 2134 EST and 2143 EST along a line generally parallel to the Langley-Quantico earth station beam, with the front moving in a direction perpendicular to the earth station beam. This analysis agrees with the rain gauge network data, which indicate virtually simultaneous

cessation of rain at all sites, the ending times ranging from 2135 EST at the 10,000 ft subpoint to 2140 EST at the 30,000 ft subpoint.

Rawinsonde data for the date showed superrefractive conditions to be prevalent over the eastern part of the experiment area until at least noon, but disappearing by 1800 EST. Quick-look significant level data received by teletype showed only some elevated layers that would have had little effect on the radio system. However, detailed refractive index profiles derived from the rawinsonde recorder charts yielded different results. Surface ducts were found at Wallops Island, Va., Hatteras, and Greensboro, N. C., but not at Washington, D. C., for 0630 EST. The temperature, relative humidity and N profiles for Wallops Island are shown in figures C-3 and C-4. At approximately 1230 EST, a special rawinsonde was launched at each of those four stations. These flights indicated superrefractive (but not ducting) at Wallops Island, Hatteras, and Greensboro, with Washington being subrefractive. At 1830 EST rawinsonde at all four stations showed saturated profiles and slightly subnormal refractive index gradients.

There is thus a good probability, based on this analysis, that radio signals could have been effected by a superrefractive/diffraction mode during the morning hours of December 16, with the probability of superrefraction on the Eastville paths being high, and the probability for Ft. Lee and Quantico being low. There is also some evidence that subrefractive conditions could have been prevalent on the Ft. Lee side of the configuration. These observations, including the description of the varying intensity of the associated rainfall have been used to help explain the anomolous radio data observed on this date.

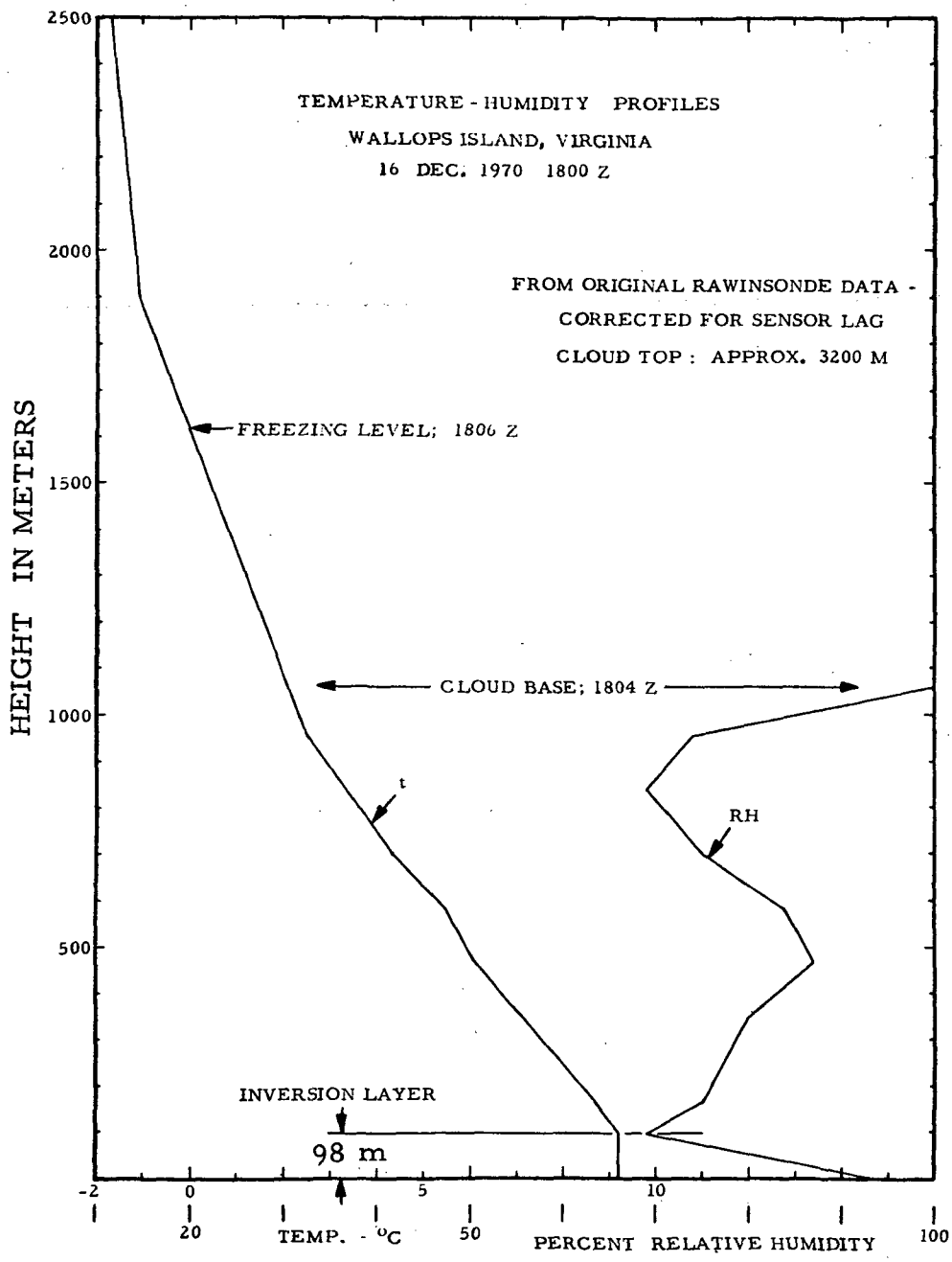

Figure C-3. Temperature-humidity profiles, Wallops Island, Va.

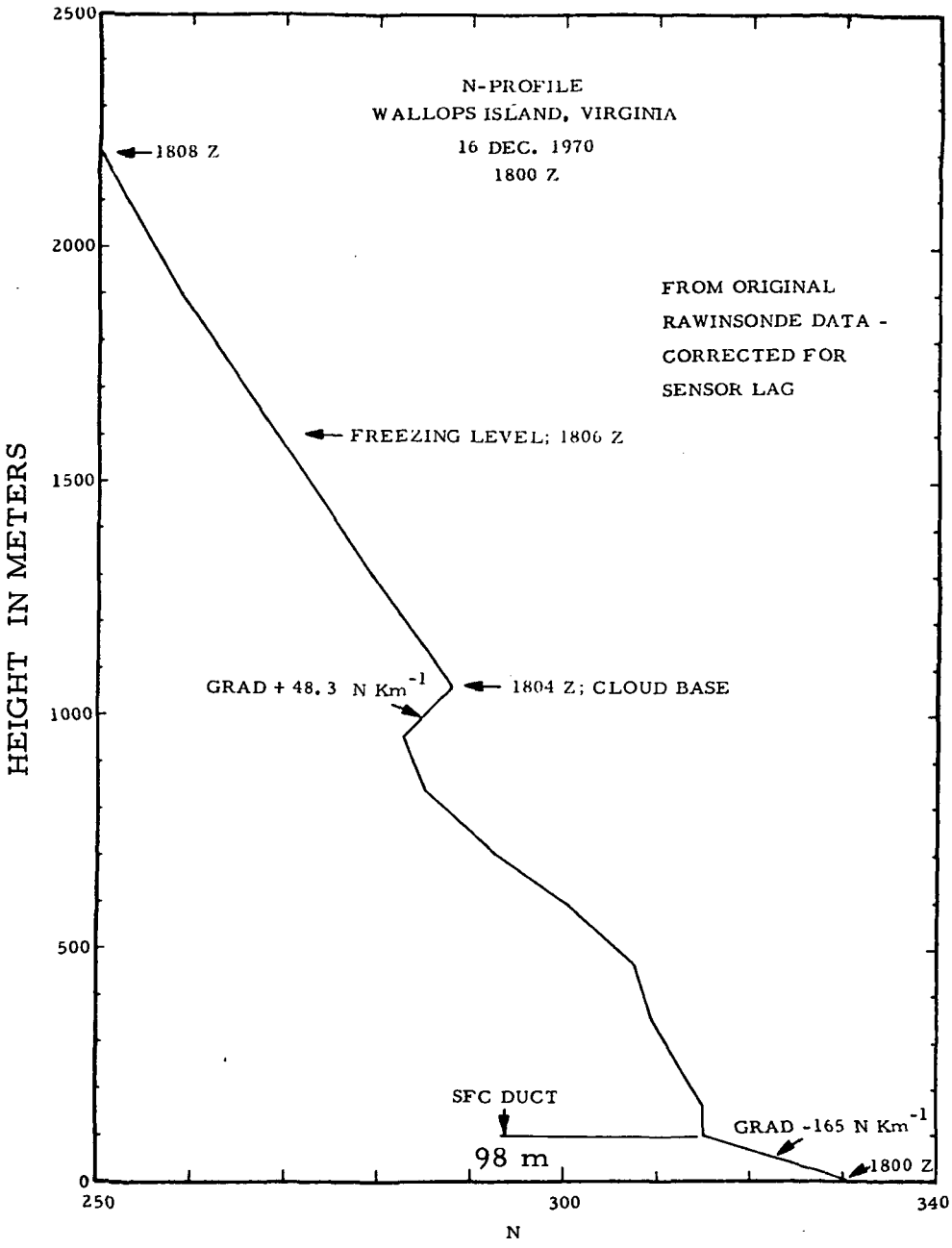

Figure C-4. N-Profile. Wallops Island, Virginia.

FORM OT-29
(3-73)

U.S. DEPARTMENT OF COMMERCE
OFFICE OF TELECOMMUNICATIONS

BIBLIOGRAPHIC DATA SHEET

1. PUBLICATION OR REPORT NO.	2. Gov't Accession No.	3. Recipient's Accession No.
OT/TRER 33 (Old Series) OT Report 73-15		

4. TITLE AND SUBTITLE
An Experimental Study of the Temporal Statistics of Radio Signals Scattered by Rain

5. Publication Date
June 1973

6. Performing Organization Code
ITS/OT

7. AUTHOR(S)
R. W. Hubbard, J. A. Hull, P. L. Rice, and P. I. Wells

9. Project/Task/Work Unit No.

8. PERFORMING ORGANIZATION NAME AND ADDRESS
U. S. Department of Commerce
Office of Telecommunications
Institute for Telecommunication Sciences
325 Broadway, Boulder, Colorado 80302

10. Contract/Grant No.

11. Sponsoring Organization Name and Address
U. S. Department of Commerce
Office of Telecommunications
Suite 250, 1325 G St., N. W.
Washington, D. C. 20005

12. Type of Report and Period Covered

13.

14. SUPPLEMENTARY NOTES

15. ABSTRACT *(A 200-word or less factual summary of most significant information. If document includes a significant bibliography or literature survey, mention it here.)*

A fixed-beam bistatic CW experiment designed to measure the temporal statistics of the volume reflectivity produced by hydrometeors at several selected altitudes, scattering angles, and at two frequencies (3.6 and 7.8 GHz) is described. Surface rain gauge data, local meteorological data, surveillance S-band radar, and great-circle path propagation measurements were also made to describe the general weather and propagation conditions and to distinguish precipitation scatter signals from those caused by ducting and other nonhydrometeor scatter mechanisms. The operating characteristics of the various system components used in the experiment are presented. The data analysis procedures were designed to provide an assessment of a one-year sample of data with a time resolution of one minute. The results to date cover the time interval of September 15, 1970, to January 31, 1971. The (continued next page)

16. Key words *(Alphabetical order, separated by semicolons)*

Coordination distances; frequency sharing; precipitation scatter; propagation; rain-rate statistics; and satellite/terrestrial communications.

17. AVAILABILITY STATEMENT

[X] UNLIMITED.

[ ] FOR OFFICIAL DISTRIBUTION.

18. Security Class *(This report)*
Unclassified

19. Security Class *(This page)*
Unclassified

20. Number of pages
147

21. Price:

☆U.S. Government Printing Office: 1973-783-893/7 Region 8

USCOMM-DC 29716-P73
USCOMM - ERL